UNIVERSITÀ
DEGLI STUDI
DI PADOVA

Head Office: Università degli Studi di Padova

Department of Biology

Ph.D. COURSE IN: Biosciences

CURRICULUM: Cell Biology and Physiology

SERIES: XXXV cycle

USP14 inhibition enhances Parkin-independent mitophagy in iNeurons

Coordinator: Prof. Ildikò Szabò

Supervisor: Prof. Elena Ziviani

Ph.D. student : Greta Bernardo

Acknowledgments

Questo percorso di dottorato è stato per me tante cose. La maggior parte del tempo è stato entusiasmo, soddisfazione, ricerca, scoperta, incontro e condivisione; ma a volte è stato anche frustrazione, lacrime, difficoltà. Non posso quindi non ringraziare tutte le persone che mi sono state vicino durante tutto questo percorso nei momenti più belli ma soprattutto in quelli un po' più duri.

Prima di tutto ringrazio Elena, il mio mentore, per la fiducia che mi ha sempre dimostrato, per avermi guidata senza imposizioni e per essere sempre stata un supporto disponibile e presente.

Un ringraziamento speciale va a Elena, è difficile dire in poche righe quanto averti avuto come collega e amica in questi anni sia stato fondamentale per me, nessuno mi aveva mai accolto con il calore con cui l'hai fatto tu e non te ne sarò mai grata abbastanza.

Ringrazio poi Margherita e Marta, compagne di gioie e di sventure, avervi al mio fianco in questi tre anni così intensi è stata la fortuna più grande; per me siete un po' delle compagne d'armi e il legame che abbiamo formato lo porterò con me per sempre.

Come non menzionare poi Sofia e Mariavittoria, vedervi crescere scientificamente è stata una grandissima soddisfazione e vi devo ringraziare per avermi supportata e sopportata, a volte avermi come collega non è proprio facile!

Devo ringraziare infine Marco e tutta la mia famiglia, mamma Federica, papà Fabio e i miei fratelli Silvia e Fausto. In tutti questi anni avete sempre creduto in me nonostante ogni tanto pensiate io sia completamente pazza e per questo vi sono infinitamente grata.

Table of Contents

SUMMARY OF THE THESIS

Neurodegenerative diseases affect millions of people worldwide and have a huge social and economic impact. They occur when cells of the brain lose function over time and ultimately die. The likelihood of developing a neurodegenerative disease rises dramatically with age, but also environmental and genetic factors can contribute to the insurgence of these disorders. First and second most common neurodegenerative disorders are Alzheimer's disease (AD) and Parkinson's disease (PD). Although some symptomatic treatments are available, AD and PD are incurable diseases, and slowing their progression is not currently feasible[1]. It is possible to observe some common themes in the pathogenesis of these disorders: mitochondrial dysfunction, oxidative stress, protein aggregation, and neuroinflammation. In particular, mitochondrial dysfunction can generate neuroinflammation and oxidative stress, which in turn leads to unfolded protein aggregation. All these mechanisms crosstalk with each other and culminate in the neurodegenerative process[2,3]. Normally the accumulation of dysfunctional mitochondria is counteracted by the activation of mitochondrial quality control (MQC) pathways, including mitochondrial dynamics, proteasome system, mitochondria-derived vesicles (MDVs), mitochondrial unfolded protein response (UPRmt), and mitophagy[4]. Mitophagy is the process that mediates the clearance of entire organelles; importantly, impairment of mitophagy is emerging as a common denominator in these diseases[5]. With that in mind, it is clear how the regulation of mitophagic pathways may be a potential target for the development of therapeutic strategies.

Mitophagy initiation requires the crosstalk between two of the best known degradative pathways in the cells: the UPS and the autophagy-lysosomal pathway that maintain cellular homeostasis through the detection and

degradation of aggregated proteins and dysfunctional organelles[6]. The signalling molecule that links these two pathways is ubiquitin (Ub), which can bind to other proteins and modulate their fate[7]. Ubiquitinated proteins on the mitochondrial surface are recognized by both the UPS, which mediate their degradation, and autophagic receptors, which promote autophagosome assembly and delivery to the lysosome[8].

Protein ubiquitination is a dynamic and reversible process controlled by two types of enzymes: Ubiquitin ligases and Deubiquitinating enzymes (DUBs). Several ubiquitin E3 ligases have been associated with the regulation of mitophagy, but the best studied is Parkin that in conjunction with the protein kinase PINK1, forms the best studied surveillance pathway for the detection and removal of dysfunctional mitochondria through Ub-dependent mitophagy. Importantly, both sporadic and genetic forms of Parkinson's disease are associated with mutation on the genes encoding for PINK1 and Parkin[9,10]. In this context, the stimulation of alternative mitophagy pathways may represent an attractive solution to counteract the neurodegeneration process. One way to do so is by acting on DUBs; enzymes able to oppose the activity of Ub-E3 ligases by eliminating Ub chains from targeted mitochondria, thus preventing their elimination[11,12]. Among these DUBs, the proteasome-associated USP14 seems a particularly appealing target thanks to its capacity to regulate both the UPS and autophagy[13–17]. Moreover, a series of potent and selective inhibitors are available for this DUB (IU1 and IU1-47), making it an ideal candidate for potential therapy development[14,18].

We recently reported that pharmacological and genetic inhibition of USP14 promotes basal mitophagy in PD patient fibroblasts while in *in vivo* PINK1/Parkin *D.melanogaster* models of PD, it restored mitochondria function and ultrastructure as well as dopamine levels. Remarkably, at the systemic level,

inhibition of USP14 extended the flies' lifespan and rescued climbing behavior[19]. At present, studies on the effects of USP14 inhibition on mitophagy in neurons of human origin have not yet been conducted.

To close this gap, we took advantage of a recently generated line of human embryonic stem cells (hESCs) able to rapidly and efficiently differentiate functional iNeurons[20,21], and tested the mitophagic effect of USP14 inhibition using the recently discovered small molecule inhibitor IU1-47[18]. After characterizing the hESCs-derived neurons, we took advantage of Tandem Mass Tagging (TMT)-based proteomics to assess the impact of USP14 inhibition on the global proteome of iNeurons. TMT analysis demonstrated that IU1-47 treatment triggers the specific degradation of mitochondrial proteins from all mitochondria compartments without impacting other cellular organelles such as ER, Golgi, and peroxisomes. Based on these results, we further investigated the effects of USP14 inhibition on mitophagy regulation using a combination of biochemical and imaging approaches on cells with different genetic backgrounds, including PINK1 KO and Parkin KO iNeurons. We were able to demonstrate that USP14 inhibition enhances autophagy and mitophagy through a PINK1/Parkin-independent mechanism. In the attempt to uncover the alternative mechanism of action through which USP14 inhibition enhances mitophagy, we evaluated the autophagic flux in neurons knock-out for known mitophagy regulators such as MUL1, BNIP3L, and MARCH5. Interestingly, we found that IU1-47-mediated autophagy is MARCH5-dependent, suggesting a possible mechanism for the mitophagic effect of USP14 inhibition. Finally, we demonstrated that by enhancing mitophagy through the inhibition of USP14, we are able to improve mitochondrial respiration and membrane potential retention in Parkin KO iNeurons, used as a model of mitophagy impairment.

In summary, we show that USP14 inhibition, with the specific inhibitor IU1-47 is able to promote mitophagy in neurons of human origin through a PINK1/Parkin independent pathway. We propose that this mechanism is MARCH5-dependent. Finally, we demonstrate that the mitophagic effect of USP14 inhibition promotes the elimination of defective mitochondria with beneficial effects on the general mitochondrial fitness in a Parkin-deficient model of mitochondrial dysfunction and MQC impairment.

LIST OF ABBREVIATIONS

Acetyl-CoA	Acetyl-coenzyme A
AD	Alzheimer's disease
ALS	Amyotrophic lateral sclerosis
APP	Amyloid precursor protein
ATP	Adenosine triphosphate
CCCP	Carbonyl cyanide m-chlorophenylhydrazone
CJs	Cristae junctions
CoQ	Coenzyme Q
CP	Core particle
ER	Endoplasmic reticulum
ETC	Electron transport chain
FAO	Fatty Acid β-oxidation
FAs	Fatty acids
HD	Huntington's disease
IMM	Inner Mitochondrial Membrane
IMS	Intermembrane space
LB	Lewy bodies
LIR	LC3-interacting region
MDVs	Mitochondria-derived vesicles
MQC	Mitochondrial quality control
mtDNA	Mitochondrial DNA
OMM	Outer Mitochondrial Membrane
OXPHOS	Oxidative phosphorylation
PD	Parkinson's disease
ROS	Reactive Oxygen Species
RP	Regulatory particle
SMA	Spinal Muscular Atrophy
SNpc	Substantia nigra pars compacta
TCA	Tricarboxylic Acid
Ub	Ubiquitin
UBD	Ubiquitin-binding domain
UPRmt	Mitochondrial unfolded protein response
UPS	Ubiquitin-proteasome system

INTRODUCTION

1.1. Mitochondrial dysfunction in aging and neurodegeneration

Neurodegenerative disorders are one of the most challenging health-related issues in modern society. They are characterized by the progressive degeneration and death of central nervous system cells, which ultimately leads to deterioration in cognitive function (e.g. memory, thinking, orientation, comprehension, calculation, learning capacity, language, and judgement), also defined as dementia[1]. The devastating effects of these diseases have a significant impact not only on the patients' lives but also on those of their families and caregivers. The mental and social burden is combined with the economic one, as the WHO states, "In 2019, the estimated total global societal cost of dementia was US$ 1.3 trillion, and these costs are expected to surpass US$ 2.8 trillion by 2030 as both the number of people living with dementia and care costs increase"[1]. Despite the significant joint effort of the scientific community and many funding organizations, so far, only symptomatic treatments are available for most of these diseases, with only Spinal Muscolar Atrophy (SMA) having a disease-modifying treatment available. This is due to the fact that the pathogenesis and molecular basis of most neurodegenerative disorders remains, to date, unclear. Multiple underlying mechanisms have been proposed; some are specific for each disease and lead to the degeneration of specific subclasses of neurons; others are shared between the different disorders and include mitochondrial dysfunction, neuroinflammation, oxidative stress, and protein aggregation[2,3,22](Figure 1). Among these, impaired mitochondrial function is characterized by decreased ATP production, morphological alterations, and increased release of mitochondrial DNA (mtDNA) and Reactive Oxygen Species (ROS). Altogether, these elements play a pivotal

role by initiating a cascade of interconnected pathogenic mechanisms that leads to neurodegeneration; mitochondrial fission and fragmentation can cause Cytochrome C release and subsequently apoptosis[23], while Reactive Oxygen Species (ROS) accumulation promotes the formation of protein aggregates and triggers the inflammatory response with mitochondrial DNA (mtDNA) release.

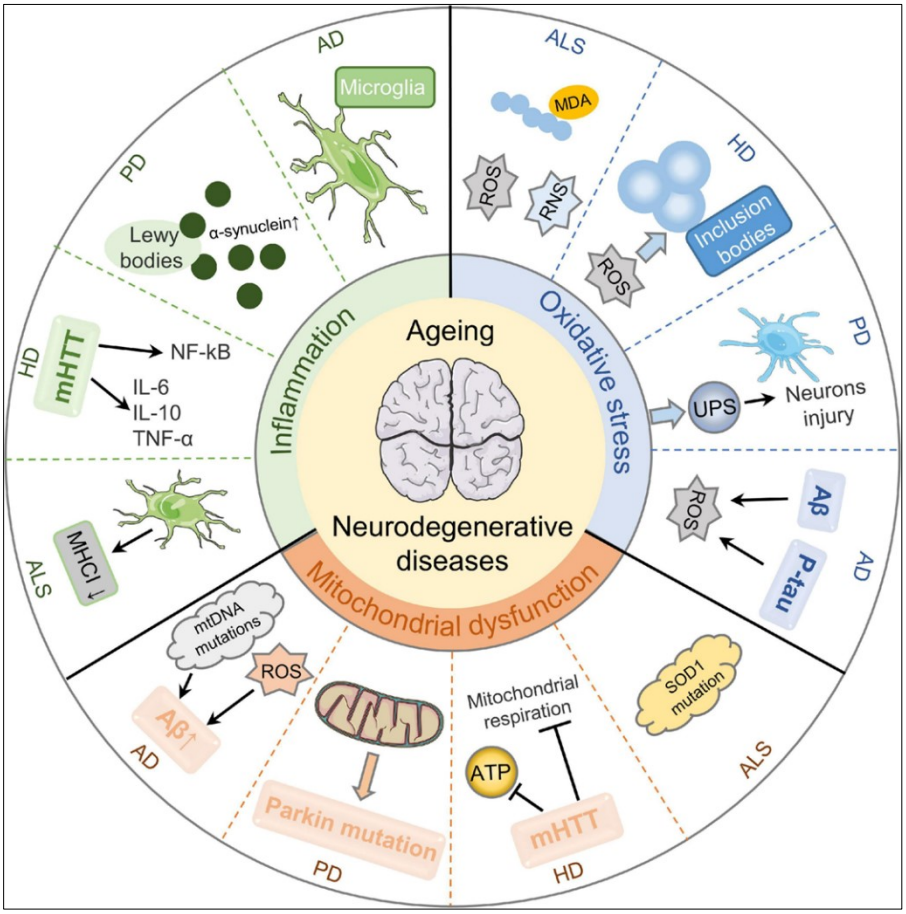

Figure 1. Pathological mechanisms of aging-related neurodegenerative diseases. Mitochondrial dysfunction, oxidative stress, and inflammation are essential cellular and molecular events in the pathogenesis of different aging-related neurodegenerative diseases[210].

To prevent the accumulation of these dysfunctional organelles and the derived detrimental effects, cells usually rely on a series of conserved mitochondrial quality control mechanisms that include mitochondrial dynamics, proteasome system, mitochondria-derived vesicles (MDVs), mitochondrial unfolded protein

response (UPRmt) and mitophagy[4]. However, in recent years, dysregulation of mitophagy has emerged as an important contributor to aging and age-associated disorders. Accumulation of dysfunctional organelles has been observed in several types of cells and tissues during ageing[24,25], and defective mitophagy has been highlighted as the cause of this accumulation, which contributes to neuronal cell death in neurodegenerative diseases[26]. Mitophagy mechanisms and the specific alterations in mitophagy associated with neurodegeneration, Parkinson's disease (PD) in particular, will be reviewed in the following chapters.

1.2. Mitochondria

Mitochondria are essential cellular organelles that, according to the "Endosymbiotic theory," originates from once free-living prokaryotes that became a stable constituent of eukaryotic cells through an endocytic uptake[27]. Thanks to their ability to generate ATP and sustain cell function through the Krebs cycle, they are primarily considered the "powerhouse of the cells"; however, since the '90s many studies have demonstrated that these organelles also play a major role in cell signalling[28]. Accordingly, they are implicated in multiple cellular processes including apoptotic cell death[29,30], autophagy[31], stem cell differentiation[32], and regulation of immune response[33,34]. The functional versatility of mitochondria is reflected by their morphological variability in terms of overall shape (length, width, roundness) and internal ultrastructure. Mitochondria organization in the cells is also highly dynamic, they can be fused together to form a tubular network, but they can also be found as isolated functional organelles. The mitochondrial network undergoes continuous remodeling through fusion and fission events; moreover, the distribution of the network in the cytosol is not casual but tightly regulated in order to match the

local energy demand of the cells[35]. Altogether, these changes in morphology, ultrastructure and distribution are defined as mitochondrial dynamics[28].

1.2.1. Mitochondrial Structure

Mitochondria are separated from the cytoplasm by the outer (OMM) and inner (IMM) mitochondrial membranes. The OMM is a protective lipid bilayer containing many pore-forming membrane proteins (porin) freely traversed by ions and small uncharged molecules[36]. It also hosts proteins fundamental to establish membrane contact sites with other subcellular compartments such as the endoplasmic reticulum (ER)[37,38], lysosomes[39], peroxisomes[40], the plasma membrane[41], and the nucleus[42] as well as with microtubules and other cytoskeletal components[43]. OMM is also crucial for mitochondrial dynamics because it is the resident site for most of the proteins involved in fission and fusion [28]. By contrast, the IMM is a barrier towards ions and molecules that can be crossed only through selective membrane transport proteins specific for individual ions or molecules. This selectivity makes possible the establishment of an electrochemical membrane potential of about 180 mV across the IMM. The formation of this gradient is fundamental to sustain the main function of the IMM, that is the synthesis of ATP through oxidative phosphorylation (OXPHOS)[36]. The IMM separates the inter-membrane space (IMS) from the central matrix and can be divided into two sub compartments: the inner boundary membrane, running parallel to the outer membrane, and the cristae, pleomorphic invaginations of the membrane which contain the majority of the machinery required for mitochondria respiration (electron transport chain complexes and ATP synthase dimers)[44]. At their base cristae are defined by cristae junctions (CJs), tight fissures which separate the content of the cristae from the IMS. The opening of these junctions and the cristae architecture is

regulated by the mitochondrial contact sites and cristae organizing system (MICOS)[45]; cristae tightening ensures the retention of metabolites, protons and ADP to enhance OXPHOS efficiency, on the other hand, following cell death stimuli, CJs widening is observed to promote cytochrome c release from the cristae lumen wherein it is normally sequestered[46–48](Figure 2).

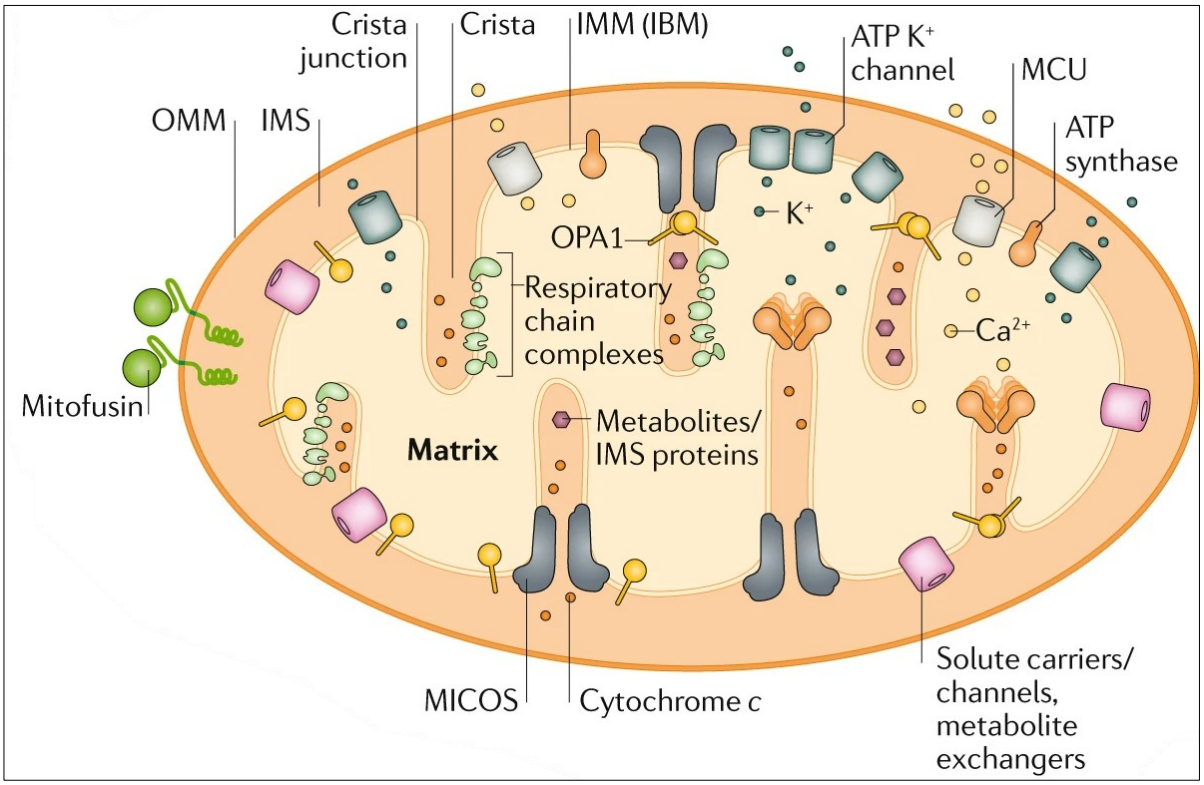

Figure 2. Mitochondrial structure. The mitochondrial lumen (named 'matrix') is surrounded by two membranes: the outer mitochondrial membrane (OMM) and the inner mitochondrial membrane (IMM). The IMM includes two main subcompartments: the inner boundary membrane (IBM) and mitochondrial cristae. Cristae are connected to the IBM via cristae junctions, which are narrow clefts that close the cristae and thereby prevent the contents of the cristae from being released into the intermembrane space (IMS). Cristae shaping depends on the mitochondrial contact site and cristae organizing system (MICOS) and dynamin-related protein optic atrophy protein 1 (OPA1)[28].

1.2.2. Mitochondrial Bioenergetics

Bioenergetics is defined as the study of energy transformations in living systems, and the fundamental issue in bioenergetics is how the energy derived from metabolic pathways is coupled to a cell's energy-requiring reaction; this is accomplished through the conservation of this energy in the form of adenosine triphosphate (ATP), an organic compound considered the "molecular unit of

currency" of intracellular energy transfer. Metabolic pathways can be divided into two types of reactions, which include both the synthesis and degradation of complex macromolecules known respectively as anabolism and catabolism[49]. Mammalian cells catabolism is mainly based on a series of aerobic reactions called Cellular Respiration. Cellular respiration can be divided into three main phases: the first requires the oxidation of organic molecules (i.e. glycolysis, Fatty Acid β-oxidation) to yield acetyl-coenzyme A (Acetyl-CoA) that is fed into the Tricarboxylic Acid (TCA) cycle, during the second phase, to release energy in the form of reduced electron carriers NADH and $FADH_2$, that are finally used by the oxidative phosphorylation to drive ATP synthesis through the electron transport chain[50].

The main players in energy catabolism are mitochondria, where, following glycolysis occurring in the cytosol, Fatty Acid β-oxidation (FAO), TCA cycle, and oxidative phosphorylation take place.

Glycolysis

Glycolysis, also known as the Embden-Meyerhof pathway, is an almost universal and central metabolic pathway for the conversion of glucose into pyruvate and ATP. The conservation of the glycolytic pathway among different species is attributable to the fact that glycolysis does not require oxygen, hence it can be used in anaerobic tissues or organisms, but it is also the first step in aerobic cellular respiration. The breakdown of glucose into two molecules of pyruvate occurs in the cytosol in two phases: an "investment" or preparatory phase and a subsequent "payoff" phase. The first phase requires the use of two ATP molecules, and this initial "investment" results, during the "payoff" phase, in the production of 4 ATP, 2 NADH, and 2 pyruvates per glucose molecule[51]. The ten-step process and the corresponding enzymes are described in Figure 3. The

destiny of the produced molecules of pyruvate depends on the microcellular environment. In erythrocytes (cell lacking mitochondria) or oxygen-deprived tissues, the pyruvate remains in the cytoplasm and is converted into lactate by lactate dehydrogenase, also resulting in the regeneration of NAD+, an oxidizing cofactor necessary to maintain the flow of glucose through glycolysis, and this process is called anaerobic glycolisis[52]. On the contrary, in mitochondria-containing cells, pyruvate, upon oxidation, enters the TCA cycle as Acetyl-CoA and undergoes oxidative phosphorylation (described later). Even if anaerobic glycolysis is much less efficient than oxidative phosphorylation, providing a net production of only 2 ATP per glucose compared to the 32 ATP of OXPHOS, it can still serve as a backup for energy, and it is essential for Acetyl-CoA synthesis in highly oxidative tissues[53].

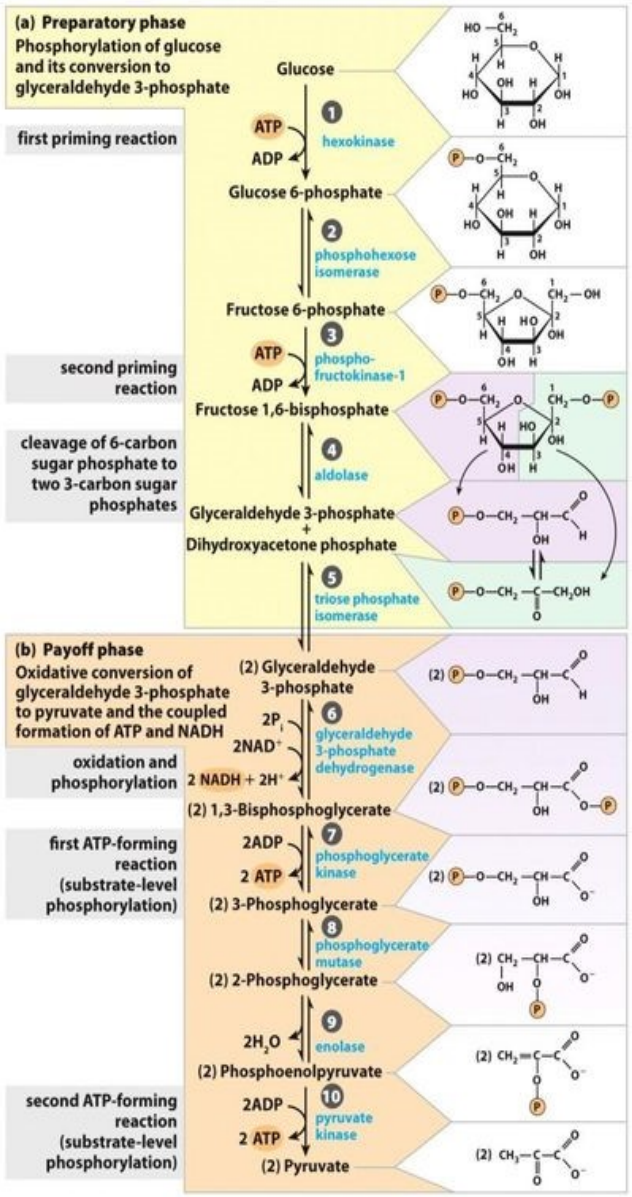

Figure 3. The two phases of glycolysis. For each molecule of glucose (a), two molecules of glyceraldehyde 3-phosphate are formed in the preparatory phase; (b). Pyruvate is the end product of the second phase of glycolysis. For each glucose molecule, two ATP are consumed in the preparatory phase and four ATP are produced in the payoff phase, giving a net yield of two ATP per molecule of glucose converted to pyruvate[50].

Fatty acid β-oxidation

Fatty acids (FAs) are an important source of energy in humans, not only during glucose depletion but also under well-fed conditions. Moreover, thanks to their anhydrous and hydrophobic nature, they allow easier storage in an anhydrous environment and a higher energy yield compared to carbohydrates. Fatty acid β-oxidation (FAO), in parallel with aerobic glycolysis, is a fundamental process in the first phase of cellular respiration and occurs in mitochondria and peroxisomes with a similar mechanism but different enzymes, regulation, and substrates[54]. FAs are "activated" in the cytosol by acyl synthetase with CoA to form Acyl-CoA to pass through the OMM. The enzyme carnitine palmitoyl transferase I (CPT1) catalyzes the transfer of the acyl group of long-chain fatty-Acyl-CoA to a carnitine molecule, releasing the CoA group. The resulting acyl-carnitine can diffuse through the pore of the OMM, reach the IMM, and be transported, via the protein carrier acyl-carnitine translocase, inside the matrix where carnitine palmitoyl transferase II (CPT2) reconverts acyl-carnitine in acyl CoA. Once inside the mitochondrial matrix, FAO can take place through a series of four sequential reactions: dehydrogenation, hydration, dehydrogenation, and thiolase cleavage. Cyclic repetition of these four reactions leads to the complete FAs degradation and the production of Acetyl-CoA, which will fuel the TCA cycle, and NADH and $FADH_2$, utilized as reducing coenzymes in the electron transport chain (ETC)[49].

The TCA Cycle

The TCA cycle, also known as the Krebs cycle, represents the second phase of cellular respiration in which the Acetyl-CoA from different sources (i.e. glycolysis, Fatty Acid β-oxidation) is fed into the TCA cycle and oxidizes to CO_2; the energy resulting from this process is preserved as reduced electron carriers

NADH and $FADH_2$ later used to fuel the OXPHOS and generate ATP. The TCA cycle comprehends a series of eight enzymatic steps, carried out in the mitochondrial matrix, and linking together carbohydrates, fats, and proteins catabolism, with OXPHOS and ETC[55]. Acetyl CoA and oxalacetate are used by the citrate synthase to catalyze the formation of citrate, which is subsequently isomerized by aconitase in isocitrate. The resulting isocitrate undergoes two subsequent reactions of oxidative decarboxylation to generate first alpha-ketoglutarate and second succinyl-CoA, which is then used by succinate thiokinase to form succinate. Succinate dehydrogenase catalyzes the formation of fumarate and generates $FADH_2$. Interestingly this enzyme is integral to Complex II and passes the $FADH_2$ electrons directly into the ETC. Fumarase is then in charge of converting fumarate into malate, which regenerates oxaloacetate by malate dehydrogenase, closing the cycle[49,50]. Each round of the TCA cycle releases energy in the form of GTP that can be converted to ATP or used in protein synthesis and reducing equivalents coenzymes NADH and $FADH_2$, later used in OXPHOS.

OXPHOS and ETC

All the previously described catabolic pathways converge in the final stage of cellular respiration: OXPHOS and ETC. The ETC consists of a series of five protein complexes located in the IMM, the function of which is to transport electrons to the final acceptor: oxygen. To support the complexes, in the IMM there are two electron carriers, coenzyme Q (CoQ) and cytochrome c, to carry electrons from complex to complex[49]. Complex I (NADH dehydrogenase) and Complex II (Succinate dehydrogenase) are the two entry-point for electrons in the ETC, as flavoprotein they can accept electrons respectively from NADH and $FADH_2$ and pass them to Complex III via CoQ. Complex III reduces cytochrome c, which in

turn reduces oxygen to water through Complex IV (Cytochrome c oxidase). Complex I, III and IV use the energy derived from reduced electron carriers (NADH and $FADH_2$) to pump protons from the matrix into the IMS (respectively $4H^+$, $4H^+$ and $2H^+$). Due to the positive charge of the protons, a concentration and pH gradient develops across the membrane, while the depletion of protons in the matrix generates an electrical potential across the membrane, equivalent to ~150-200 mV. The electrochemical gradient created is finally used to propel the conversion of ADP to ATP through Complex V (ATP synthase)[56].

1.2.3. Mitochondrial dynamics, trafficking, and biogenesis: a neuronal perspective

Mitochondrial Dynamics

Mitochondria do not exist as single organelles in cells; they form a highly interconnected network whose dynamics are regulated by the metabolic demands of the cell[57]. Large GTPases regulate mitochondrial dynamics. In particular, Mitofusin 1 and 2 (Mfn1/2), which are expressed on the OMM, coordinate the fusion of OMM by forming trans hetero- and homo-oligomeric complexes[58]. In parallel, IMM-resident protein Optic atrophy 1 (Opa1) regulates IMM fusion and cristae remodelling[28]. Mitochondrial fission is mediated by dynamin-related protein 1 (Drp1). Drp1 is recruited from the cytosol to OMM, where it oligomerizes to form ring-like structures that enclose and constrict the mitochondrion at specific sites, marked by the endoplasmic reticulum (ER), to promote mitochondrial fission[59]. Several dedicated adaptor proteins ("receptors") for Drp1 have been identified on the OMM (such as Fis1, Mff, MiD49, and MiD51), which can mediate Drp1 recruitment to mitochondria and Drp1 docking[60,61]. Coordination of fission and fusion events maintains the shape, ultrastructure, distribution, number, and homeostasis of mitochondria, which is

essential for mitochondrial function. In particular, mitochondrial dynamics are implicated in the propagation of apoptotic signalling, regulate cell proliferation, and are intimately involved in the switch between glycolytic and respiratory energy metabolism, which accompanies the transition between pluripotent and differentiated states[62]. Moreover, elongated mitochondrial morphology is associated with enhanced OXPHOS activity [63] and seems to play a fundamental role in the assembly of respiratory complexes to maximize mitochondrial respiration[46,64]. Conversely, mitochondrial fission is known to promote uncoupled respiration as a means to reduce oxidative stress, which, when elevated, triggers mitochondrial quality control mechanisms to remove damaged mitochondrial components[28]. All these pieces of evidence underline the crucial role of mitochondrial dynamics in the regulation of mitochondrial function. This is particularly relevant for neurons that are post-mitotic, energetically demanding cells due to their limited glycolytic capacity and extremely metabolically active nature. Thus, neuronal cells activity deeply relies on mitochondrial function and this makes them particularly sensitive to alteration in mitochondrial dynamics[65,66]. Not surprisingly, increasing pieces of evidence link disturbed mitochondria dynamics with neurodegenerative disorders like Alzheimer's disease (AD), PD and Huntington's disease (HD)[67–70]. Of note, two groups of human neuropathies, Dominant Optic Atrophy (DOA) and Charcot–Marie–Tooth disease (CMT), have been directly linked to mutations in mitochondrial shaping proteins Mfn2 and Opa1, respectively[71,72], and expression of the dominant negative mutation of Drp1 in humans induces severe neonatal disorder[73,74].

Mitochondrial Trafficking

Mitochondrial trafficking is strictly linked to mitochondrial dynamics, especially in neurons. As highly polarized cells, their function requires mitochondrial

transport from the cell body to the presynaptic terminal[75,76], and mitochondrial fission and fusion are fundamental in the regulation of this process. Not surprisingly, deficiency of mitochondrial fusion and fission regulators such as Drp1, Opa1, Mfn1, Mfn2, and Fis1 or the expression of their respective dominant-negative mutants impairs mitochondrial trafficking, leading to mitochondrial depletion in neurites and synapses, and eventually to dendritic spines and synapsis loss[67]. Aberrant mitochondrial accumulation is often observed in cells body of neuronal models of neurodegeneration[77,78], underlying a significant correlation between mitochondrial dynamics, trafficking, and neurodegenerative diseases. The interplay between dynamics and trafficking suggests that by targeting mitochondrial dynamics, it may be possible to also rescue disrupted mitochondrial trafficking. In support of this notion, in two recent studies, neurons challenged with extracellular Aβ or neurons expressing amyloid precursor protein (APP) displayed mitochondrial trafficking deficits, which were alleviated with overexpression of Drp1[79,80]. Another important component of the mitochondrial transport machinery is Miro1, an OMM protein that attaches to kinesin and dynein motors for microtubule transport[81,82]. Healthy mitochondria are transported from the soma to synapse with the mitochondrial transport machinery consisting of the Miro, Milton, and Kinesin heavy chain complex, whereas, for the retrograde transport, Miro and Milton interact with Dynein[83]. Depletion of this protein causes reduced neuronal survival[84] and has been reported in AD and Amyotrophic lateral sclerosis (ALS) patients[85]. Miro turnover in healthy cells is regulated by PINK1, Parkin, and LRRK2, three proteins (all mutated in familial PD), which identify dysfunctional organelles and promote Miro degradation to promote mitochondrial quality control[86–88]. Accordingly, Miro accumulation has been observed in PD patients[86], and the reduction of Miro in a fly model of PD rescued mitochondrial movement

and the neurodegeneration phenotype[86,89]. Miro is also a fundamental protein regulating mitochondrial Ca2+ homeostasis at the ER-mitochondrial contact sites (ERMCs)[90]. At the ERMCs, Miro interacts with Porin/VDAC and Mfn2, a protein that tethers mitochondria to the ER and a core component of the mitochondrial fusion machinery. At the microtubule/mitochondria contact site, Miro interacts with the microtubule-associated protein Tau, and the knockdown of Miro enhances Tau-induced neurodegeneration[91].

Mitochondrial Biogenesis

The maintenance of a healthy mitochondrial pool is necessary for cellular homeostasis, particularly for neurons, and it is obtained through the balance between interconnected and highly regulated processes: mitochondrial dynamics (fusion and fission), trafficking, *de novo* mitochondrial biogenesis and mitochondrial quality control (MQC) (discussed later)[92]. Mitophagy, one of the best characterized mechanisms of MQC, and biogenesis are two faces of the same coin, that is mitochondrial quality control (MQC), in fact, in physiological conditions, dysfunctional organelles are eliminated through mitophagy, but this needs to be balanced with the creation of new mitochondria to ensure the maintenance of the homeostasis[93]. Not surprisingly, impaired mitochondrial biogenesis contributes to mitochondrial dysfunction and plays a role in the pathogenesis of several neurodegenerative diseases [94–96]. Mitochondrial biogenesis is mostly regulated at the transcriptional level and is dependent on different signalling cascades and transcriptional complexes that promote the formation and assembly of mitochondria[97]. The master regulator of mitochondrial biogenesis is PGC1α, which, once activated (by either phosphorylation or deacetylation), stimulates a series of nuclear transcription factors, including the nuclear respiratory factor-1 and 2(NRF-1/2), estrogen-

related receptor-α (ERR-α), and increases expression of mitochondrial transcription factor A (TFAM), the final effector of mtDNA transcription and replication[98]. In recent years, mitochondrial biogenesis has become an attractive candidate for therapeutic approaches aimed to boost MQC in the context of neurodegeneration; however, only a limited number of studies is available to date[99,100].

1.3. Mitochondrial quality control and mitophagy

Mitochondrial dysfunction has been associated with a broad spectrum of pathologies spanning from rare mitochondrial disorders, consequences of nuclear or mitochondrial DNA mutations, to metabolic and neurodegenerative diseases resulting from ATP deprivation, oxidative stress, and impaired signalling, all signs of mitochondrial damage[101]. Cells have developed sophisticated quality control mechanisms to protect cellular homeostasis from the detrimental effects of defective mitochondria. The best characterized is mitophagy, a form of autophagy able to selectively remove entire mitochondria. Mitophagy, in a physiological context, can be classified as basal, stress-induced, or programmed (Figure 4).

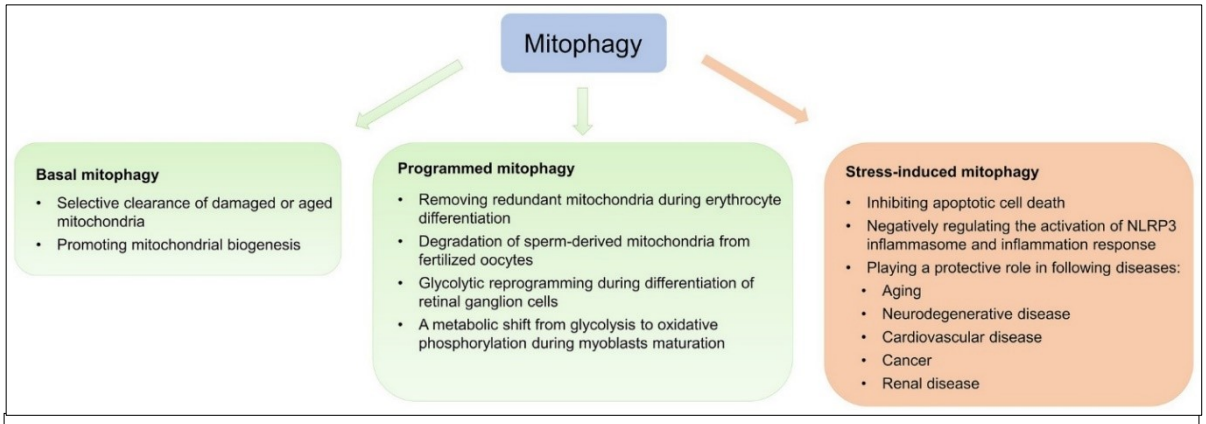

Figure 4. Physiological and pathological effects of mitophagy. Mitophagy is classified as basal, programmed, or stress-induced. Basal mitophagy is essential for routine mitochondrial maintenance. Programmed mitophagy removes redundant mitochondria during differentiation and development. Stress-induced mitophagy occurs under pathological conditions[211].

Basal mitophagy

This class of mitophagy refers to the continuous and constitutive elimination and recycling of old organelles aimed at the maintenance of a healthy mitochondrial population. The contribution of basal mitophagy *in vivo* has not been completely clarified yet; indeed, until recently, the majority of the studies were based on stimulus-induced mitophagy *in vitro*[9]. A fundamental breakthrough in this field has been the generation by the Ganley and Finkel laboratories of two reporter mouse lines: mitoQC and mtKeima. Both transgenic mice showed that basal mitophagy is active in most cells, and it is highly heterogeneous between tissues and cell types. For example, highly energetic compartments such as the heart, skeletal muscle, nervous system, and hepatic and renal tissue exhibit higher levels of basal mitophagy compared to the spleen and thymus[102,103]. Interestingly, different studies in mouse and fly models have established that basal mitophagy is independent of the PINK1-Parkin pathway [104,105](discussed later), suggesting that there are other mechanisms, yet to be unraveled, that drive basal mitophagy in a tissue/cell-specific manner.

Stress-induced mitophagy

Under stressful conditions, mitophagy has a double function: to mediate the metabolic rewiring necessary for the cells to adapt their metabolism in response to a challenging environment and to eliminate dysfunctional mitochondria to avoid the accumulation of defective organelles, which might turn into an additional source of stress[103]. Stress-induced mitophagy is strongly activated upon treatment with mitochondrial uncouplers (e.g. carbonyl cyanide m-chlorophenylhydrazone- CCCP)[106], oxidative stress (e.g. H_2O_2, rotenone) [107], or alternatively during starvation or hypoxia[108,109]. Interestingly, in yeast, mitophagy is selectively induced under starvation depending on the available

carbon source. This mechanism is Atg32-dependent and, more importantly, is distinct from bulk autophagy[108]. However, *in vivo* studies in mice reveal that even though mitochondria can be eliminated by starvation-induced autophagy, they do not appear to be the selectively targeted[104].

Programmed mitophagy

Mitophagy is fundamental to remove redundant mitochondria during development and differentiation. In early embryogenesis, upon fertilization, paternal mitochondria are selectively removed from fertilized oocytes preventing paternal mtDNA inheritance[110,111]. Moreover, during erythrocyte differentiation, NIX-dependent mitophagy is activated to achieve the complete removal of mitochondria, a typical characteristic of mature red blood cells in most mammalians[107]. During differentiation, programmed mitophagy drives the metabolic switch necessary to meet specific cells' energy demands. Stemness is maintained through a specific set of mitochondrial characteristics which are defined as “metabolic stemness” and include: low mitochondria abundance, underdeveloped ultrastructure, low network complexity, reduced membrane potential, and low ROS emission[112]. It is now clear that to differentiate, stem cells need to undergo complete mitochondrial ultrastructure and metabolic remodeling to support the specific needs of terminally differentiated cells. In line with this statement, increased mitophagy has been observed in different models of cell differentiation such as neurons[113], Retinal Ganglion cells (RGCs)[114], myoblast[115], and Cardiac Progenitor cells (CPCs)[116].

Mechanistically, mitophagy involves a series of elaborated processes that can be summarized in three steps: (1) isolation of excess or damaged mitochondria from the mitochondrial network, (2) priming with an “eat me” signal for recognition by the autophagy machinery, (3) autophagosome engulfment of the

primed mitochondria, and delivery to the lysosome for degradation. Depending on the nature of the "eat me" signal attached to the mitochondria, mitophagy pathways can be divided into ubiquitin-dependent or -independent[117] (Figure 5).

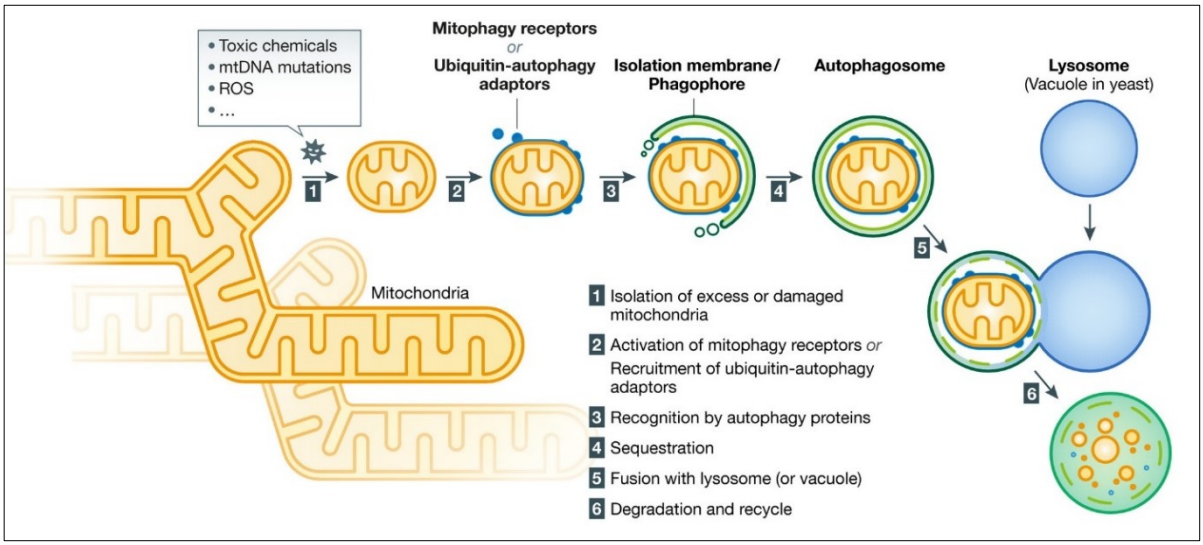

Figure 5. Mitophagy steps: (1) Intra- and extracellular cues promote isolation of excess or damaged mitochondria via fragmentation of the tubular network. (2) Mitophagy receptors or ubiquitin–autophagy adaptors that confer selectivity for degradation are recruited and/or activated on the surface of mitochondria. (3) Core autophagy-related proteins target to mitochondria and generate the isolation membrane/phagophore surrounding mitochondria. (4) Targeted mitochondria are enclosed and sequestrated by autophagosomes. (5) Autophagosomes are transported and fused with lytic compartments such as vacuoles in yeast or lysosomes in mammals. (6) Lysosomal or vacuolar acidic hydrolases flow into autophagosomes to degrade mitochondria, and the contents will be recycled[117].

1.3.1. Ubiquitin-dependent mitophagy

PINK1-Parkin pathway

The discovery of the PINK1-Parkin pathway carried out in Youle's and Tanaka's lab represents one of the milestones in the study of mitophagy, and for this reason, it is also one of the best characterized mechanisms[118–120]. The main actors in this pathway are the mitochondrial serine/threonine protein kinase, PINK1, and the cytosolic E3 ubiquitin ligase, Parkin. Briefly, in functional mitochondria, PINK1 is imported in the IMM through mitochondrial translocases

(TOM and TIM complexes) and is subsequently cleaved by several proteases and released into the cytosol to be degraded by the proteasome. Following a mitophagy stimulus (e.g. membrane depolarization), PINK1 is stabilized on the OMM where it is activated through autophosphorylation; once activated, PINK1 induces Parkin translocation on the OMM and induces its ubiquitin (Ub) E3-ligase activity by phosphorylating Parkin itself or phosphorylating pre-existing ubiquitin chains on OMM proteins (pSer65-Ub). In both scenarios, Parkin ubiquitinates OMM proteins creating new substrates for PINK1 phosphorylation, thereby creating a feedforward mechanism that amplifies mitophagy signals[121]. The ubiquitin chains formed by Parkin in the OMM display linkage types typical of both autophagy and proteasomal degradation. Ubiquitination of OMM proteins Mfn1/2, Miro1/2, VDAC, and TOMs leads to their chaperone p97/VCP-mediated extraction from OMM for proteasomal degradation[122,123]. Mfn1/2 removal abolishes mitochondrial fusion supporting the isolation of defective organelles from the healthy mitochondrial network, while degradation of Miro, a Rho–GTPase that anchors mitochondria to the cytoskeleton, inhibits mitochondrial transport; both mechanisms contribute to mitophagy execution[124]. Parkin-mediated ubiquitination can also trigger the recruitment of autophagic cargo receptors, such as optineurin (OPTN), p62, AMBRA1, TAX1BP1, and NDP52 on the OMM. These receptors possess a ubiquitin-binding domain (UBD), through which they bind ubiquitinated-OMM proteins, and an LC3-interacting region (LIR) able to recruit the Microtubule Associated Protein-Light Chain 3 (LC3) that is localized on the autophagosome membranes, thus enabling the delivery of mitochondria to autophagosome for degradation[8]. Even though it is the most studied mitophagy pathway, several studies have started to question its relevance in a physiological context (previously discussed). Therefore, recently many researchers have focused on

the identification of alternative pathways that are Ub-dependent but Parkin-independent (Figure 6).

Parkin-independent pathways

Several other ubiquitin E3 ligases, such as Gp78, SMURF1, SIAH1, MUL1, and ARIH1, have been identified as mitophagy regulators in pathways that act alternatively or in parallel to the PINK1-Parkin pathway. Their mechanism of action is similar to the one of Parkin: they generate ubiquitin chains on the OMM that trigger the recruitment of the already mentioned autophagy adaptors (e.g. OPTN, NDP52, and p62), which in turn bind to LC3 to promote the formation of the autophagosome around the mitochondria. MUL1, in particular, is a multifunctional protein anchored on the OMM and, thanks to its dual function, ubiquitination and sumoylation, regulates several biological processes such as mitochondrial dynamics and mitophagy. Several different mechanisms for MUL1-mediated mitophagy have been proposed, but they still lack consensus. MUL1 ubiquitinates mitochondrial fusion protein Mfn2, enhancing its degradation through the UPS and resulting in fragmented mitochondrial morphology, one of the prerequisites for mitophagy[125]. This capacity to regulate Mfn2 levels has also been suggested as a mitophagy-inducing mechanism in MEFs cells treated with CCCP[126]. Another indication that MUL1 is involved in mitophagy regulation comes from an *in vivo* study in Drosophila, in which they show that MUL1-mediated Mfn2 degradation suppresses PINK1 and Parkin-mutants phenotypes, thus suggesting that this pathway works in parallel or as an alternative to the PINK1/Parkin canonical pathway[126] (Figure 6).

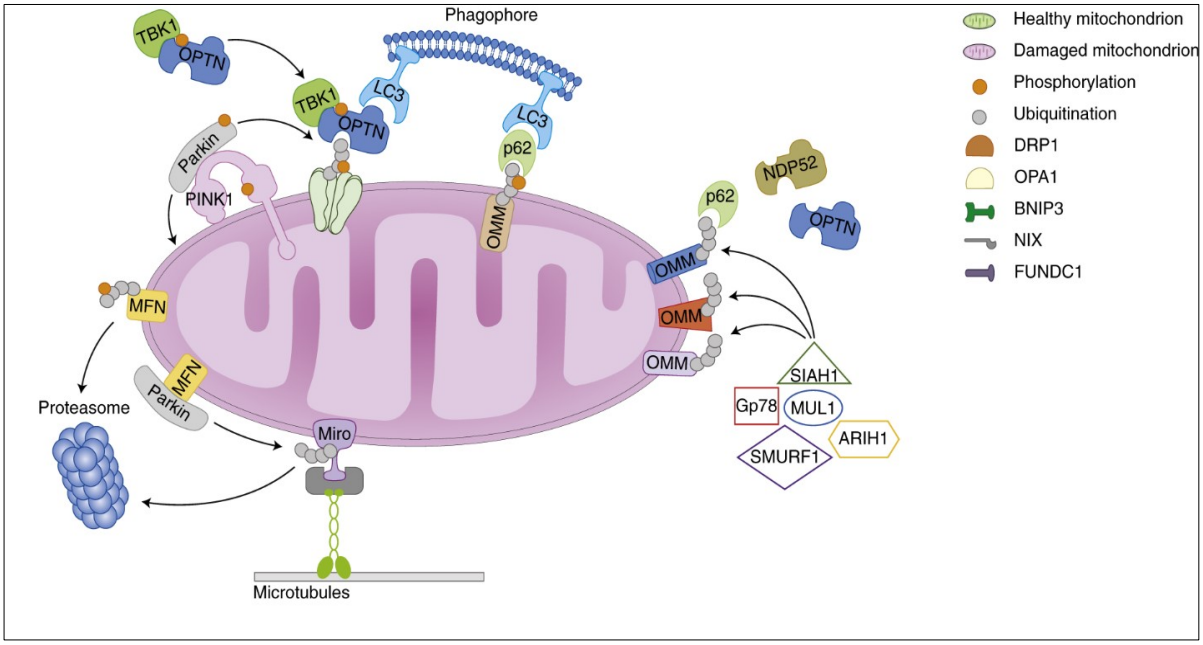

Figure 6. Ubiquitin-dependent mitophagy. Following stress, PINK1 is stabilized on the OMM, promoting Parkin recruitment. Parkin ubiquitinates several outer membrane components. Poly-Ub chains are subsequently phosphorylated by PINK1 serving as an "eat me" signal for the autophagic machinery. Adaptor proteins (p62, OPTN, NDP52) recognize phosphorylated poly-Ub chains on mitochondrial proteins and initiate autophagosome formation through binding with LC3. TBK1 phosphorylates OPTN, thereby enhancing its binding affinity to Ub chains. The OPTN–TBK1 complex establishes a feed-forward mechanism promoting mitochondrial clearance. Gp78, SMURF1, MUL1, SIAH1 and ARIH1 represent alternative E3 ubiquitin ligases targeting OMM proteins prior to mitophagy. The PINK1–Parkin pathway modulates mitochondrial dynamics and motility by targeting MFN and Miro for proteasomal degradation[124].

1.3.2. Ubiquitin-independent/receptor-mediated mitophagy

Some mitochondrial proteins can act as mitophagy receptors without the need for Ub chains to attract autophagic cargo proteins. These proteins are mostly located on the OMM and have their own LIR motifs through which they are able to directly interact with LC3 and GABARAP autophagosomal membrane proteins[8]. Receptor-based mitophagy is regulated by transcriptional or post-transcriptional modification, and unlike the PINK1/Parkin pathway, it seems to be most active in basal conditions and in response to chronic stress[127]. The first mitophagy receptor characterized was BCL-2-like protein 13 (BCL2L13), the mammalian homolog of the Atg32 protein in yeast. BCL2L13 mediates both mitophagy and mitochondrial fragmentation in a Parkin-independent

manner[128]. Other OMM mitophagy receptors are available in response to a plethora of stimuli. NIX (NIP3-like protein or BNIP3L) controls programmed mitochondrial degradation during differentiation[113]. It shares 56% amino acid content with another receptor, BH3-domain containing protein (BNIP3), and they are both under the transcriptional regulation of hypoxia-inducible factor 1 (HIF1), which increases their expression upon a hypoxic stimulus to induce mitophagy[129]. The activation of both these proteins requires phosphorylation of the LIR domain by different kinases to stimulate the autophagosome recruitment on the targeted mitochondria[130,131]. Interestingly, NIX and BNIP3 have been shown to participate in the PINK1/Parkin pathway by promoting the accumulation of these proteins on damaged mitochondria and facilitating mitophagy[132,133], thus highlighting the crosstalk that takes place between different mitophagy pathways. Another important OMM mitophagy receptor is the FUN14 domain containing 1 (FUNDC1); like NIX and BNIP3, it is activated during hypoxic-induced mitophagy, but unlike them, it is not overexpressed in response to the stimuli. FUNDC1 activity is modulated through a series of phosphorylation/dephosphorylation reactions to switch from the inactive to the active state[134,135]. Moreover, its activity is also controlled by the mitochondrial E3 ubiquitin ligase MARCH5 (or MITOL), which enhances proteasomal degradation of FUNDC1 to inhibit hypoxia-induced mitophagy[136]. Besides its function in FUNDC1 regulation, MARCH5 seems to play a role in the PINK1/Parkin mitophagy pathway, in response to mitochondria depolarization. In particular, MARCH5-mediated ubiquitination of OMM proteins might function as a "seed" for PINK1 phosphorylation and Parkin recruitment to initiate their feedforward mechanism in the initiation of mitophagy[137]. Another study demonstrated that MARCH5 promotes the degradation of Mfn2 to induce mitochondrial fission and mitophagy in melanoma cells [137], further confirming a possible function in the regulation of alternative mitophagy pathways. However, studies on the mechanism of action of MARCH5 in the control of mitochondrial dynamics, mitophagy, and apoptosis are very contradictory,

with evidence pointing in all directions. Therefore, further studies are needed to clarify MARCH5 role in all these different pathways[138] (Figure 7).

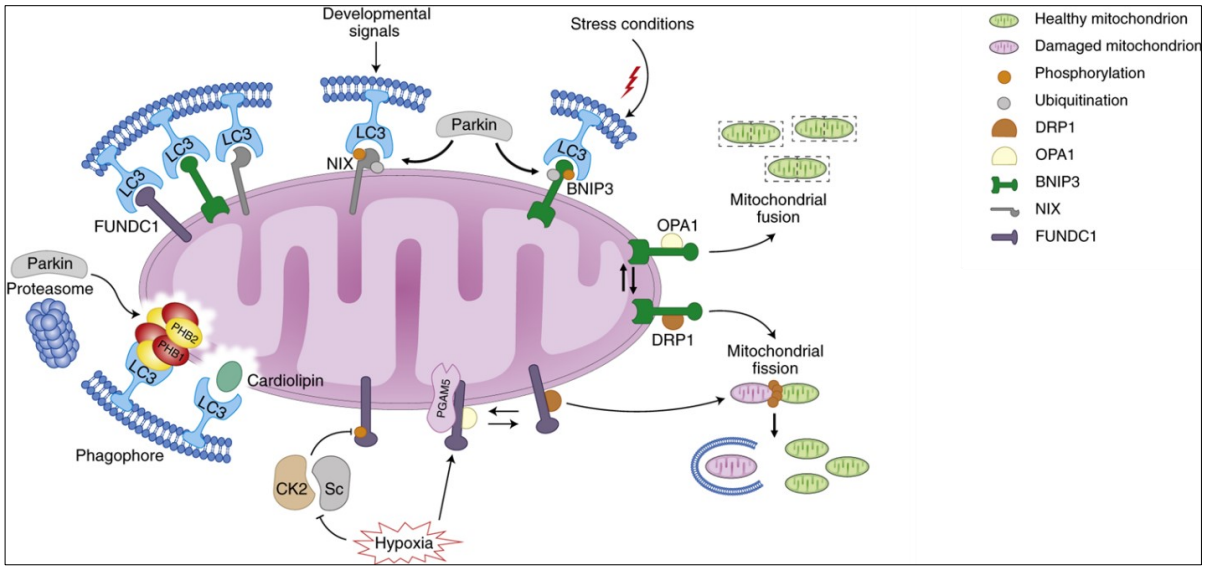

Figure 7. Ubiquitin-independent/Receptor-mediated mitophagy. BNIP3, NIX and FUNDC1 mitophagy receptors localize to the OMM and interact directly with LC3 to mediate mitochondrial elimination. PHB2 and cardiolipin are externalized to OMM and interact with LC3 following mitochondrial impairment. Different receptors ensure specificity of the process in different tissues and following diverse stimuli. NIX and BNIP3 phosphorylation enhances their association with LC3. Mitophagy receptors promote fission of damaged organelles through the disassembly and release of OPA1, and the recruitment of DRP1 on the mitochondrial surface. Parkin-dependent ubiquitination of NIX and BNIP3 highlights an intricate crosstalk between receptor-mediated mitophagy and the PINK1–Parkin pathway[124].

1.4. Ubiquitin Proteasome System and Autophagy: the two sides of quality control in cells

The two main quality control systems for proteins and organelles in cells are the ubiquitin-proteasome system (UPS) and autophagy. These two pathways crosstalk with each other to maintain cellular homeostasis through the detection and degradation of aggregated proteins and dysfunctional organelles. Ubiquitin is an important signalling protein in both these pathways; it is a small 8,5 kDa protein covalently attached to lysine (Lys) residues of other proteins to modulate their fate. Ubiquitin contains 7 Lys residues, each of which can bind

other ubiquitin, forming Ub chains[7]. Based on how the different blocks of the chain are connected, different types of chains (linear, branched, mixed) can be formed. Effector proteins specifically recognize the different chains leading to different outcomes: K48 and K11 chains are specific for proteasomal degradation, while K6, K27, K33, and K63 are devoted to signal transduction[10]. Protein ubiquitination is a dynamic and reversible process controlled by two types of enzymes: Ub-ligase and Deubiquitinating enzymes (DUBs). Three types of ligase participate in the conjugation process E1, E2, and E3 ligases. Ub is activated by an E1 enzyme and then is transferred to the E2 active site forming an E2-Ub intermediate; finally, an E3 ligase binds to both the E2-Ub and the substrate catalyzing the transfer of Ub on it[139]. The number of E1 and E2 enzymes is limited in humans, while over 600 E3 Ub ligases have been described allowing substrate and cell type specificity[140]. On the other hand, DUBs ensure the reversibility of the ubiquitination process, catalyzing the reaction of removal of Ub chains from the substrates. The eukaryotic 26S proteasome is a large multi-subunit complex composed of two subcomplexes called 20S core particle (CP) and 19S regulatory particle (RP). The CP it is a conserved barrel-shaped cylinder where proteolytic degradation of proteins occurs, whereas the RPs complexes are positioned on both sides of the CP barrel and are crucial for substrate recognition; many different RP complexes exist, but their specific function is still unknown[141]. Substrate size is the limiting factor for the UPS activity, in fact, only soluble unfolded polypeptides can enter the proteasome channel for degradation. Bigger structures, such as protein aggregates or entire organelles, are processed through the autophagic pathway. Autophagy is a cellular degradation pathway, which consists in the formation of a double membrane structure, called autophagosome, around the target cargo which is subsequently fused with lysosome resulting in the hydrolyzation of their content

and release of the single components in the cytosol for recycling[8]. The link where the crosstalk between the UPS and autophagy occurs is represented by the previously described autophagic receptors (e.g. p62/SQSTM1, NBR1, NDP52, OPTN, and TAX1BP1). Components of the autophagic machinery are able to directly recognize their LIR motifs, while they conjugate to Ub protein aggregates or Ub proteins on organelles surface through their UBD[6] (Figure 8).

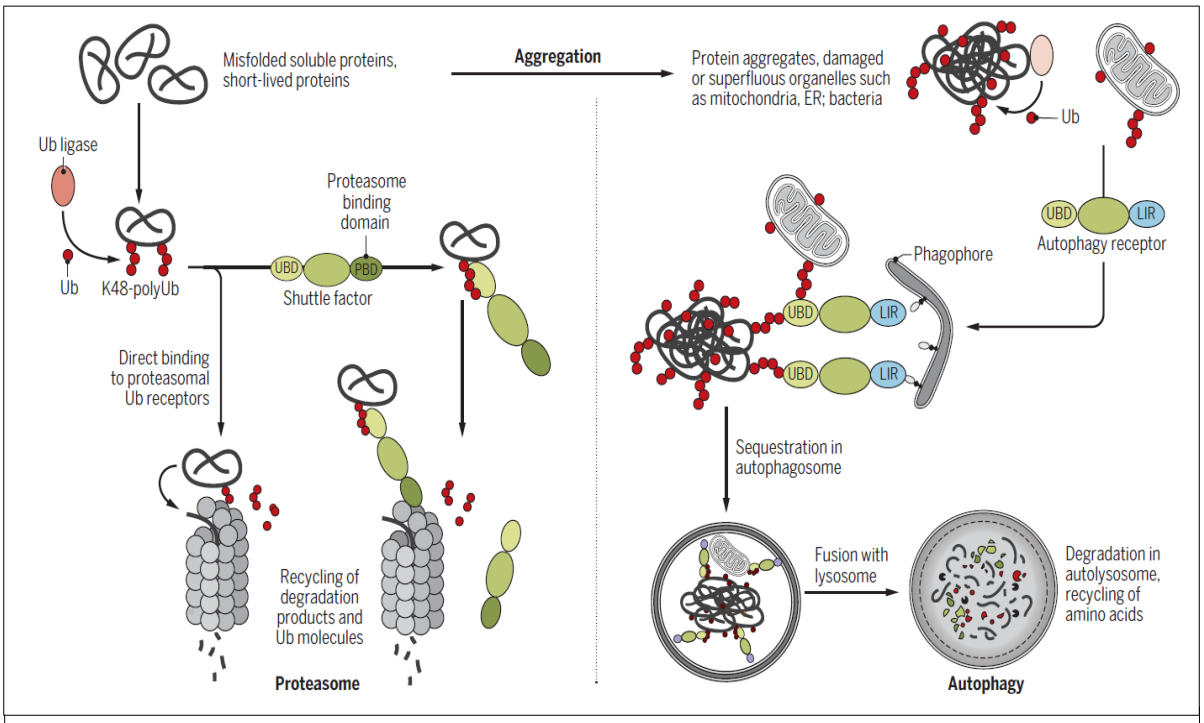

Figure 8. Overview and comparison between the UPS and autophagy. Left: The UPS is characterized by the strong dependence on Ub as a degradation signal and its degradation capacity is limited by the substrates size. Soluble single proteins are polyubiquitinated in an inducible and reversible manner. Poly-Ub chains on the substrates are recognized either by intrinsic Ub receptors of the proteasome or shuttle factors that are equipped with both an ubiquitin binding domain (UBD) and a domain that binds to the proteasome. Right: Selective autophagy is able to degrade large and heterogeneous cytosolic material, including aggregated proteins, organelles, bacteria, and molecular machines. Substrate labels recognized by the autophagic machinery are more diverse and include Ub, lipid-based signals, or organelle-intrinsic autophagy receptors that become exposed to the cytosol. A growing phagophore engulfs autophagic cargo that is connected to the ATG8/LC3-decorated membrane via LIR motif–containing autophagy receptors. Eventually, the phagophore closes around the cargo to give rise to the autophagosome that finally fuses with the lysosome[6].

Decreased functioning of cellular quality control pathways is typical in aging, and it is one of the causes of the onset of neurodegenerative diseases like AD, PD,

and ALS, characterized by the accumulation of mutated, aggregated proteins and dysfunctional organelles (e.g. mitochondria). Therefore, these pathways are becoming prominent therapeutic targets in the neurodegeneration field.

1.5. Mitophagy in neurodegenerative disease: a focus on PD

It has already been discussed how a strict association exists between the aging process and the onset and spreading of mitochondria dysfunction, in particular in the brain. The aberrant accumulation of these dysfunctional organelles is usually kept under control by different mechanisms of MQC that have been described in the previous chapter. However, in recent years many studies have highlighted how the pathogenesis of neurodegenerative diseases is correlated with an inefficient clearance of dysfunctional mitochondria leading to their accumulation. Due to their high-energy requirements and post-mitotic nature, neurons are particularly vulnerable to the disruption of cell homeostasis, with the accumulation of aggregated proteins or dysfunctional organelles being the main cause of neuronal cell death and contributing to the pathogenesis of neurodegenerative diseases.

Alzheimer's Disease (AD)

AD is the most common neurodegenerative disease; the main symptoms are severe memory loss and cognitive disorders. It is characterized by intracellular accumulation of hyper-phosphorylated Tau protein (pTAU) and extracellular amyloid β plaque[142]. Defective mitophagy and accumulation of dysfunctional mitochondria have been shown in post-mortem tissues of AD patients and in neurons derived from induced pluripotent stem cells (iPSCs) of AD patients[143]. Moreover, the autophagic/lysosomal/endosomal system is affected in AD as described by ultrastructural analysis of AD post-mortem brains in which neurons

exhibit depleted lysosomes and accumulation of autophagosomes[144]. This is accompanied by a decreased expression of transcription factor EB (TFEB), the main transcriptional regulator of lysosome biogenesis and autophagy[145]. Recently some groups have found a connection between AD and Parkin-dependent mitophagy. In particular, they proposed that in Tau overexpressing cells Parkin recruitment on the OMM is hindered through different mechanisms. Importantly, Parkin overexpression seems to be sufficient to prevent mitophagy deficits in several models of neurodegeneration[146,147]. It is still unclear if impairment of mitophagy is an early event or a consequence of Tau pathology in AD; however, data derived from clinical studies indicate that pharmacological enhancement of mitophagy rescues cognitive deficit in worm and mouse models of AD[5,143].

Amyotrophic Lateral Sclerosis (ALS)

ALS is characterized by the selective degeneration of motor neurons. Clinically, it manifests mainly at the level of motor function (weakness and atrophy). Similarly to AD, ALS is characterized by the accumulation of aggregated proteins, the main components of these aggregates are superoxide dismutase 1 (SOD1), TDP43, and fused in sarcoma (FUS)[148]. Studies on genetic forms of ALS have identified the link with several genes related to MQC, such as the mitophagy receptors OPTN and p62. Accordingly, *in vitro* studies demonstrated that ALS-linked mutations in the previously mentioned genes affect selective autophagy, thereby contributing to the accumulation of defective mitochondria[149].

Parkinson's Disease (PD)

PD is the second most common neurodegenerative disease after AD; clinical manifestation can be divided into motor and non-motor symptoms. The most common motor symptoms are bradykinesia, resting tremors, rigidity, and

postural instability. These manifestations of the disease usually appear later in the life of the patient when the neurodegenerative process is already at an advanced stage[150]. Conversely, non-motor symptoms, such as depression, sleep deprivation, olfactory impairment, constipation, and cognitive deterioration, may develop years before the onset of the typical motor symptoms and are classified as premotor or prodromal phase of PD. These symptoms have an adverse effect on patient's well-being; therefore, early diagnosis and treatment of prodromal symptoms have the potential to improve the quality of life of PD patients and allow more effective neuroprotective therapies[151]. The most common neuropathological features of PD are the selective loss of dopaminergic neurons in the substantia nigra pars compacta (SNpc) and the presence of intracellular protein aggregates called Lewy bodies and Lewy neurite. The main component of Lewy bodies (LB) is an abnormal, post-translationally modified, and aggregated form of the presynaptic protein alpha-synuclein (α-syn). In addition to LB pathology, PD patients exhibit the selective loss of dopaminergic neurons in the SNpc that leads to the decrease of dopamine levels in the striatum. Dopamine loss is recognized as the main cause of the motor dysfunction underlying PD[150]. Over the past years, a wide range of evidence has suggested that mitochondrial dysfunction plays a pivotal role in PD pathogenesis. The first evidence came from the observation that mitochondrial complex I inhibitors (e.g. MPTP, rotenone, paraquat) administered to rhesus monkeys and mice induce selective death of DA neurons and PD-like phenotypes[152]. Another important lead that connects PD with mitochondrial dysfunction and defective MQC is the fact that among the genes identified as causative of autosomal recessive forms of PD are PARK2 and PARK6, encoding for Parkin and PINK1, respectively, the two main players in the PINK1/Parkin mitophagy pathway, as described above[153]. The role of this pathway *in vivo*

remains controversial; basal mitophagy seems to be independent of PINK1/Parkin, which mostly acts in response to mitochondrial stress. These findings are in line with the fact that most PINK1 KO and Parkin KO mouse models do not recapitulate PD phenotype unless they are triggered by stress stimuli such as exhaustive exercise or increased mtDNA damage[154]. Importantly, PINK1 and Parkin also regulate other aspects of mitochondrial homeostasis, such as mitochondrial dynamics and biogenesis. Both PINK1 and Parkin promote UPS degradation of fusion proteins Mfn1/2, while PINK1 promotes mitochondrial fission by recruiting DRP1 to mitochondria[155]. Parkin also regulates PARIS (Parkin Interacting Substrate, ZNF746) degradation. Parkin deficiency leads to the accumulation of PARIS, which acts as a repressor of peroxisome proliferator-activated receptor gamma coactivator 1-alpha (PGC-1α), a key transcriptional regulator of mitochondrial biogenesis[95,156]. Other genes, correlated with genetic forms of PD, translate into proteins involved in mitochondrial maintenance; some examples are α-synuclein, which leads to complex I deficiency and interacts with the mitochondrial protein import machinery; DJ-1, a pro-survival protein which prevents neuronal death induced by oxidative stress, and leucine-rich repeat kinase 2 (LRRK2), which potentiates the pro-fission activity of DRP1[157].

1.6. Enhancing mitophagy as a therapeutic approach for neurodegenerative diseases

Taken together, the pieces of evidence discussed so far demonstrate that mitochondrial dysfunctions and impaired MQC are common features in many neurodegenerative disorders. Thus, the discovery of small molecules or chemicals able to selectively enhance mitophagy holds an outstanding clinical interest in the neurodegeneration field.

1.6.1. Mitophagy inducers

Several mitophagy inducers have been discovered to date with promising results regarding neuronal protection and increased healthspan in animal models and human cell lines. In a recent paper, Fang et al. demonstrated that mitophagy-inducers such as urolithin A(UA), actinonin (AC), and nicotinamide mononucleotide (NMN), a NAD^+ precursor, were able to ameliorate cognitive decline in *C.elegans* and in a mouse model of AD[143]. Moreover, treatment with another NAD^+ precursor, nicotinamide riboside (NR), rescued mitochondrial defects and dopaminergic neuronal loss in iPSC and fly models of PD[158]. Interestingly, clinical trials for these small molecules demonstrated that UA and NR are orally bioavailable and safe[159,160]. Additional clinical trials are ongoing to assess the effects of NR on brain function, cognition, and memory in people diagnosed with mild cognitive impairment (MCI) (NTC02942888 and NTC03482167). Other promising compounds are rapamycin and metformin, two FDA-approved mTOR inhibitors well known to stimulate autophagy. These molecules exhibit anticancer and antiaging properties and have been correlated with Parkin-mediated mitophagy[161–163]. However, additional studies are required to uncover the underlying mechanism of mitophagy activation and to understand their applicability in the context of neurodegenerative diseases.

1.6.2. Deubiquitinating enzymes (DUBs)

As described in previous chapters, the ubiquitin-dependent mitophagy pathways rely on E3 ubiquitin ligases to mediate poly-ubiquitination of OMM proteins leading to their recognition by autophagy adaptors or their proteasomal degradation. This process can be counteracted by deubiquitinating enzymes (DUBs), which can eliminate ubiquitin chains from the mitochondrial surface. Essentially, mitochondrial homeostasis seems to be regulated by a

balance between ubiquitination and deubiquitination events, with poly-Ub functioning as an “eat-me” signal for damaged organelles[124]. In this context, the regulation of DUBs activity represents a promising target for therapeutic intervention aimed at increasing mitophagy and mitochondrial turnover. Recent works identified several DUBs involved in the modulation of ubiquitin-dependent mitophagy, such as ataxin-3, USP14, USP15, USP30, and USP35 [19,21,164–166](Figure 9).

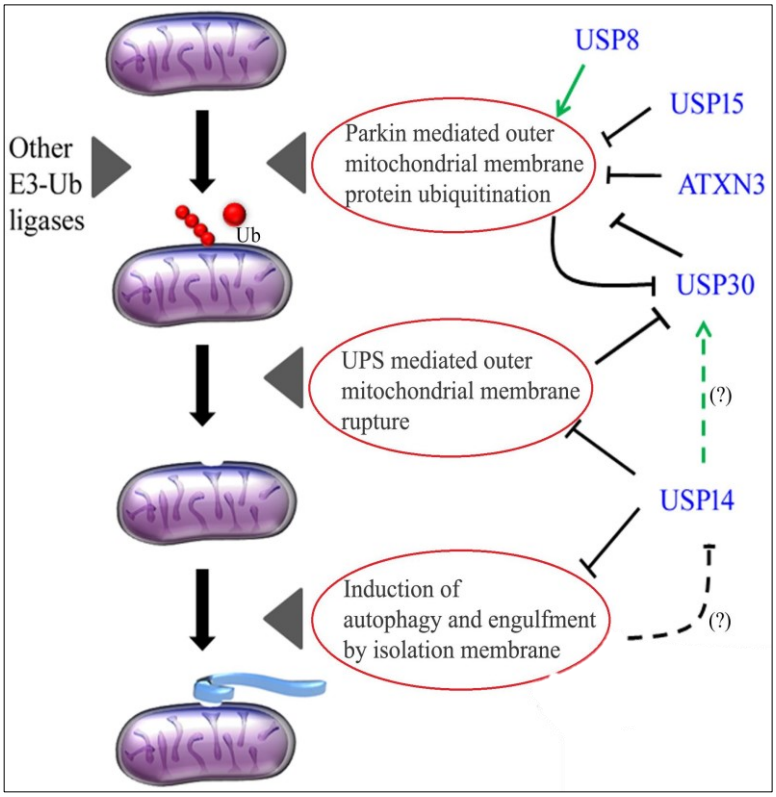

Figure 9. DUBs in the regulation of mitophagy. USP8 positively regulates Parkin mitochondrial recruitment and mitophagy, whereas USP15, ATXN3, and USP30 negatively impact Parkin activity. Parkin has in turn a negative feedback loop on USP30. USP14 can tune the ubiquitin proteasome system (UPS) as well as autophagy. It is yet to be demonstrated whether USP14 stability can be regulated by autophagy in a negative feedback loop (?), and whether USP14 can impact USP30 stability (?). Green arrows indicate positive impact while blunt lines indicate negative / antagonizing feedback[183].

These DUBs act with different mechanisms enhancing mitophagy under basal or depolarized conditions, suggesting an intricate crosstalk between different DUBs and E3 ubiquitin ligases that might also be cell-specific. Currently, studies to develop DUBs inhibitor are ongoing, however, due to their similarity in terms of sequence and structure, finding specific inhibitors have proven to be challenging. Despite the complexity of the task, some groups were able to

identify small molecules able to regulate DUBs catalytic activity. USP30 is one of the most characterized mitochondrial anchored DUB, which is able to inhibit Parkin-dependent mitophagy[167,168]. In the last years, thanks to an increased interest in DUBs inhibitors, a few promising small molecules targeting USP30 were identified. One example is MF-094, identified with an *in vitro* study, this compound selectively inhibits USP30 with an IC_{50} of 0,12 µM and has been shown to accelerate mitophagy in C2C12 cells[169]. More recently, another similar compound was synthesized from the same lab and proved to be efficient in restoring mitophagy levels in dopaminergic neurons generated from iPSCs derived from PD patients carrying Parking mutations[170]. Finally, a peptide (Q14) derived from the transmembrane domain of USP30 was reported to inhibit USP30 with nanomolar IC_{50} values and to induce mitophagy in A172 cells[170]. Another promising DUB in the context of neurodegenerative diseases and MQC is USP14. The best known inhibitor available for this DUB is IU1, which inhibits USP14 with an IC_{50} of 4-5 µM[14](Figure 10A). Interestingly it was reported that IU1 promotes basal mitophagy in SH-Sy5y cells and fibroblasts from PD patients. Moreover, IU1 inhibition of USP14 *in vivo* corrected mitochondria dysfunction and locomotion impairment of PINK1/Parkin *D. melanogaster* models of PD[19]. The need for even more specific inhibitors has recently led to the discovery of a new potent USP14 inhibitor, IU1-47, an IU1-derivative tenfold more potent and with lower IC_{50} (0,6 µM)[171], orally bioavailable and able to cross the Blood Brain Barrier (Figure 10B). IU1-47 was tested on murine primary neurons and neurons derived from iPSCs, where it accelerates the degradation of the microtubule-associated protein Tau, which accumulation is implicated in many neurodegenerative diseases[18]. Studies evaluating the effect of USP14 inhibition on mitophagy in neuronal models of neurodegeneration are still lacking, for this

reason in our lab we are focusing on dissecting the role of USP14 inhibition on MQC using iNeurons generated from human embryonic stem cells.

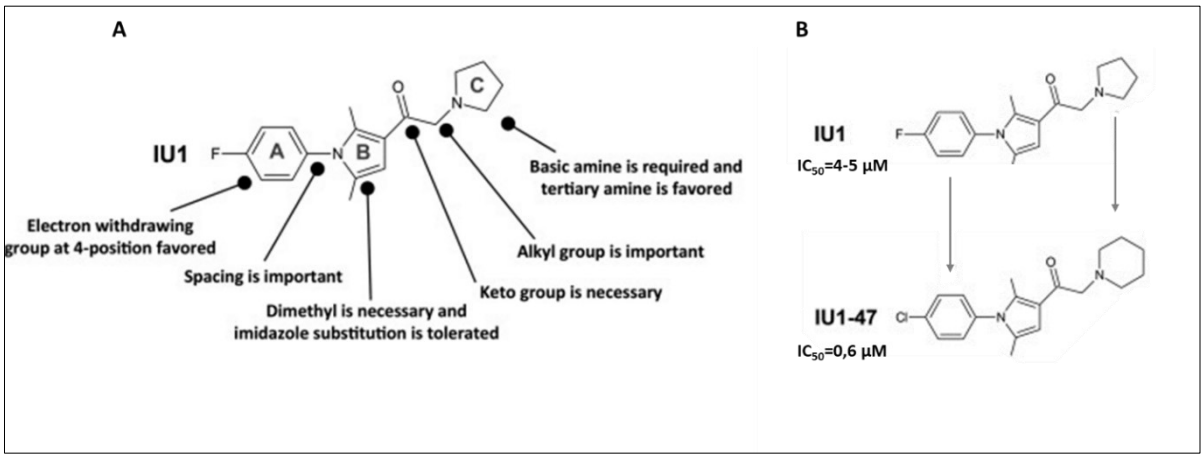

Figure 10. Structures of small molecules USP14 inhibitors (A) IU1 and (B) IU1-47[18].

1.7. USP14

More than 100 human DUBs have been identified and classified into six families depending on their structure and function: ubiquitin-specific proteases (USPs), ubiquitin C-terminal hydrolases (UCHs), Machado-Joseph domain-containing proteases, ovarian tumor proteases, motif-interacting with ubiquitin containing proteases, and JAMM/MPN domain-associated Zn-dependent metalloproteases[11]. USP14 is part of the USPs family, and it contains 494 amino acids that form two structural domains: an N-terminal ubiquitin-like (UBL) domain and a C-terminal catalytic USP domain. The UBL domain regulates UPS activity, while the USP domain contains the enzymatic pocket where deubiquitination occurs. The catalytic domain consists of three subdomain structures (finger, palm, and thumb), which provide specificity for ubiquitin binding. Structural analysis revealed that two surface loops on the palm subdomain (BL1 and BL2), positioned above the catalytic binding site, are

extremely dynamic and undergo conformational changes during binding with the C-terminal of Ub chains[172](Figure 11).

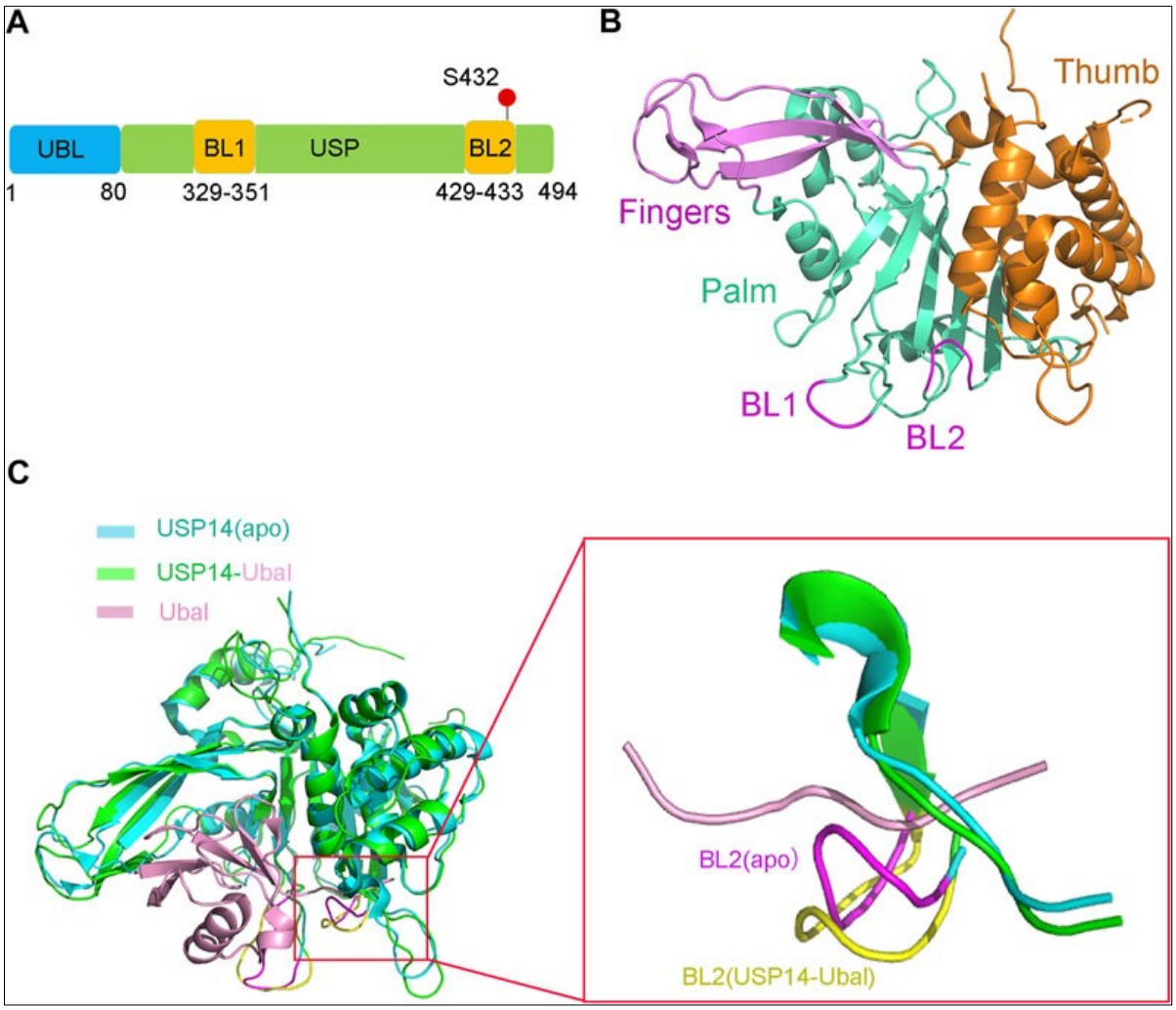

Figure 11. Structure of USP14 in the inactive and active conformation with Ubal. (A) Domain structure and modification of the full-length USP14. (B) Inactive crystal structure of USP14. (C) Crystal structure of USP14 in complexed with Ubal. Left: Comparison between the structures of USP14 (apo) and USP14-Ubal (Ub-conjugated). Right: Comparison between the BL2 of USP14(apo) and USP14-Ubal(complex)[172].

USP14 activity depends on its association with the proteasome. When it is not bound, USP14 can be found in an autoinhibited state. Once conjugated to the 26S subunits of the proteasome, it is activated and removes ubiquitin chains from different substrates preventing their degradation[11]. Importantly, the USP14 association provides specificity to the proteasome by targeting with

greater specificity substrates bearing multiple ubiquitin chains compared to single chain conjugates[173]. Chemical inhibition of USP14 *in vitro* triggers an enhancement of proteasome activity and degradation of different substrates, in particular, some implicated in neurodegenerative disorders[14]. USP14 also negatively regulates autophagy by cutting K63 ubiquitin chains from Beclin1, a regulatory element in the Beclin1/VPS34 complex necessary for autophagosome nucleation. In line with this mechanism, several studies have reported an enhancement of autophagy upon USP14 inhibition[15–17].

The importance of UPS and autophagy as the two main degradative pathways in the cells has been extensively emphasized in the previous chapters. Due to its cardinal role in the regulation of both pathways, USP14 is considered of particular interest in the context of the modulation of cellular homeostasis and MQC and a potential therapeutic target for neurodegenerative diseases intervention.

Of note, USP14 overexpression has been found in different kind of cancer, including lung cancer, breast cancer, and pancreatic ductal adenocarcinoma, and it is correlated with a worst prognosis[174]. Accordingly, inhibition of USP14 has proven to be remarkably successful in cancer treatment by reducing cell proliferation, migration and by inducing apoptosis[175]. At least one clinical trial for breast cancer treatment utilizing an available USP14 inhibitor is already ongoing[176], and over the last few years, the interest from pharmaceutical companies in developing new compounds has grown exponentially.

AIM OF THE THESIS

The selective removal of damaged mitochondria via autophagy, a process called mitophagy, is one of the integral aspects of mitochondrial quality control (MQC). Increasing pieces of evidence show that the deregulation of MQC and accumulation of defective mitochondria as a consequence of impaired mitophagy is one of the causative mechanisms leading to neurodegeneration. The most dissected mitophagy pathway is regulated by PINK1 and Parkin, and mutations in their encoding genes are associated with juvenile forms of PD. PINK1 is a mitochondrial-targeted serine/threonine kinase that recruits Parkin, an E3 ubiquitin ligase, to the OMM upon mitochondrial damage. Ubiquitination of several OMM proteins by Parkin leads to the recognition of damaged mitochondria by the two main cellular degradative systems, UPS and autophagy-lysosome pathway, triggering their removal and degradation. Thus, the ubiquitination of mitochondria plays a pivotal role in the clearance of the dysfunctional organelle. The action of Ub ligases can be counteracted by the activity of deubiquitinating enzymes (DUBs). Therefore, the inhibition of specific DUBs can potentially enhance PINK1/Parkin-independent mitophagy by stabilizing ubiquitin chains on the mitochondrial surface. Among these DUBs, Ubiquitin specific protease 14 (USP14) appears as a promising candidate because its inhibition can positively regulate both the UPS and autophagy. Furthermore, highly specific and potent inhibitors of USP14, such as IU1 and its derivative IU1-47, are available.

Previous studies in my lab have reported that genetic and pharmacological inhibition of USP14 activity induces PINK1/Parkin independent mitophagy and rescues the pathological phenotype of two well-established *D.melanogaster* models of PD, the PINK1 and Parkin KO flies. At present, studies on the

“mitophagic” effects of USP14 inhibitors in neurons of human origin have not yet been conducted.

With that in mind, the central aims of this study are: (i) to validate the PINK1/Parkin-independent mitophagic effect of USP14 inhibition in human neurons; (ii) to evaluate the potential beneficial effect of USP14-mediated enhanced mitophagy on the general fitness of neurons displaying mitochondrial dysfunctions; (iii) to identify target(s) of USP14 inhibition that account for its pro-mitophagic effect.

RESULTS

USP14 inhibition enhances Parkin-independent mitophagy in iNeurons

Bernardo Greta[1], Prado Miguel A.[2], Daniel Finley[3], Elena Ziviani[1]

[1] Department of Biological Sciences, University of Padova, Padova, Italy.
[2] Instituto de Investigación Sanitaria del Principado de Asturias (ISPA), Oviedo, Spain.
[3] Department of Cell Biology, Harvard Medical School, Boston, USA.

Graphical Abstract

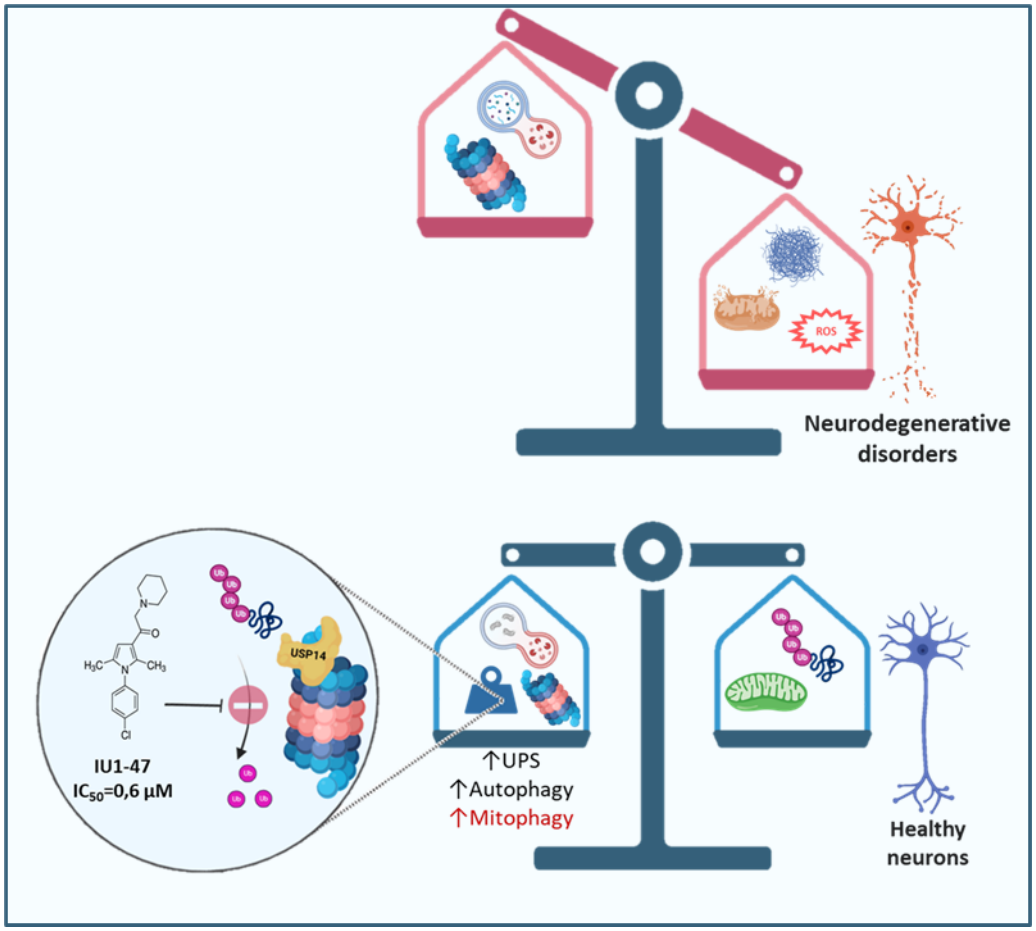

Address correspondence to
Elena Ziviani: elena.ziviani@unipd.it

Abstract

Loss of proteostasis is well documented during aging and depends on the progressive pathological decline in the activity of two major degradative mechanisms: the ubiquitin-proteasome system (UPS) and the autophagy-lysosomal pathway. Although a physiological decline in proteostasis during aging is expected, this seems to be exacerbated in age-associated neurodegenerative diseases. Indeed, patients display an accumulation of aggregated proteins and dysfunctional mitochondria, which becomes pathologically relevant because it leads to enhanced neuroinflammation and ROS production, culminating in neuronal death. In this context, approaches aimed to enhance proteins and organelles' homeostasis are promising targets for therapeutic applications. Supporting this hypothesis, we recently reported that inhibition of the deubiquitinating enzyme USP14, which is known to enhance both the UPS and autophagy, increases lifespan and rescues the pathological phenotype of two fly models of neurodegeneration. Studies on the effects of USP14 inhibition in mammalian neurons have not yet been conducted.

To close this gap, we exploited iNeurons differentiated from human embryonic stem cells (hESCs) to investigate the potential beneficial effect of enhancing proteostasis in two *in vitro* models, which are known to accumulate dysfunctional mitochondria: PINK1 and Parkin KO iNeurons. Quantitative global proteomics analysis performed following genetic ablation or pharmacological inhibition of USP14 demonstrated that USP14 inhibition specifically promotes mitochondrial autophagy, i.e. mitophagy, in iNeurons. Accordingly, our biochemical and imaging data showed that USP14 inhibition enhances autophagy and mitophagy in these neurons of human origin. Importantly, the mitophagic effect of USP14 inhibition rescued the mitochondrial defects of

Parkin KO neurons, supporting the use of small-molecule inhibitors of USP14 for therapeutic intervention.

Introduction

In the last two decades, increasing life expectancy and declining fertility have been fueling an exponential increase in the population over 65 years of age. As a result, age-related neurodegenerative diseases such as PD, AD, and ALS are becoming serious public health problems affecting both the social and economic spheres of society. Despite great efforts of the scientific community, to date, only a few pharmaceutical treatments, able to alleviate the symptoms or slow down the neurodegeneration process, have been developed. A better understanding of the pathogenesis of these diseases is fundamental for the development of drugs targeting neurodegeneration. In this context, more and more pieces of evidence are pointing to a prominent role of mitochondrial dysfunction and impaired MQC in the neurodegenerative process[5]. Mitochondrial homeostasis depends on the balance between biogenesis and the removal of damaged mitochondria through a selective form of autophagy named mitophagy[177]. Mitophagy initiation requires the crosstalk between two of the best characterized degradative pathways in the cells, the UPS and the autophagy-lysosomal pathway that maintain cellular homeostasis through the detection and degradation of aggregated proteins and dysfunctional organelles[6]. The fundamental signalling molecule that links these two pathways is ubiquitin, a small 8,5 kDa protein covalently attached to Lys residues of other proteins to modulate their fate[7]. Ubiquitinated proteins on the mitochondrial surface are recognized by both the UPS, which mediate their degradation, and autophagic receptors, which promote autophagosome assembly and delivery to the lysosome[8]. Protein ubiquitination is a dynamic and reversible process

controlled by two types of enzymes: Ubiquitin ligases, which conjugate ubiquitin moieties to the target protein, and Deubiquitinating enzymes (DUBs), which counteract this process. Several ubiquitin E3 ligases have been associated with the regulation of mitophagy, but the best studied is Parkin. Parkin, in conjunction with the protein kinase PINK1, forms a surveillance pathway for the detection and removal of dysfunctional mitochondria through Ub-dependent mitophagy[9,10]. In functional mitochondria, PINK1 is imported, cleaved, and rapidly degraded. Following a mitophagy stimulus, PINK1 is stabilized on the OMM where it is activated through autophosphorylation; once activated, PINK1 induces Parkin translocation to the OMM, and induces its ubiquitin E3-ligase activity by phosphorylating Parkin itself or by phosphorylating pre-existing ubiquitin chains on OMM proteins (pSer65-Ub). In both scenarios, Parkin ubiquitinates OMM proteins creating new substrates for PINK1 phosphorylation, thereby creating a feedforward mechanism that amplifies mitophagy signals[118,120,121]. The ubiquitin chains formed by Parkin on the OMM display linkage types typical of both autophagy and proteasomal degradation[123,178].

Notably, the two genes encoding for Parkin and PINK1 (PARK2 and PARK6, respectively) were identified as causative of autosomal recessive forms of PD, providing a mechanistic link between impaired mitophagy and a very common aged-associated neurodegenerative disorder[153].

The relevance of the PINK1/Parkin-dependent mitophagy in neuronal cells is controversial due to the mild phenotype developed by PINK1 or Parkin KO mouse models. However, PINK1/Parkin depletion generates PD-like phenotypes, including loss of dopaminergic neurons and motor defects, in *Drosophila* models[179,180] and in mice subjected to mitochondrial stress (exhaustive exercise, increased mtDNA damage)[154]. These findings suggest that

the PINK1/Parkin-dependent mitophagy is probably dispensable under physiological conditions but might become important to counteract neurodegeneration in the presence of pathological stimuli such as protein aggregation and inflammation[181,182].

In this context, the stimulation of alternative mitophagy pathways may represent an attractive solution to counteract the neurodegeneration process.

One way to do so is by acting on DUBs; these enzymes are able to oppose the activity of Ub E3 ligases by eliminating Ub chains from targeted proteins or organelles such as mitochondria, thus preventing their elimination through the UPS and autophagy-lysosome pathway[11,12]. Hence, inhibition of specific DUBs activity represents a promising target for therapeutic intervention aimed at enhancing mitophagy and mitochondrial turnover[164,183].

Recent works reviewed by Burtscher et al. [100] have identified several DUBs involved in the modulation of ubiquitin-dependent mitophagy, such as ataxin-3, USP14, USP15, USP30, and USP35 [21,164–166]. Among these DUBs, the proteasome-associated USP14 seems a particularly appealing target thanks to its capacity to regulate both the UPS and autophagy[13–17]. Moreover, a series of potent and selective inhibitors are available for this DUB, making it an ideal candidate for potential therapy development. The first described inhibitor, IU1 (IC_{50} of 4-5 µM), was developed in Finley lab in 2010 [14], and recently the same lab synthesized a new compound called IU1-47, which derives from the same family of IU1. IU1-47 is tenfold more potent, has a lower $IC_{50,}$ and, more importantly, is orally bioavailable and able to cross the BBB, both important features for its use for clinical purposes[171]. We recently reported that pharmacological and genetic inhibition of USP14 promotes basal mitophagy in PD patient fibroblasts while in two *in vivo* PINK1 and Parkin *D.melanogaster* models of PD, it restored mitochondria function and ultrastructure as well as dopamine levels.

Remarkably, at the systemic level, inhibition of USP14 extended the PINK1 and Parkin KO flies' lifespan and rescued climbing behavior[19]. At present, studies on the effects of USP14 inhibition on mitophagy in neurons of human origin have not yet been conducted.

To close this gap, we took advantage of a recently generated line of hESCs able to rapidly and efficiently differentiate functional iNeurons[20,21], and tested the mitophagic effect of USP14 inhibition.

We found that USP14 inhibition promotes mitophagy in these neurons of human origin. More importantly, we demonstrated that USP14 inhibition rescues mitochondrial impairment of Parkin KO iNeurons.

Results

Efficient differentiation of hESCs into iNeurons by Ngn2 forced expression

Previous studies in my lab have shown that genetic downregulation of USP14 or its pharmacological inhibition by specific inhibitor IU1 induces autophagy and PINK1/Parkin independent mitophagy in different cell models[19]. Moreover, USP14 inhibition restored mitochondria function and ultrastructure, as well as dopamine levels in two well-established *D.melanogaster* models of PD, the PINK1 and Parkin KO flies. At the systemic level, USP14 inhibition extended flies' lifespan and rescued the climbing impairment of both PINK1 and Parkin KO flies [19], presumably by enhancing proteostasis and mitochondrial quality control. Aiming to extend these findings to mammals, we next wanted to evaluate the effect of USP14 inhibition in neurons of human origin. To this end, we took advantage of H9 human embryonic stem cells (hESCs) lines produced by Harper's lab to differentiate hESCs in neurons with a fast and efficient protocol [20,21]. Briefly, hESCs were subjected to CRISPR-Cas9-based gene editing to homozygously insert a doxycycline-inducible Neurogenin-2 (Ngn2) cassette into the AAVS1 locus and obtain human neurons by forcing the expression of this transcription factor. Ngn2 regulates the commitment of neural progenitors to neuronal fate during development and induces early postnatal astroglia into neurons. It is known that overexpression of Ngn2 and Sox11 (another transcription factor involved in neuronal induction) promotes the differentiation of primary fibroblasts into cholinergic neurons while it inhibits (GABA)-ergic neuronal differentiation. Accordingly, Ngn2 expression in hESCs produces excitatory layer2/3 cortical neurons that exhibits AMPA-receptor-dependent spontaneous synaptic activity and a relatively smaller NMDA-receptor-mediated synaptic current. These so-called iNeurons (induced Neurons) express

glutamatergic synaptic proteins such as vesicular glutamate transporter 1 (vGLUT1), postsynaptic density-95 (PSD95), synapsin1 (SYN1), and display excitatory synaptic function when in co-culture with mouse glial cells[184–186]. Harper's lab kindly provided us with these modified H9 hESCs with different relevant genotypes (WT, PINK1 KO, PARK2 KO, USP14 KO, BNIP3L KO, MUL1 KO, and MARCH5 KO). The yield of neuronal conversion obtained is nearly 100%, and this protocol allows generating neurons with a mature neuronal morphology, and reproducible neuronal properties in less than two weeks. In particular, after 11-12 days of differentiation, cells start to develop a clear neuronal network (**Figure 1A**), and at the end of the differentiation process, iNeurons exhibit the expression of the typical neuronal markers MAP2 and βIII-tubulin (**Figure 1B**), while expression of stem cell pluripotency markers Oct3/4 and Sox2 was almost completely abolished (**Figure 1B**). Quantitative RT-PCR analyses revealed that iNeurons expressed ~ 30 to ~ 100-fold increased levels of endogenous Ngn2 as well as of three neuronal markers NeuN, MAP2, and Tuj1 compared to undifferentiated H9 hESCs (**Figure 1C**). Immunoblotting experiment confirmed that stem cell marker OCT3/4 is only present until day 2 of differentiation while the expression of neuronal marker βIII-Tubulin gradually increased until day 14 upon induction (**Figure 1D**). Finally, our representative electron microscopy (EM) images of iNeurons after 14 days of differentiation show neuronal cells with distinguishable neuronal soma, axon hillock, and axonal and dendritic projections (**Figure 1E,F**). Released neurotransmitter molecules are visible at synaptic clefts (**Figure 1F**), and detectable levels of NMDAR 2B are expressed, which we assessed by western blotting analysis (**Figure 1G**). The different KO lines were tested using Western Blot approach to confirm the absence of each analyzed protein (**Figure S1A**). Thus, these cells of the desired genotype fully develop as neurons and seem to make functional synapsis.

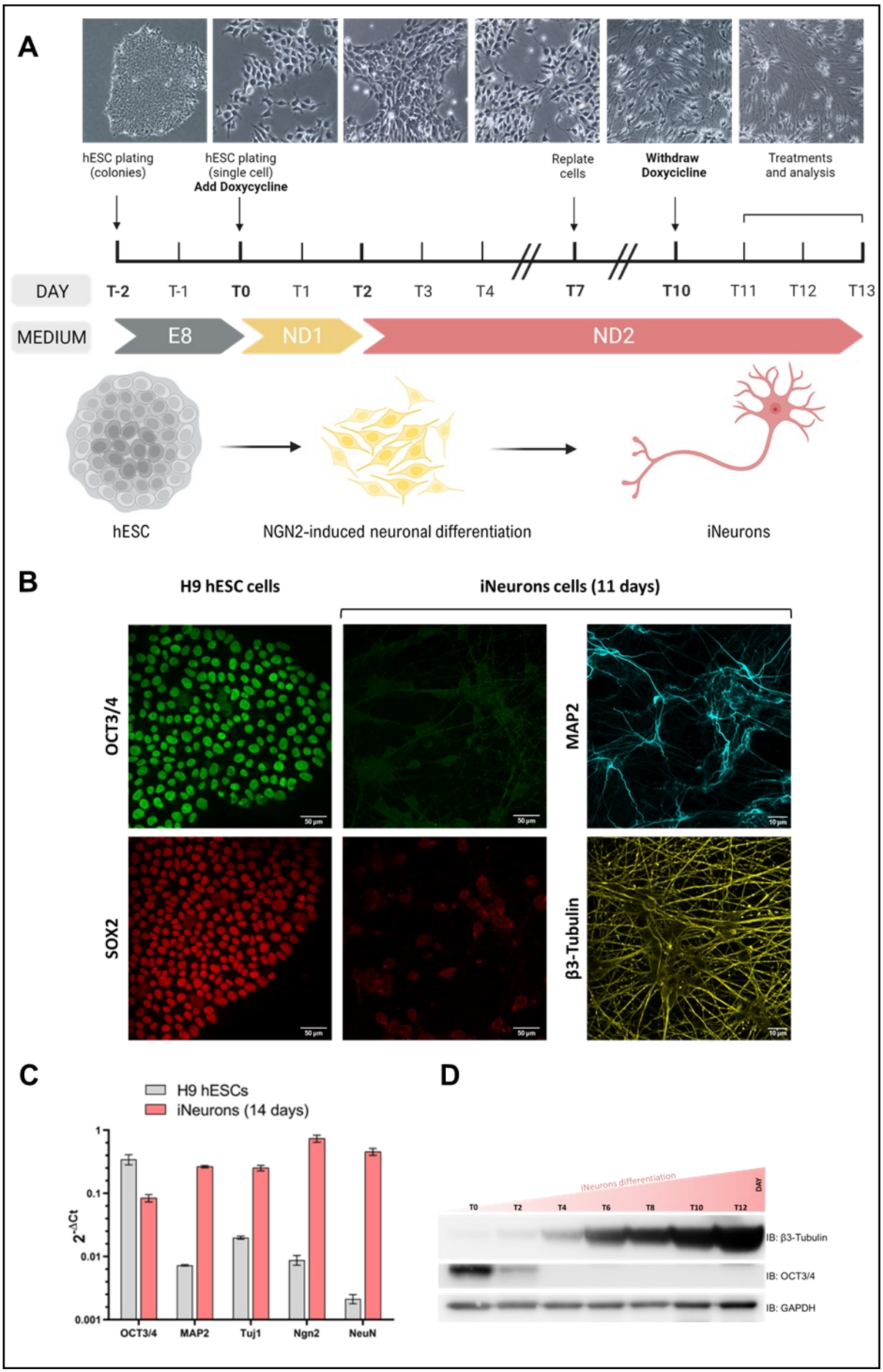
A
hESC plating (colonies)
hESC plating (single cell)
Add Doxycycline
Replate cells
Withdraw Doxycicline
Treatments and analysis
DAY
T-2
T-1
T0
T1
T2
T3
T4
T7
T10
T11
T12
T13
MEDIUM
E8
ND1
ND2
hESC
NGN2-induced neuronal differentiation
iNeurons
B
H9 hESC cells
iNeurons cells (11 days)
OCT3/4
MAP2
SOX2
β3-Tubulin
C
H9 hESCs
iNeurons (14 days)
2^-ΔCt
OCT3/4
MAP2
Tuj1
Ngn2
NeuN
D
iNeurons differentiation
DAY
IB: β3-Tubulin
IB: OCT3/4
IB: GAPDH

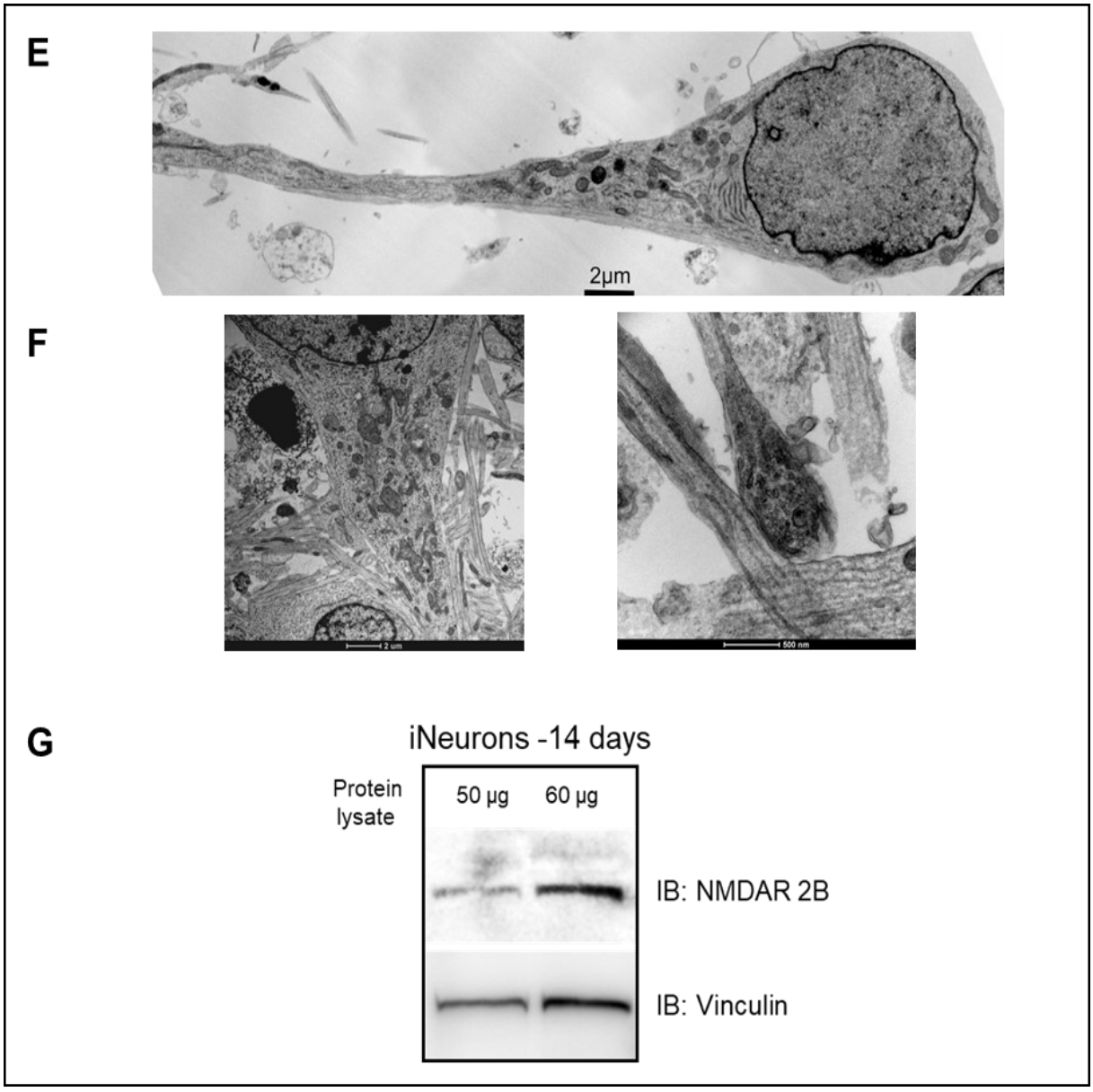

Figure 1. Characterization of hESCs-derived iNeurons (A) Timeline of Ngn2-neuronal induction strategy from H9 hESCs, and representative bright-field images of the corresponding time-points showing the development of neuronal morphology and the high conversion yield of iNeurons. **(B)** Undifferentiated hESCs (left) and hESC-derived iNeurons after 11 days of differentiation (right) were stained for pluripotency markers OCT3/4 (green), SOX2 (red), MAP2 (cyan), and βIII-tubulin (yellow); differentiated iNeurons exhibit the expression of the typical neuronal markers MAP2 and βIII-tubulin (Tuj1) while the expression of pluripotency markers OCT374 and SOX2decreases upon differentiation; **(C)** Real-time qPCR analysis of OCT3/4, MAP2, Tuj1, Ngn2, and NeuN mRNA expression from H9-hESCs and 2-weeks old iNeurons, normalized to GAPDH. iNeurons showed increased expression of neuronal markers MAP2 (37.1-fold), Tuj1 (13.1-fold), Ngn2 (79.5-fold), NeuN (225-fold). **(D)** Western-blot analysis of H9-hESCs iNeurons samples collected every other-day after induction of differentiation. Samples were immunoblotted for βIII-tubulin, which shows an exponential increase, and OCT3/4, which disappears after 4 days of differentiation. GAPDH was used as loading control. **(E,F)** Representative Electron Microscopy images of iNeurons 11-days post differentiation displaying axonal (E), dendritic projections and neurotransmitter release at synaptic clefts (F). Scale bar are represented in each image. **(G)** Immunoblot analysis of iNeurons, 14 days post induction, showing high expression levels of synaptic glutamate receptors NMDAR 2B.

In iNeurons USP14 inhibition induces differential remodelling of the mitochondrial proteome

To dissect the molecular pathway underlying USP14 inhibition and identify the repertoire of USP14 substrates in neurons of human origin, we next chose to perform a mass spectrometry-based analysis of iNeurons in which USP14 activity was inhibited. In order to assess the impact of USP14 inhibition on cell viability, we first performed a dose-response MTT assay to evaluate the potential toxicity of IU1-47, a potent and highly selective inhibitor of USP14. MTT is a colorimetric assay that measures cellular metabolic activity as an indicator of cell viability, proliferation, and cytotoxicity. NAD(P)H-dependent oxidoreductase enzymes in metabolically active cells can reduce the yellow MTT to purple formazan crystals. Thus, the darker the solution, the greater the number of viable, metabolically active cells. IU1 is the first of a series of inhibitors that have been developed to inhibit USP14 specifically. In 2017 Boselli et al.[18] synthesized a new inhibitor called IU1-47, which is 10-fold more potent and more selective compared to IU1 (IC50 IU1 = 5,5 µM; IC50 IU1-47 = 0,6µM). We treated iNeurons with increasing dosages (1-200µM) of IU1-47 for 24H and reported the obtained data in a cell survival curve. We found that at doses up to 10 µM, at least 80% of viability is retained (**Figure S2A**). The effect is reduced in USP14 KO cells as expected, while at higher concentrations (>50µM), we detected some level of toxicity in both cell lines, which is probably due to the high amount of DMSO in which IU1-47 is resuspended. These results fully support previously reported evidence on the relatively not toxic and well-tolerated effect of IU1-47 in cells, which we also recorded in SH-SY5Y (**Figure S2B**).

To examine the impact of USP14 inhibition on the total proteome, we treated WT iNeurons with 5µM and 10µM IU1-47 for 24H and compared them with untreated samples (DMSO). Samples treatments were performed in

quadruplicate (DMSO and 5µM IU1-47) or triplicate (10µM IU1-47), and total cell extracts obtained in the lab, were subjected to 11-plex Tandem Mass Tagging (TMT)-based proteomics performed by our collaborator Dr. Daniel Finley at Harvard Medical School (HMS) **(Figure 2A)**. Replicates were highly correlated and Principal Component Analysis (PCA) revealed clustering of replicates, with PC1 clearly separating treated samples (IU1-47) and CTR (DMSO) (**Figure S2C**). Since only one of the CTR samples was separated from the others in PC2 (DMSO_4), we decided to exclude this sample from the subsequent analysis. TMT proteomics quantified 8018 proteins, and through annotation of mitochondrial proteins using the MitoCarta 3.0 database, we found major alterations in the abundance of the mitochondrial proteome following USP14 inhibition with both 5µM **(Figure 2B)** and 10µM (**Figure S2D**) IU1-47 treatment. Indeed, the majority of proteins annotated as mitochondria were downregulated in IU1-47 treated iNeurons compared to CTR, as indicated in the volcano plots (leftward skew of coloured dot in **Figure 2B Figure S2D**). Proteins with decreased abundance were enriched for IMM, Matrix, and to a less extent, OMM sub-organelle compartment categories, consistent with degradation of the entire organelle (**Figure 2C**). Importantly other organelles were not negatively affected by IU1-47 treatment; in fact we found an increase of protein belonging to the ER, Golgi, and Peroxisomes, together with an upregulation of the lysosomal compartment, pointing towards a potential autophagic effect of USP14 inhibition (**Figure 2D**). We next performed Gene Ontology analysis on the subset of data obtained from the treatment with 5µM of IU1-47 compared to CTR, and we found that GO Cellular Compartment analysis confirmed the previous results obtained with protein annotation. Indeed, we found enrichment of mitochondrial proteins in the downregulated subset (**Figure 2E**), while the upregulated subset was enriched in proteins belonging to ER and Golgi

(**Figure 2G**). On the same dataset, we also performed KEGG pathway enrichment analysis, which highlighted a downregulation of pathways involved in different neurodegenerative diseases, including PD, AD, and ALS (**Figure 2F**). Interestingly this is in line with multiple findings in the literature that correlate USP14 inhibition with enhanced clearance of intracellular protein aggregates such as tau protein, ataxin-3, TDP-43, and α-synuclein [18,187]. KEGG Pathway enrichment also showed upregulation of "lysosome", "phagosome", and "protein processing in the ER" pathways, corroborating the previous results, further supporting the hypothesis of an autophagic effect of USP14 inhibition (**Figure 2H**). Importantly, comparing WT and USP14 KO iNeurons using the same TMT-based approach (**Figure S2E,F**)the downregulation of mitochondrial proteins is detectable but much less pronounced. Moreover, in contrast with the results obtained with the USP14 inhibitor, we did not found an upregulation of the lysosomal compartment in USP14 KO iNeurons compared to the WT (Figure S2G).

Conclusively, these results indicate that treatment of iNeurons with a specific USP14 inhibitor IU1-47 is not toxic at concentrations lower than 10µM. Most importantly, USP14 inhibition induces selective autophagy of mitochondria, also known as mitophagy, without impacting the degradation of other cellular organelles.

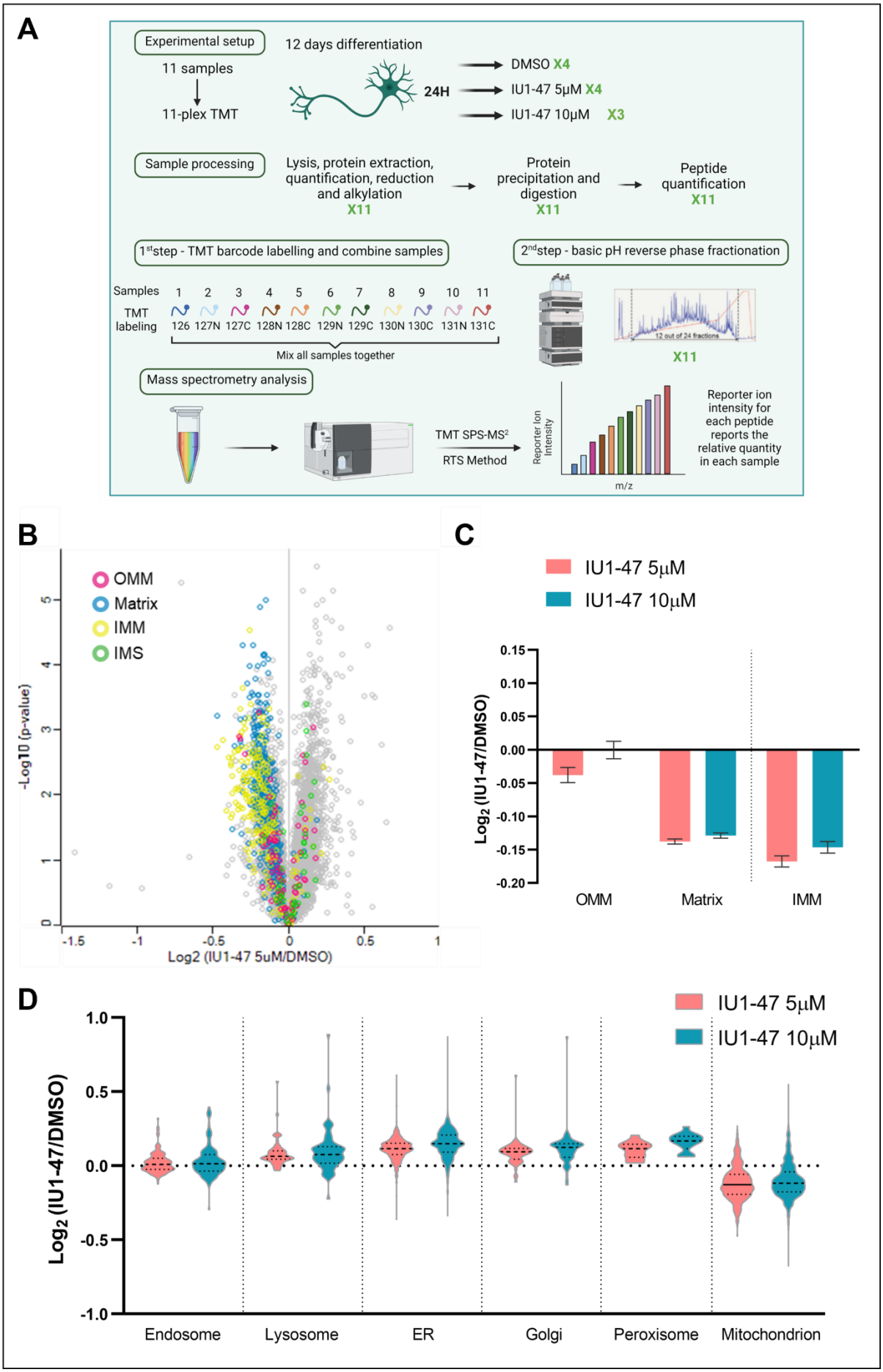
A
Experimental setup
11 samples
11-plex TMT
12 days differentiation
24H
DMSO X4
IU1-47 5µM X4
IU1-47 10µM X3
Sample processing
Lysis, protein extraction, quantification, reduction and alkylation X11
Protein precipitation and digestion X11
Peptide quantification X11
1ststep - TMT barcode labelling and combine samples
2ndstep - basic pH reverse phase fractionation
Samples 1 2 3 4 5 6 7 8 9 10 11
TMT labeling 126 127N 127C 128N 128C 129N 129C 130N 130C 131N 131C
Mix all samples together
12 out of 24 fractions
X11
Mass spectrometry analysis
TMT SPS-MS2
RTS Method
Reporter Ion Intensity
m/z
Reporter ion intensity for each peptide reports the relative quantity in each sample
B
OMM
Matrix
IMM
IMS
-Log10 (p-value)
Log2 (IU1-47 5uM/DMSO)
C
IU1-47 5µM
IU1-47 10µM
Log2 (IU1-47/DMSO)
OMM
Matrix
IMM
D
IU1-47 5µM
IU1-47 10µM
Log2 (IU1-47/DMSO)
Endosome
Lysosome
ER
Golgi
Peroxisome
Mitochondrion

E

GO Cellular Component (CC)
downregulated proteins
P-value < 0,05

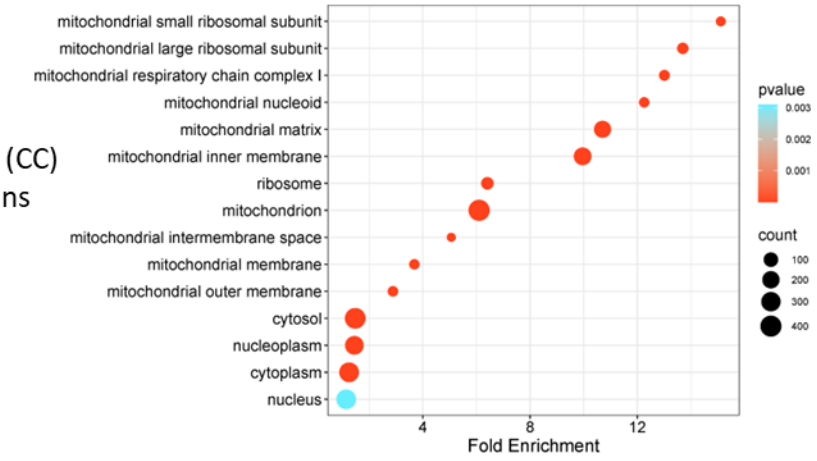

F

KEGG Pathways
downregulated proteins
P-value < 0,05

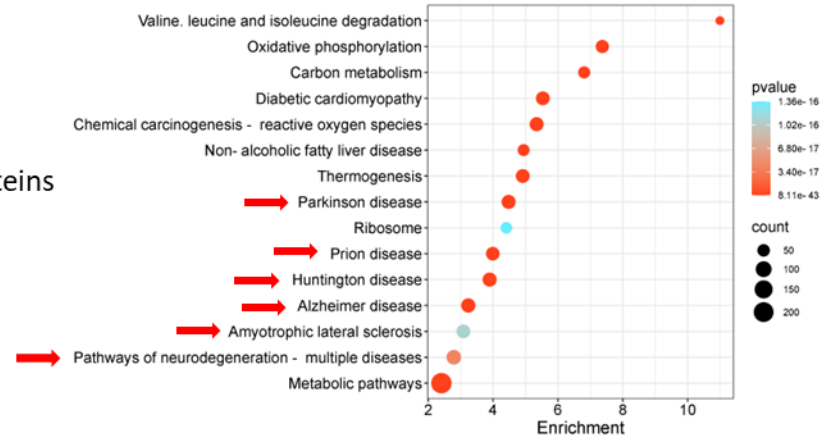

G

GO Cellular Component (CC)
upregulated proteins
P-value < 0,05

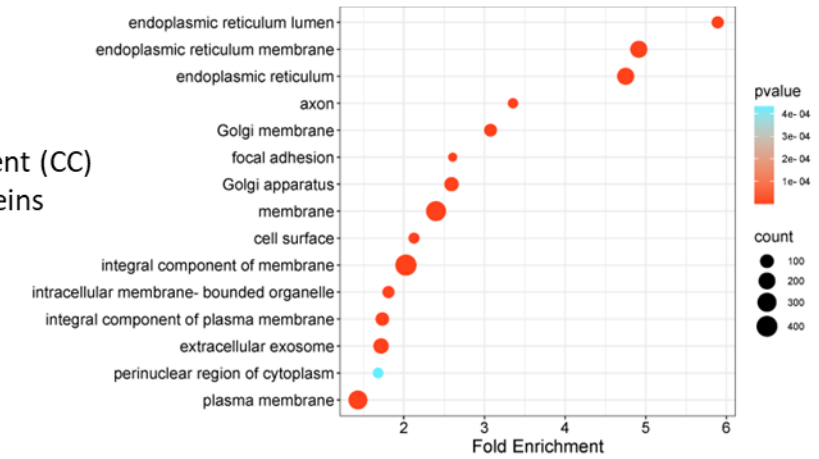

H

KEGG Pathways
upregulated proteins
P-value < 0,05

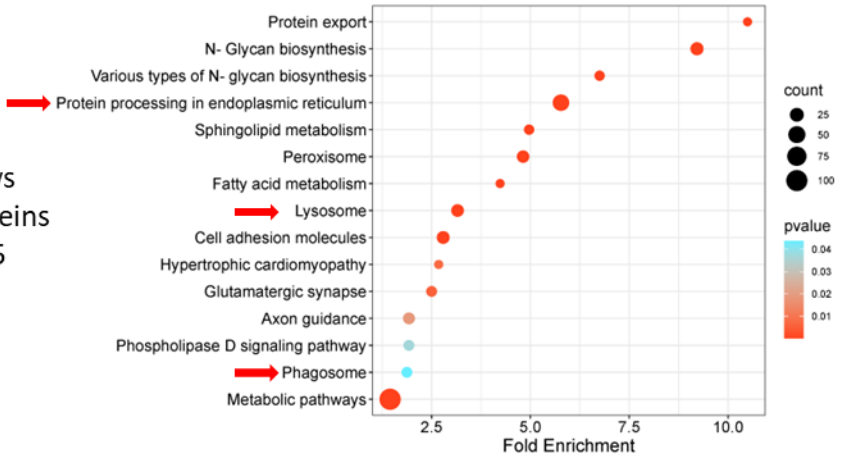

(legend on next page)

Figure 2. TMT-analysis of iNeurons upon USP14 inhibition (A) Workflow for TMT-based proteomics of iNeurons, treated with USP14 inhibitor as indicated. 11-plex proteomics was performed on 4 biological replicates for Control (DMSO) and IU1-47-5μM treatment, and 3 biological replicates for IU1-47-10μM treatment. **(B)** Volcano plots representing the abundance of the 8018 identified proteins in the WT iNeurons treated with 5μM IU1-47 for 24H compared to untreated cells (DMSO). Mitochondrial proteins (identified by comparison with MitoCarta 3.0[208]) are represented with coloured dots based on their reported mitochondria localization: OMM proteins (magenta), matrix proteins (blue), IMM proteins (yellow), IMS proteins (green). **(C)** Bar graph shows changes distribution compared to control (DMSO) in protein abundance upon IU1-47 treatment (5μM/24H-pink bar; 10μM/24H-blue bar) for proteins that localize in the indicated mitochondrial compartments (OMM, mitochondria matrix and the IMM respectively). **(D)** Distribution of changes in protein abundance for proteins that localize in individual organelles or protein complexes as indicated in iNeurons treated with 5μM (pink) or 10μM (blue) IU1-47 for 24H compared to untreated cells (DMSO). **(E)** GO-term Cellular Component enrichment analysis of proteins significantly downregulated (p-value<0.05) in iNeurons treated with 5μM IU1-47-24H compared to control (DMSO). **(F)** Kegg pathway enrichment analysis of proteins significantly downregulated (p-value<0.05) in iNeurons treated with 5μM IU1-47/24H compared to control (DMSO). **(G)** GO-term Cellular Component enrichment analysis of proteins significantly downregulated (p-value<0.05) in iNeurons treated with 5μM IU1-47/24H compared to control (DMSO). **(H)** Kegg pathway enrichment analysis of proteins significantly downregulated (p-value<0.05) in iNeurons treated with 5μM IU1-47/24H compared to control (DMSO). Red arrows identify pathways that are potentially relevant for this study.

Inhibition of USP14 induces autophagy in iNeurons

Considering the correlation between USP14, autophagy and mitophagy highlighted in previous works[15,17,19], and the identification in our TMT analysis of specific downregulation of the mitochondrial proteome, we next wanted to evaluate mitophagy levels in iNeurons when USP14 activity is altered.

Mitophagy can be defined as the lysosome-dependent autophagic turnover of damaged mitochondria [188]. For this reason and to understand if USP14 is able to regulate mitophagy (i.e. mitochondrial degradation via autophagy) we analysed the autophagic flux in iNeurons upon USP14 inhibition.

We assessed autophagy by western blotting analysis of LC3 levels. An increased ratio between the lipidated (LC3II) and normal (LC3I) forms of LC3 protein can be interpreted as an indication of enhanced autophagy and can be easily evaluated via immunoblotting (**Figure 3A**). In WT iNeurons, USP14 inhibition by IU1-47 (10μM-24H) induces an increase of autophagy, represented by an

increased LC3II:LC3I ratio, while IU1-47 does not seem to affect the LC3II:LC3I ratio in USP14 KO cells (**Figure 3B,C**). This result confirms the high specificity of the inhibitor for USP14 in that the autophagic effect of USP14 inhibition is completely abrogated in USP14 KO background, as expected. Importantly, we observed a further increase in LC3II levels when cells were co-incubated with IU1-47 and bafilomycin (10nM-24H), a common drug that is used to inhibit the autophagic flux. This result indicates that USP14 inhibition does not lead to a blockage of the autophagic flux but rather enhances autophagy (**Figure 3C**).

Next, in order to examine whether the autophagic effect of USP14 inhibition is PINK1/Parkin dependent, we assessed autophagy in iNeurons differentiated from PINK1 KO and Parkin KO hESCs. Importantly, IU1-47 induces an increase of autophagy also in PINK1 KO and PARK2 KO iNeurons, demonstrating that this effect of USP14 inhibition is PINK1/Parkin independent (**Figure 3D,E**). We obtained similar results with the USP14 inhibitor, IU1 (100µM/24-48hrs), for which we observed a significant increase in the LC3II:LC3I ratio, both in WT and PINK1 KO iNeurons (**Figure S3A**). Electron microscopy (EM) analyses also revealed a significantly increased number of autophagic vesicles after IU1 treatment in both genotypes (**Figure S3B**). Importantly, IU1 seems to display off-target effects because the autophagic response triggered by IU1 was not abrogated in USP14 KO background (**Figure S3C-D**).

In summary, USP14 inhibition enhances autophagy in iNeurons with a mechanism that is PINK1/Parkin independent and more importantly it does not impact the autophagic flux.

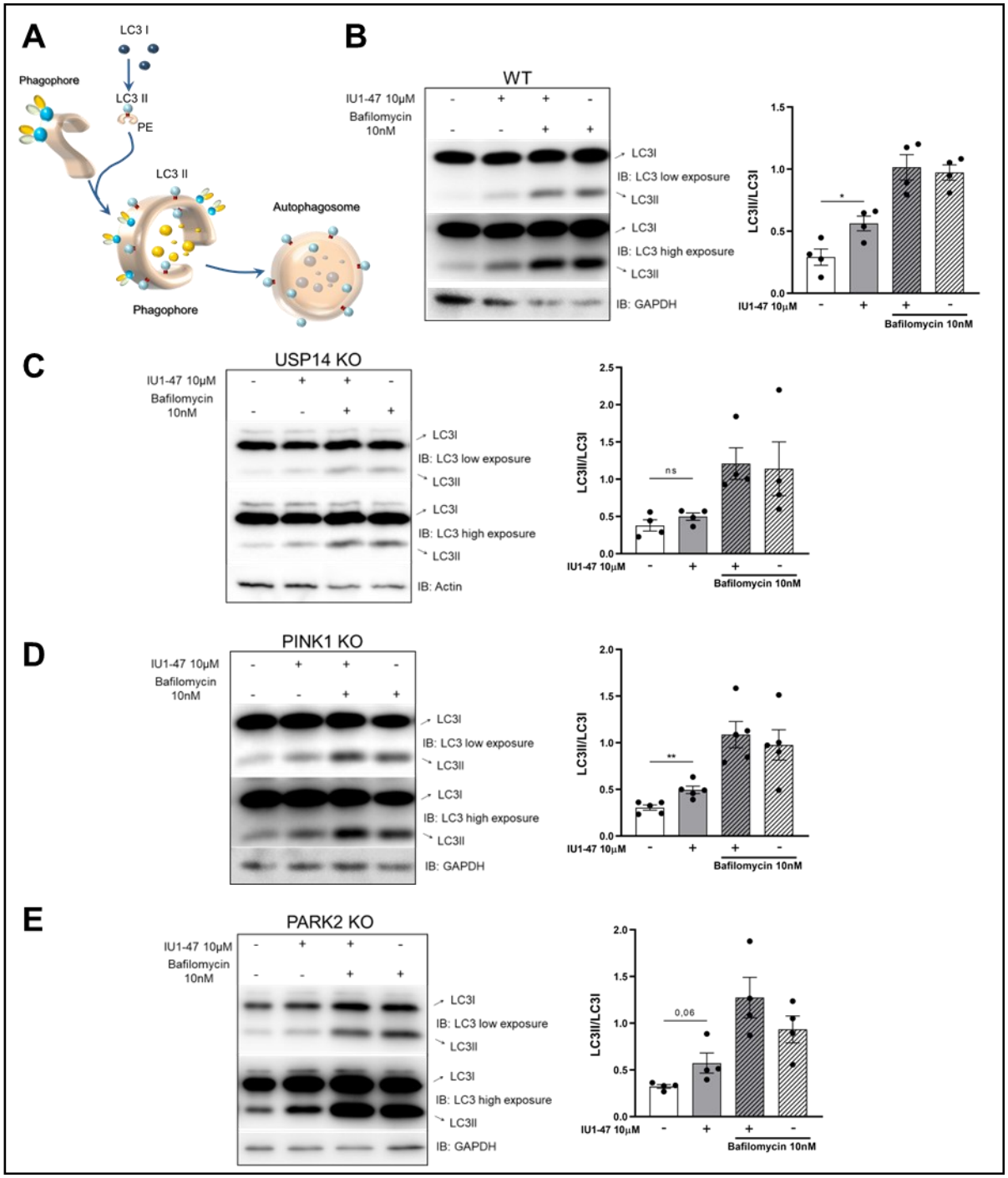

Figure 3. USP14 inhibition enhances autophagy in iNeurons (A) Picture depicts schematic representation of LC3I to LC3II conversion during autophagosome formation. **(B,C)** Western Blot analysis and corresponding quantifications (right) of WT (B) and USP14 KO (C) iNeurons treated with 10 µM IU1-47 for 24H. Treated samples display a significant increase in LC3II:LC3I ratio compared to control in WT cells but not in USP14 KO, indicating specificity of the inhibition. Treatment with Bafilomycin A1 (10nM) alone, and in combination with IU1-47 was used to monitor the autophagic flux. Graph bar represent mean±SEM of N=4 independent experiments. **(D,E)** Western Blot analysis and corresponding quantifications (right) of PINK1 KO (D) and PARK2 KO (E) iNeurons treated with 10µM IU1-47 for 24H. Treatment with Bafilomycin A1 (10nM) alone, and in combination with IU1-47 was used to monitor the autophagic flux. Graph bars represent Mean±SEM of N≥4 independent experiments.

Inhibition of USP14 induces mitophagy in iNeurons

Our results fully support the hypothesis of a proteostatic effect of USP14 inhibition in iNeurons, which specifically affects the mitochondrial proteome (**Figure 2**), and involves the activation of autophagy in a PINK1/Parkin independent fashion (**Figure 3**). What about mitophagy? The importance of PINK1/Parkin-dependent mitophagy in neuronal cells is controversial, this is due to the fact that PINK1 and PARK2 KO mouse models do not display a clear impairment of the mitophagic flux [181], and studies in neurons using flux reporters are still scarce[5]. However, in 2020 Kumar et al., using the mitophagic reporter mito-Keima, demonstrated that basal mitophagy is impaired in DA neurons derived from PARK2 KO hESCs and from iPSCs of patients with Parkin mutations[156]. Also, in 2020 Ordureau et al. showed that the mitophagy flux can be measured in post-mitotic cells like neurons and that stress-induced mitophagy in iNeurons is PINK1-dependent[21]. Based on these studies, and to evaluate basal mitophagy in iNeurons upon USP14 inhibition, we took advantage of a new mitophagy flux reporter developed by Ordureau et al. [21] called mtx-QC^{XL}. mtx-QC^{XL} is a matrix-targeted mCherry- GFP protein that undergoes quenching of the GFP moiety upon acidification in the lysosome but retains mCherry fluorescence, allowing the flux to be examined microscopically (**Figure 4A**). These constructs were stably introduced into engineered hESCs (WT, PINK1 KO, and PARK2 KO) **(Figure S4A)**. We differentiated hESCs of the indicated genotype (WT, PARK2 KO, and PINK1 KO) into iNeurons as previously described, and we treated them with IU1-47 (5-10 µM – 24H). As a positive control for mitophagy induction, iNeurons were treated with 0,5µM antimycinA/0,5µM oligomycin for 24H (AO, sub-threshold depolarization). Mitophagy flux was assessed using live-cell imaging evaluating the presence of mCherry-positive puncta in mtx-QC^{XL}. WT iNeurons displayed a significantly

increased mitophagy flux upon USP14 inhibition with IU1-47 in a concentration-dependent way; interestingly, this increase is comparable with the one obtained upon stress-induced mitophagy with AO **(Figure 4B, quantified in 4E)**. As previously reported, we also found that in PARK2 KO iNeurons, stress-induced mitophagy triggered by AO treatment was almost completely abolished, while an enhancement of mitophagy was observed upon IU1-47 treatment (5-10 µM – 24H) **(Figure 4C, quantified in 4E)**. Similar results were obtained in the PINK1 KO background, in which we see a clear trend towards increased mitophagy upon USP14 inhibition, which needs to be consolidated with additional biological replicates **(Figure 4D, quantified in 4E)**.

To summarize, USP14 inhibition enhances mitophagy in human neurons in a PINK1/Parkin-independent fashion.

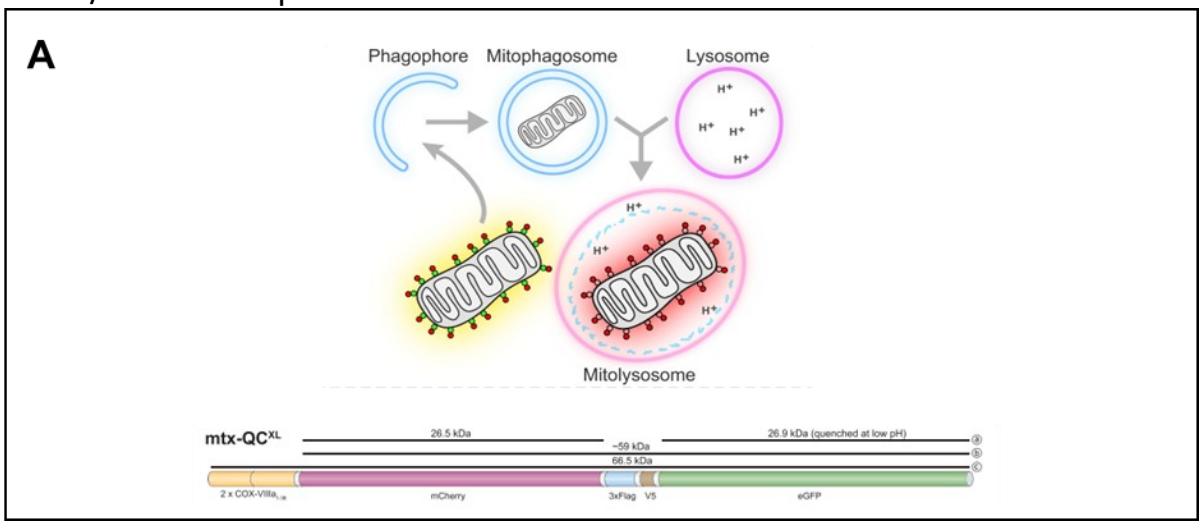

(Figure 4 continues on next page)

Figure 4. USP14 inhibition enhances mitophagy in iNeurons (A) Scheme of the mitophagic flux assay mitoQC (see text for details). Schematic representation of the flux reporter construct (below). mtx-QCXL contains COXVIII mitochondrial targeting sequences, mCherry, and GFP. **(B,C)** Representative confocal images of (B) WT and (C) PARK2 KO iNeurons expressing mtx-QCXL treated with 5µM and 10µM IU1-47 for 24H or 0.5 µM antimycin A/0.5 µM oligomycin (sub-threshold depolarization) for 24H, and imaged for mCherry (red) and GFP (green) signal. ROIs of the quantified mitolysosome are depicted in yellow (GFP and mCherry channel) and in white (merge) **(D)** Representative images of PINK1 KO iNeurons expressing mtx-QCXL treated with IU1-47 as indicated and imaged for mCherry (red) and GFP (green) signal. ROIs of the quantified mitolysosome are depicted in yellow (GFP and mCherry channel) and in white (merge). **(E)** Quantification of the mitophagic flux of WT, PARK2 KO and PINK1 KO iNeurons (as described in Material and Methods) Dots represent biological replicates. For each replicate, N≥10 images per treatment were analyzed. Error bars represent Mean±SEM.

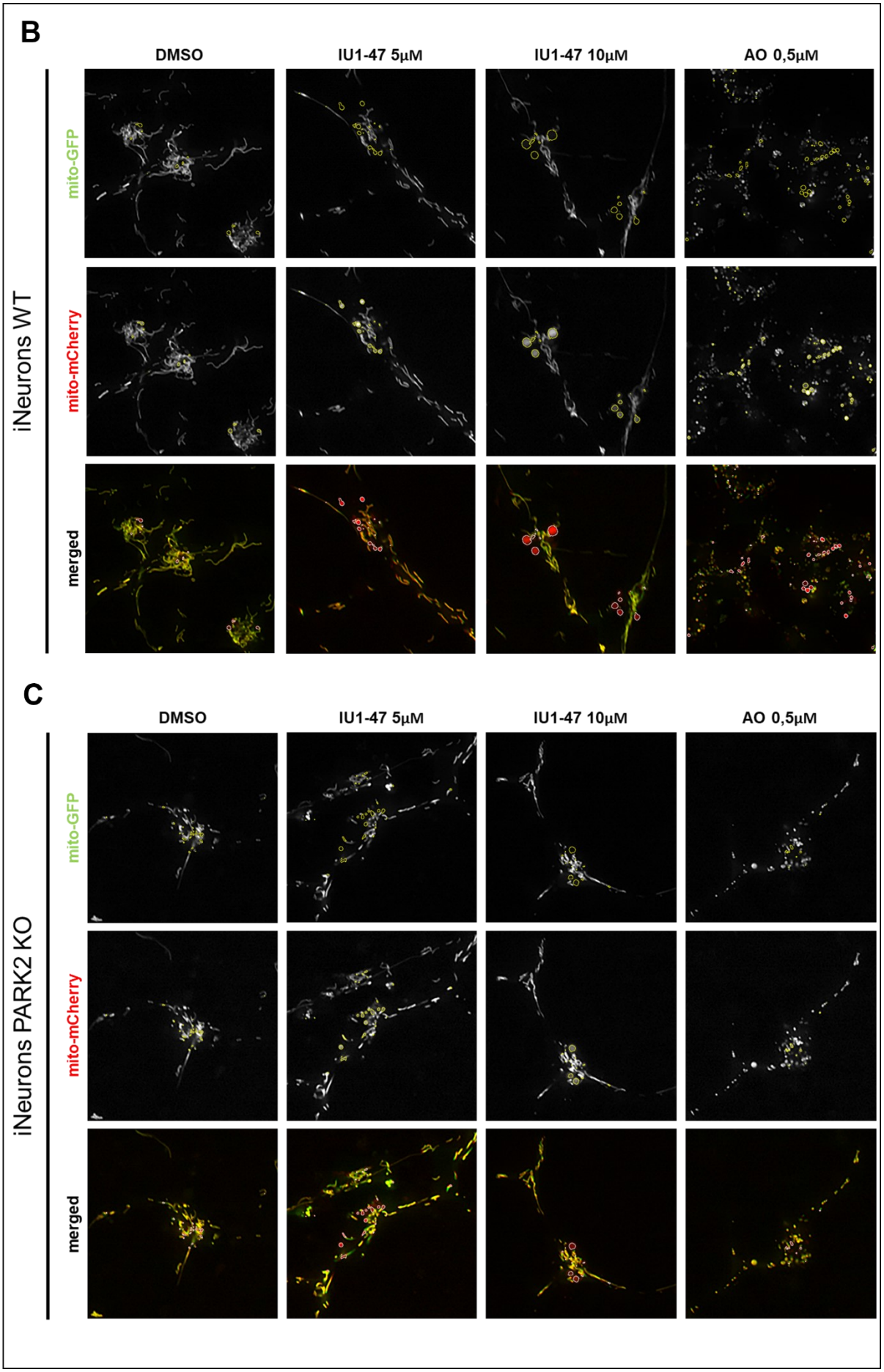
B
DMSO
IU1-47 5µM
IU1-47 10µM
AO 0,5µM
iNeurons WT
mito-GFP
mito-mCherry
merged
C
DMSO
IU1-47 5µM
IU1-47 10µM
AO 0,5µM
iNeurons PARK2 KO
mito-GFP
mito-mCherry
merged

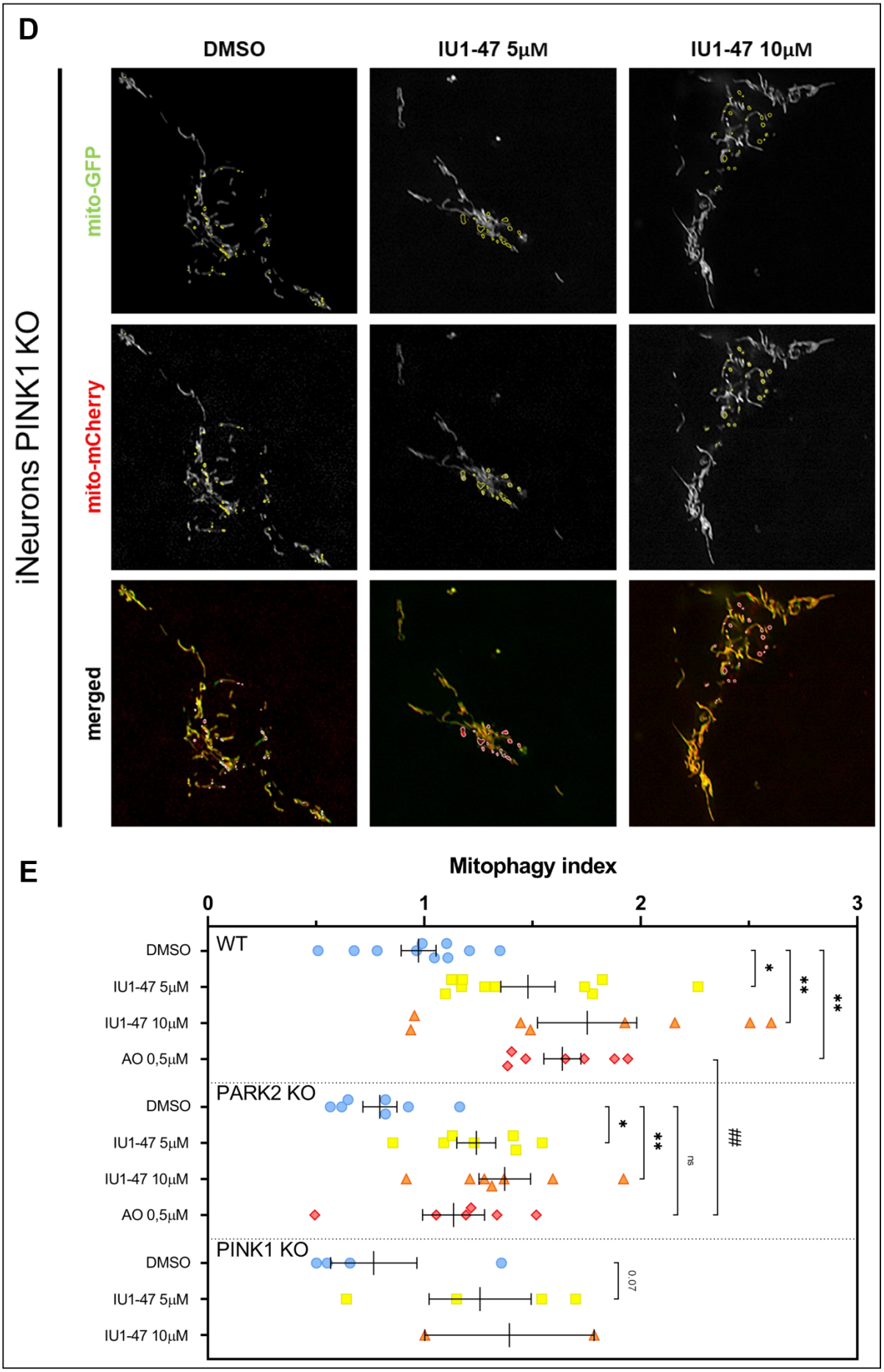
D
DMSO
IU1-47 5µM
IU1-47 10µM
iNeurons PINK1 KO
mito-GFP
mito-mCherry
merged
E
Mitophagy index
0
1
2
3
WT
DMSO
IU1-47 5µM
IU1-47 10µM
AO 0,5µM
PARK2 KO
DMSO
IU1-47 5µM
IU1-47 10µM
AO 0,5µM
PINK1 KO
DMSO
IU1-47 5µM
IU1-47 10µM
*
**
**
*
**
ns
##
0.07

IU1-47 induced autophagy is MARCH5-dependent

Our data indicate the existence of a yet uncharacterized mitophagic pathway that is activated upon USP14 inhibition, which does not operate via the canonical PINK1/Parkin pathway. Thus, in order to explore the molecular mechanism leading to the mitophagic effect of USP14 inhibition, we took advantage of different hESCs cell lines lacking specific mitophagy receptors and/or regulators, namely BNIP3L/NIX KO, MUL1 KO, and MARCH5 KO. BNIP3L/NIX is an autophagic receptor that localizes on mitochondria and has been identified by several studies as a key regulator of PINK1/Parkin independent mitophagy induced by iron chelation (DFP), hypoxia[189], and organelle remodeling during differentiation[113]. MUL1, is a multifunctional mitochondrial membrane protein that acts as an E3 ubiquitin ligase that binds, ubiquitinates, and degrades Mfn2[190] and as a SUMO E3 ligase towards Drp1 to regulate mitochondrial fission[191]. Mul1 can also regulate Parkin-independent mitophagy even though the mechanism is still elusive[192,193], and it acts as an early checkpoint to suppress neuronal mitophagy, under mild stress, by degrading Mfn2 and enhancing ER-Mito coupling[194]. Finally, MARCH5 (also named MITOL) is a mitochondrially localized RING finger E3 ubiquitin ligase involved in mitochondrial dynamics, ubiquitinating different mitochondrial substrates such as Fis1, Mfn1, Mfn2, and MiD49[138]. MARCH5 regulates hypoxia-induced mitophagy through ubiquitination of mitophagy receptor FUNDC1[136], thus placing it at the crossroad between regulation of mitochondrial dynamics and quality control (**Figure 5A**). We found these proteins to be valid candidates as possible regulators of the mitophagic effect of USP14 inhibition. For this reason, we differentiated iNeurons from BNIP3L/NIX KO, MUL1 KO and MARCH5 KO hESCs, treated them with IU1-47 (5-10µM – 24H), and evaluated autophagy. As before, we used bafilomycin (10nM-24H) as a control to monitor the

autophagic flux. We found that IU1-47 induces autophagy in BNIP3L/NIX KO (**Figure 5B**) and MUL1 KO neurons (**Figure 5C**), while this was not the case in MARCH5 KO background (**Figure 5D**).

In summary, these results indicate that USP14 inhibition may act on autophagy (and potentially on mitophagy) in a MARCH5-dependent way.

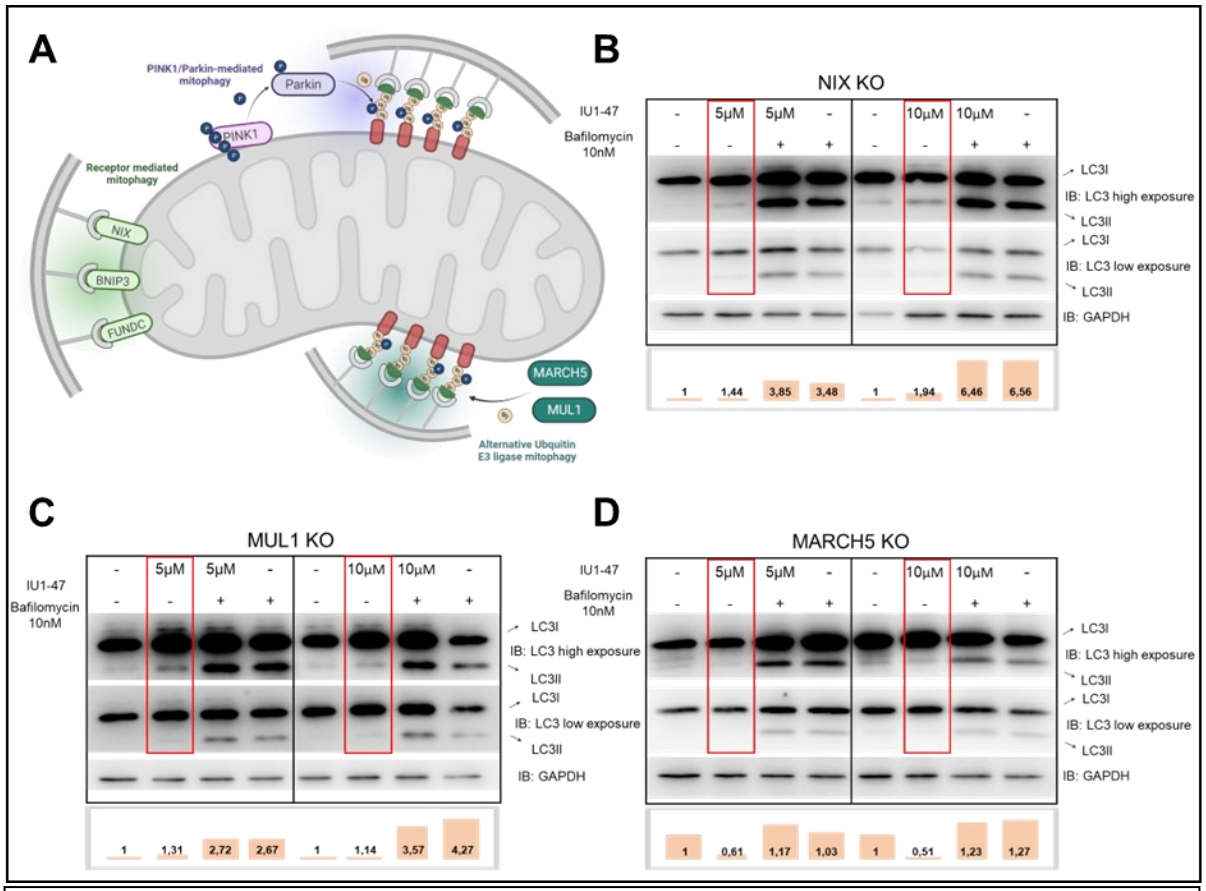

Figure 5. USP14-mediated autophagy is MARCH5-dependent (A) Picture depicts different mitophagy pathways with specific focus on the localization and potential role of NIX, MUL1 and MARCH5. **(B-D)** Western Blot analysis and corresponding quantification (graph bar below) of **(B)** NIX KO, **(C)** MUL1 KO, and **(D)** MARCH5 KO iNeurons treated with 5 and 10 μM IU1-47 for 24H. Treatment with Bafilomycin A1 (10nM) alone, and in combination with IU1-47 was used as control to monitor the autophagic flux. N=2 independent experiments.

USP14 inhibition rescues mitochondrial respiratory defects of PARK2 KO iNeurons

The observation that USP14 inhibition promotes proteostasis by enhancing the autophagic flux and mitophagy, points to a potential beneficial effect of USP14 inhibition in models in which accumulation of misfolded proteins and dysfunctional mitochondria is implicated. Thus, after establishing that we can induce PINK1/Parkin-independent mitophagy through USP14 inhibition, we sought to understand if this enhanced mitochondrial turnover is beneficial for the overall fitness of PARK2 KO neurons, which develop aberrant mechanisms of proteostasis[156,195]. To this aim, we measured mitochondrial respiration in WT and PARK2 KO iNeurons using Seahorse XF24 Flux Analyzer (Agilent Technologies, USA). We found a significant reduction in the Respiratory Control Ratio (RCR) of Parkin-deficient neurons compared to WT, confirming the results of Kumar et al. in DA neurons [156]. Treatment with IU1-47 (5µM– 24H) rescued the impaired mitochondrial phenotype of PARK2 KO iNeurons, while it did not have a significant impact on the respiration of WT cells **(Figure 6A)**. A similar trend was also found for PINK1 KO iNeurons; however, neither the respiration impairment nor the rescue was found to be significant in this genotype **(Figure S5A)**. To consolidate this finding, we also evaluated mitochondrial membrane potential using MitoCMXRos, a membrane potential-dependent probe, in conjunction with TOMM20 immunostaining. We found a 32% reduction in mitochondrial membrane potential in PARK2 KO iNeurons compared to WT that was completely recovered upon IU1-47 treatment (5µM – 24H) **(Figure 6B)**.

In conclusion, we were able to demonstrate that the mitochondrial defects of Parkin KO iNeurons can be rescued upon inhibition of USP14 with specific inhibitor IU1-47. The inhibitor seems to be completely benign in WT background.

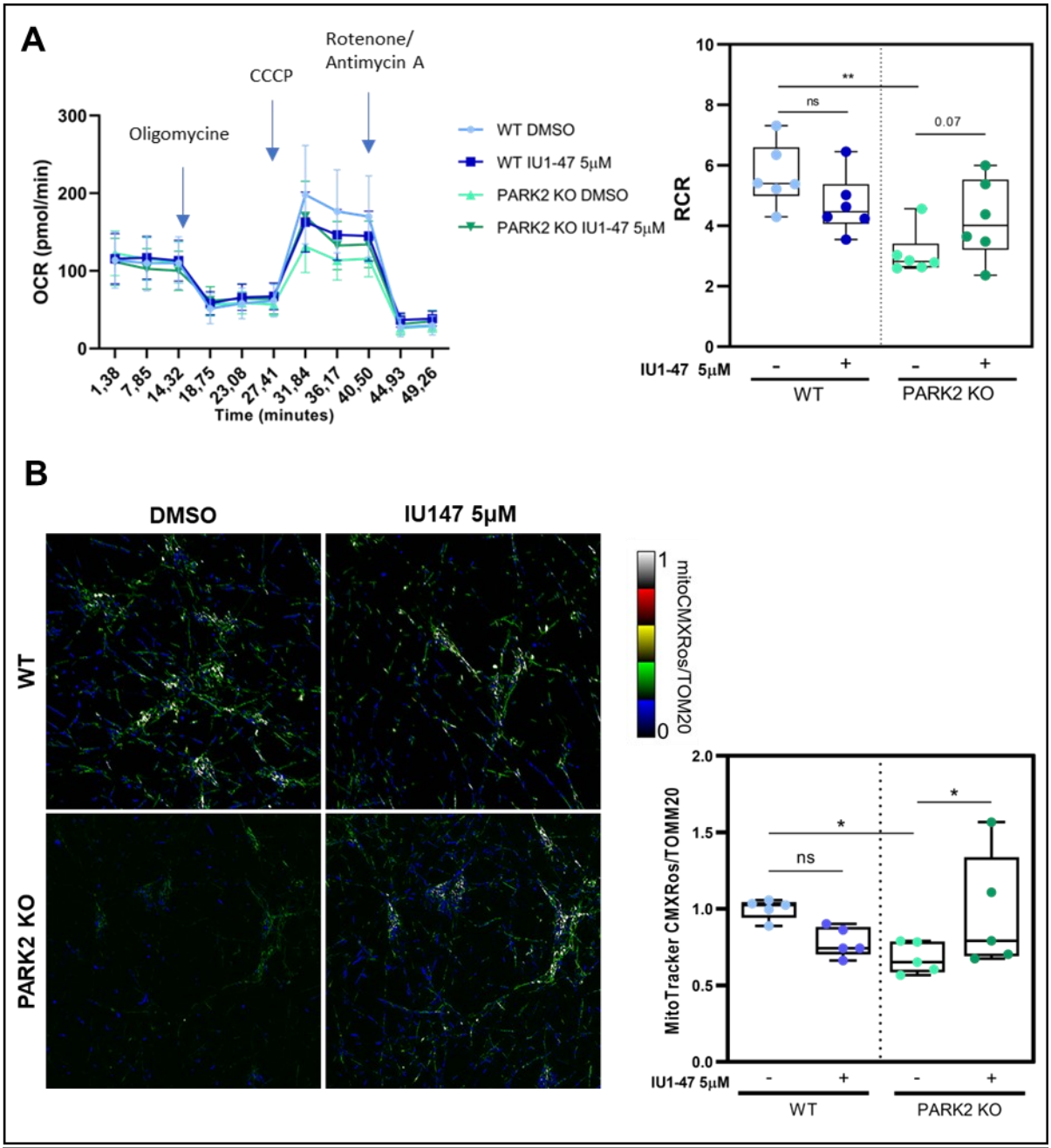

Figure 6. IU1-47 driven mitophagy rescues the mitochondrial phenotype of PARK2 KO iNeurons **(A)** (Left) Plot showing mitochondrial oxygen consumption rate measurements (OCR) of WT and PARK2 KO iNeurons treated with 5µM IU1-47 for 24H. OCR measurements were performed using the Seahorse XFe24 using the indicated treatments. (Right) Corresponding quantification of respiratory control ratio (RCR) calculated as State 3/ State 4. Each dot represents one independent experiment (N=6). Box plot represents Mean±SEM. One-way ANOVA with multiple comparisons was used to compare the RCR. **(B)** (Left) Immunofluorescence staining of mitochondrial marker Tom20 and MitoTracker Red CMXRos in WT and PARK2 KO iNeurons, treated with 5µM IU1-47 for 24H. Images represent fluorescence ratio (MitoTracker Red CMXRos/Tom20) between the two probes with representative colors depicted in the colored scale bar. (Right) Corresponding quantification of MitoTracker Red CMXRos/Tom20 intensity ratio. Each dot represents one independent experiment (N=5). Box plot represents Mean±SEM. One-way ANOVA with multiple comparisons was used to compare the RCR.

Discussion and conclusions

Loss of mitochondrial homeostasis and consequent accumulation of dysfunctional mitochondria is emerging as one of the main features in the pathogenesis of neurodegenerative disorders[5]. The maintenance of mitochondrial homeostasis is controlled by a series of interconnected pathways defined as mitochondrial quality control (MQC). MQC is regulated by different mechanisms that include the degradation of misfolded mitochondrial proteins by the mitochondrial proteases (the so-called mitochondrial unfolded protein response-mtUPR), delivery of mitochondrial particles to the lysosomes by mitochondria-derived vesicles (MDVs), mitochondrial fission and fusion, mitochondrial biogenesis, and ultimately degradation of the entire organelle via mitochondrial autophagy or mitophagy[4]. In many of these processes, the activation of the ubiquitin-proteasome system (UPS) is crucial. Moreover, a fundamental factor in the regulation of both the UPS and mitophagy is ubiquitination, which bridges the two processes by acting as a signal for degradation of single proteins or entire organelles[6]. Therefore, regulators of protein ubiquitination have started to be recognized as attractive candidates in the development of drugs to target the neurodegeneration process[100].

Among the regulators of protein ubiquitination, deubiquitinating enzymes (DUBs) are particularly attractive thanks to their capacity to fine-tune the ubiquitination status of proteins through the removal of ubiquitin chains from their surface[183]. One interesting DUB in this context is USP14, which regulates both UPS and autophagy[11,15,16]. USP14 inhibition is protective in different models of neurodegeneration; it enhances clearance of intracellular protein aggregates such as tau protein, ataxin-3, TDP-43, and α-synuclein[18,187]. Moreover, a previous study performed in our lab showed how inhibition of this DUB promotes basal mitophagy in SH-Sy5y cells and fibroblasts from PD patients,

while genetic and pharmacological ablation of USP14 activity *in vivo* corrects mitochondria dysfunction and locomotion impairment of PINK1/Parkin *D.melanogaster* model of PD, presumably by enhancing mitochondrial proteostasis[19].

Studies directed to the restoration of mitophagy in neuronal models are still scarce; for this reason, starting from the previous results obtained in the lab[19], we decided to evaluate the potential "mitophagic" effect of USP14 inhibition in human neurons. To do so, we took advantage of a recently generated line of hESCs, able to rapidly differentiate functional iNeurons within two weeks[20,21] (Figure 1). The choice of this model over others is particularly relevant in the study of mitophagy correlation with neurodegenerative disease; in fact, due to their peculiar architecture, high energetic demands, and post-mitotic state, neurons are particularly vulnerable to the impairment of mitochondrial homeostasis.

The selective inhibition of USP14 was obtained thanks to the use of a small-molecule inhibitor recently developed in Finley lab, IU1-47, which derives from the same family of IU1, the inhibitor used in our previous study. The new compound is tenfold more potent, has a lower $IC_{50,}$ and, more importantly, is orally bioavailable and able to cross the BBB, both important features for its potential use for clinical purposes[171]. We started by investigating the toxicity of this molecule in our cell model using a cell proliferation assay, which revealed that doses up to 10 µM are not toxic for neuronal cells. This is in line with other studies where IU1-47 was used at similar concentrations on hippocampal and cortical murine primary neurons[18,196]. Once established the proper concentration to treat iNeurons, we sought to use an unbiased approach to evaluate the effect of USP14 inhibition on the total proteome of these cells. Samples treated with different concentrations of IU1-47 (5-10 µM) were

compared with their untreated counterpart using TMT-based proteomics. The results revealed a general decrease of mitochondrial mass in the sample treated with the inhibitor, affecting all three mitochondrial sub-compartments (OMM, IMM, and Matrix). This was specific for mitochondria because other organelles, such as the ER, Golgi, and peroxisomes, were not altered by the treatment, thus indicating that USP14 inhibition specifically led to mitochondrial autophagy (Figure 3). GO analysis confirmed these results and, in line with previous literature, highlighted the role of USP14 inhibition in multiple neurodegenerative diseases[187]. The same analysis was performed comparing WT and USP14 KO iNeurons; however, the results obtained with the genetic ablation of USP14 do not completely recapitulate the ones obtained with the pharmacological inhibition of USP14 in that the downregulation of mitochondrial proteins in USP14 KO background is less pronounced (Figure S2E,F) and there is no upregulation of the lysosomal compartment (Figure S2G). These findings are corroborated by EM images and Western Blot analysis, in which we did not observe a basal upregulation of autophagy in this background. Our hypothesis is that USP14 KO iNeurons have developed some kind of compensatory mechanism to cope with the continuous activation of selective mitochondrial autophagy that might be too demanding for neuronal survival. To corroborate, using a genetic approach, the results obtained with the pharmacological inhibition of USP14, in the future we are planning to generate inducible USP14 knockdown hESCs lines to overcome the limitations of the stable knockout line.

Despite the informative results obtained from this analysis, we were not able to identify a specific mitochondrial target of USP14 deubiquitylation activity, as no mitochondrial protein showed a drastic drop in its abundance. This was also confirmed by immunoblotting analysis of different mitochondrial resident

proteins in neurons and SH-Sy5y cells, which were found unaltered upon USP14 inhibition (data not shown). Since the maintenance of a healthy mitochondrial population requires both the clearance and the biogenesis of newly generated functional mitochondria, the coordination between mitophagy and mitochondrial biogenesis is essential for mitochondria homeostasis, especially in high metabolic-demanding cells like neurons[177]. Thus, we speculate that USP14 inhibition possibly enhances both these aspects of MQC, and if this is true, degradation of specific mitochondrial proteins target of USP14 might be masked by the simultaneous activation of biogenesis. Further studies are needed to investigate this aspect of USP14-mediated MQC regulation in neuronal cells.

To corroborate the results obtained from the proteomic analysis, we next used a combination of biochemical and imaging approaches to evaluate the mitophagic effect of USP14 inhibition. Firstly, since mitophagy is considered a selective type of autophagy, we evaluated the autophagic flux in iNeurons upon USP14 inhibition. The ability of USP14 to regulate autophagy has been illustrated by several studies; however, there is still an open debate regarding the "direction" of this regulation. Indeed some groups demonstrated that USP14 inhibition induces autophagy[15–17] while another showed that it blocks the autophagic flux, delaying autophagosome-lysosome fusion[173]. Our data agree with the former, showing a robust and selective induction of autophagy with IU1-47 treatment not associated with a blockage of the flux as shown by the comparison with the Bafilomycin-treated samples used as control (Figure 3). Of note, IU1-47-mediated enhancement of autophagy was also found in PINK1 and Parkin KO background, thus indicating that the autophagic effect of USP14 inhibition is PINK1/Parkin independent. PINK1 and Parkin are two fundamental proteins because they lay at the interface between mitophagy and

neurodegenerative diseases, PD in particular. Mutations on PINK1 and PARK2 genes are the main cause of genetic forms of PD[153,197], moreover the PINK1/Parkin pathway is the most dissected stress-induced mitophagy pathway. The importance of PINK1/Parkin-dependent mitophagy in neuronal cells is controversial, and this is because PINK1 KO and PARK2 KO mouse models do not display a clear impairment of the mitophagy flux[181], and studies in neurons using flux reporters are still scarce. However, a recent study showed that mitochondrial stress mimicked by exhaustive exercise or increased mtDNA damage in PINK1 and Parkin KD mice exacerbated their inflammation status, generating PD-like phenotypes including loss of dopaminergic neurons and motor defects[154]. These findings suggest that in pathogenic conditions, the alteration of the PINK1/Parkin pathway, in conjunction with additional stimuli such as protein aggregation and inflammation, hallmarks of neurodegeneration, exacerbates the accumulation of dysfunctional mitochondria and may contribute to dopaminergic neurons' demise[198]. Our results indicate that USP14 inhibition boosts autophagy in a PINK1/Parkin-independent fashion, but what about mitophagy? Our mass spec data indicates that the autophagy we observe is specifically targeted to mitochondria, supporting the hypothesis of a specific "mitophagic" effect of USP14 inhibition. To validate this deduction, we took advantage of a probe specifically created to measure the mitophagy flux, the mtx-QC^{XL}. In mtx-QC^{XL} expressing iNeurons, IU1-47 treatment was able to enhance mitophagy in a concentration-dependent way in WT cells, and more importantly, this effect was replicated in PARK2 KO and PINK1 KO genetic backgrounds. The fact that USP14 inhibition enhances mitophagy regardless of PINK1/Parkin expression is particularly relevant because it indicates that we are looking at a mechanism that exploits alternative mitophagy pathways and can

potentially benefit patients with loss-of-function mutations in one of these two genes.

In the attempt to uncover the alternative mechanism of action through which USP14 inhibition enhances mitophagy, we pointed our attention to some known mitophagy regulators such as BNIP3L/NIX[113,189], a mitochondrial-localized autophagic receptor and MUL1[192–194] and MARCH5[136,138], E3 ubiquitin ligases resident on the OMM. Treating iNeurons, knock-out for each of these proteins, with IU1-47, we found that induction of autophagy is MARCH5-dependent, suggesting the same conditional relationship for mitophagy. However, further work to specifically analyse the mitophagy flux, is needed to support the hypothesis of a MARCH5-mediated mitophagic effect of USP14 inhibition.

Finally, as our ultimate aim is to find a way to enhance alternative mitophagy pathway(s) with the long-term perspective to translate the results in the clinical field, it was important for us to understand if the mitophagy boost has an actual impact on the general fitness of the mitochondrial network in neurons. In this context, we found that IU1-47 significantly ameliorates mitochondrial respiration and membrane potential in PARK2 KO iNeurons, with little impact on WT cells. In the future, we aim to confirm these results in PINK1 KO background and possibly move to an *in vivo* approach. This will be possible also thanks to the current availability of new, more potent, and selective inhibitors of USP14 developed by pharmaceutical companies interested in the potential application in the field of both neurodegenerative diseases and cancer treatment.

Supplemental Information

Supplementary Figure S1. Relevant to Figure 1

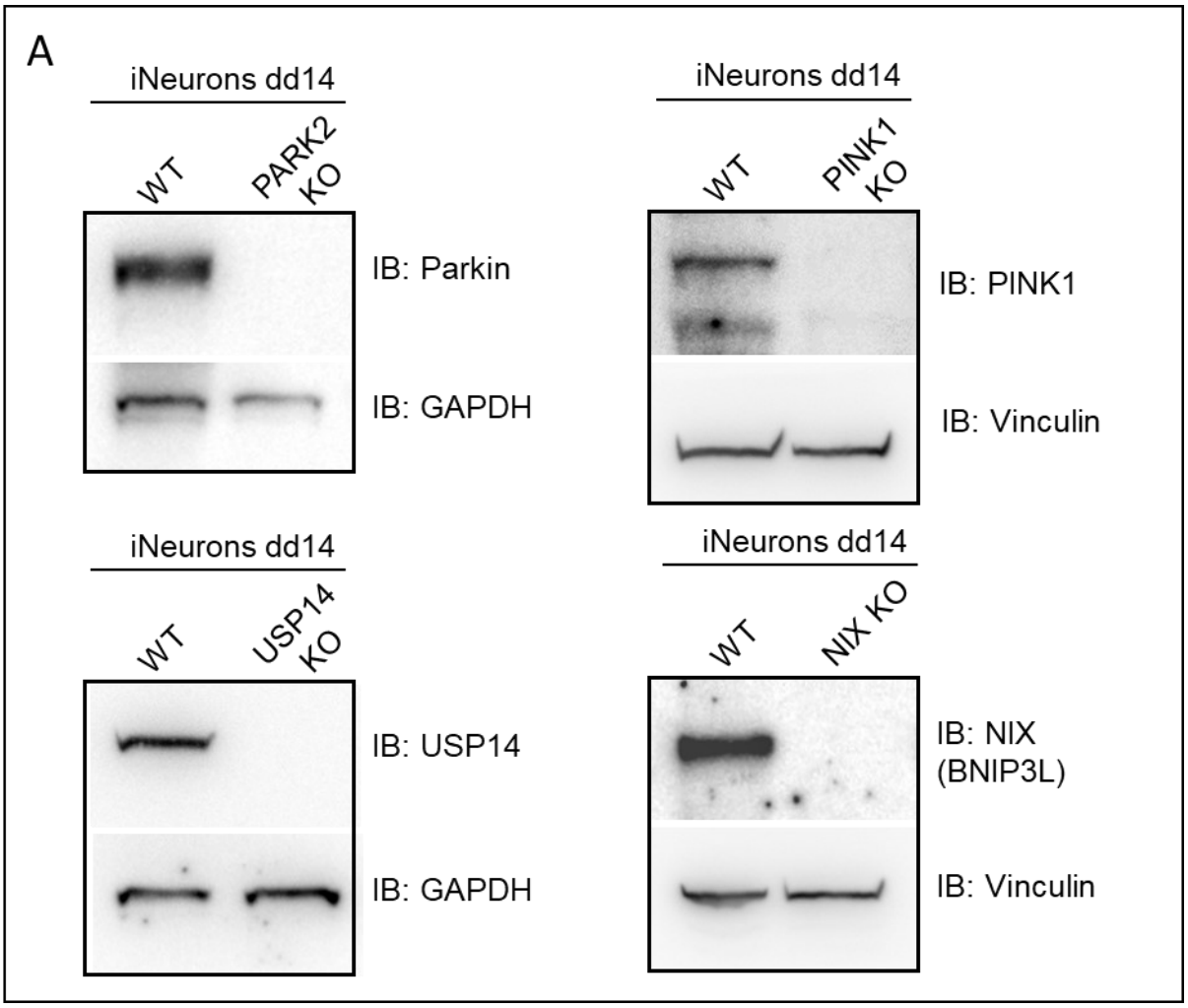

Figure S1. (A) Immunoblot analysis of different KO cell lines used in the paper. Cell lysate of iNeurons, 14 days post induction, were subjected to WB analysis to verify genotype.

Supplementary Figure S2. Relevant to Figure 2 (legend on next page)

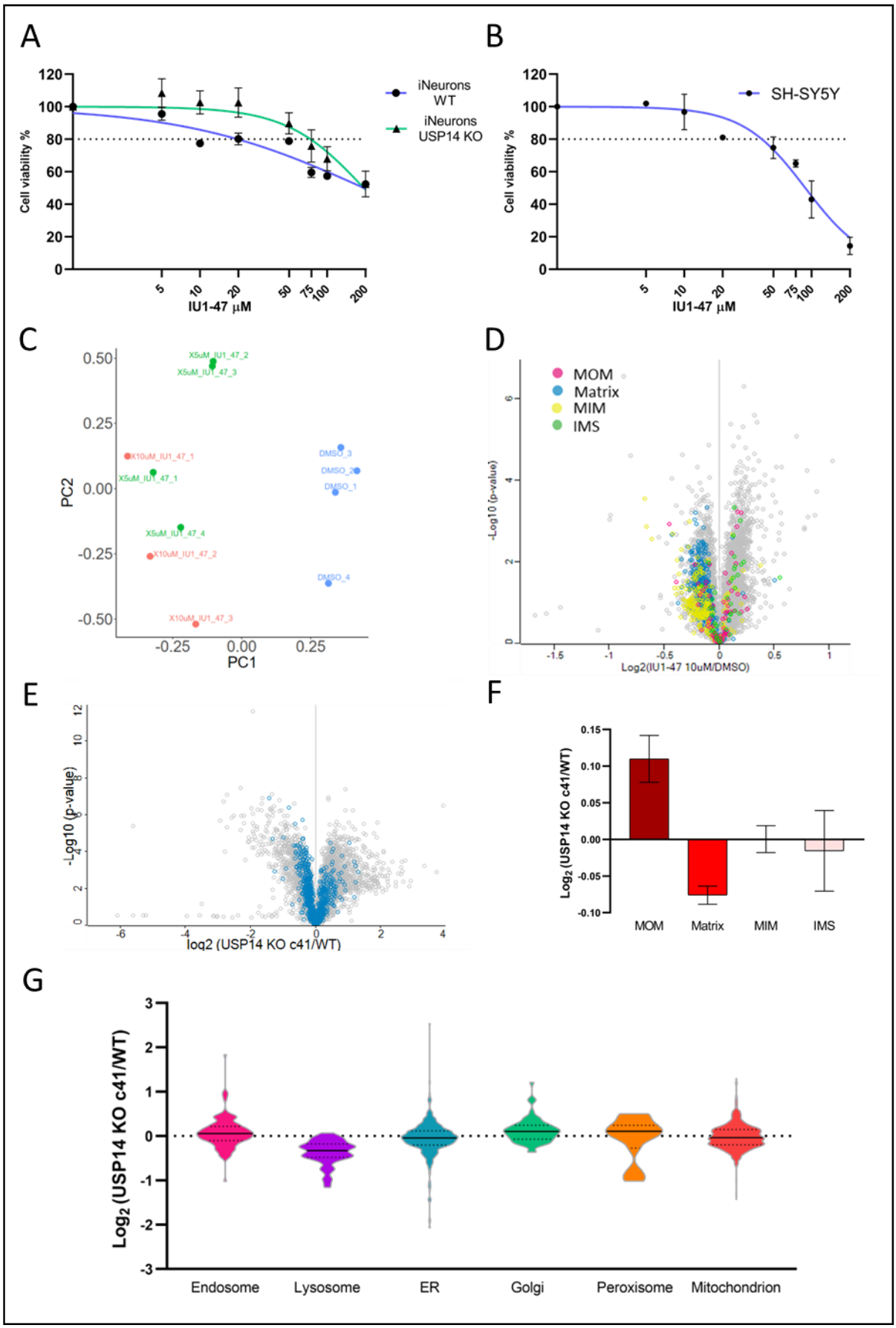

Figure S2. (A) WT and USP14 KO iNeurons were treated with increasing concentration of IU1-47 (0-200μM) and cell survival was assessed with the MTT assay. Results are reported as a cell survival curve. N=3 independent experiments. Error bars represent Mean±SEM. **(B)** SH-Sy5Y cells were treated with increasing concentration of IU1-47 (0-200μM) and cell survival was assessed with the MTT assay. Results are reported as a cell survival curve. Doses >50 μM reduce cell viability, whereas doses up to 20 μM have little or no effect on cell viability (>80% cell survival). N=3 independent experiments. Error bars represent Mean±SEM. **(C)** PCA analysis for for ~8000 proteins quantified by TMT proteomics in individual replicates for the experiment outlined in Figure 2A. **(D)** Volcano plots representing the abundance of the 8018 proteins quantified by TMT proteomics of the WT iNeurons treated with 10μM IU1-47 for 24H compared with untreated cells (DMSO). Mitochondrial proteins (identified by comparison with MitoCarta 3.0[208]) are represented with colored dots based on their reported mitochondria localization: OMM proteins (magenta), matrix proteins (blue), IMM proteins (yellow), IMS proteins (green). **(E)** Volcano plots representing the abundance of the ~8000 proteins quantified by TMT proteomics of USP14 KO iNeurons compared to WT iNeurons. Mitochondrial proteins (identified by comparison with MitoCarta 3.0[208]) are represented with blue colored dots. **(F)** Distribution of changes in protein abundance for proteins that localize in the mitochondria matrix, the IMM, or the OMM in USP14 KO iNeurons treated compared to WT iNeurons. **(G)** Distribution of changes in protein abundance for proteins that localize in individual organelles or protein complexes in USP14 KO iNeurons compared to WT iNeurons.

Supplementary Figure S3. Relevant to Figure 3 (continue on next page)

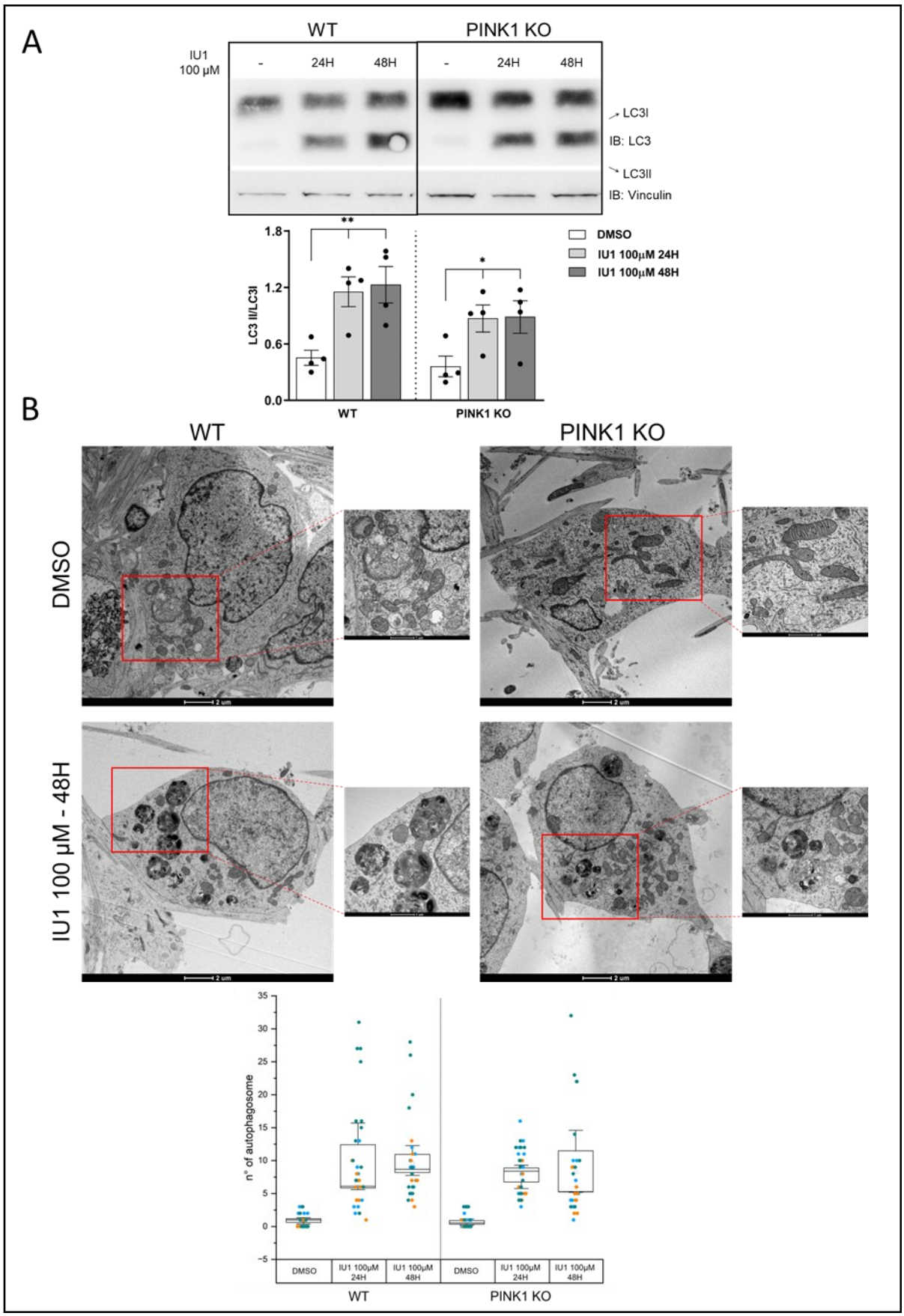

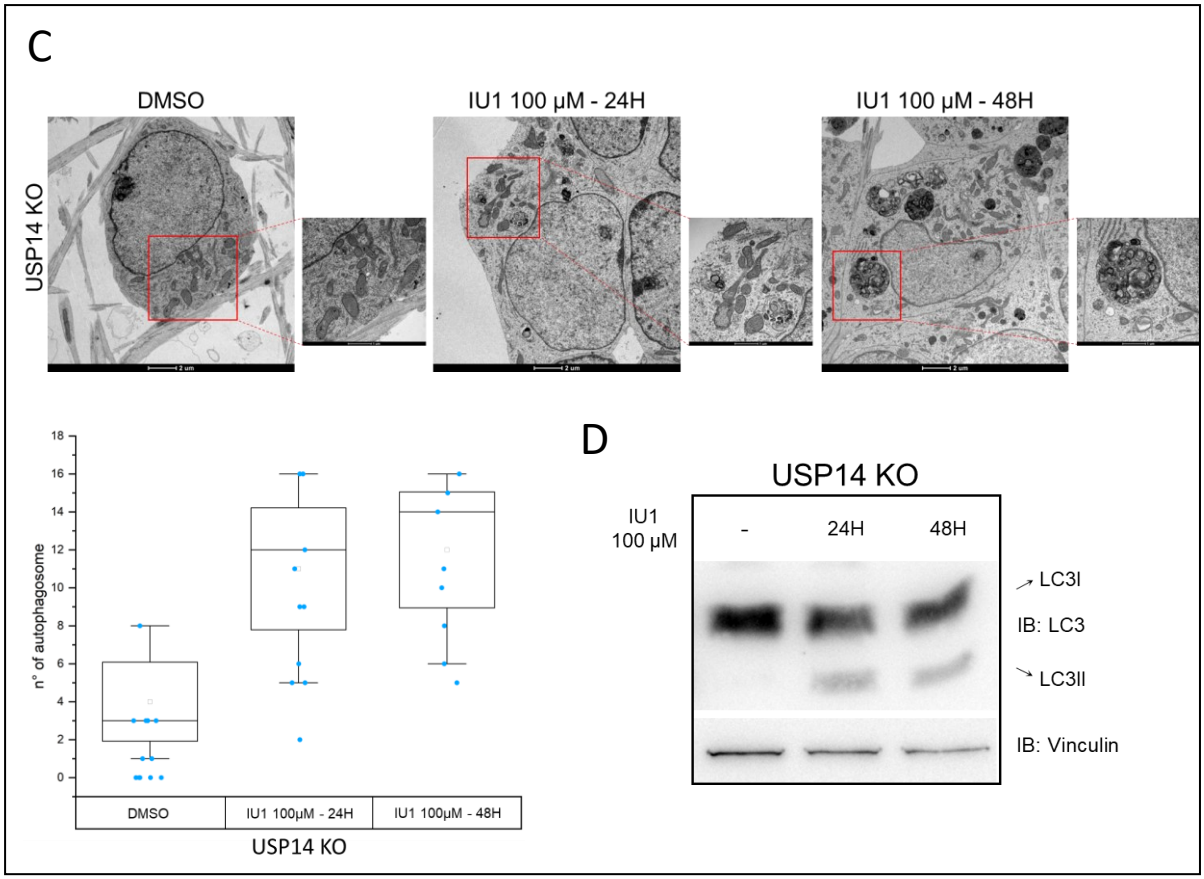

Figure S3. (A) Western Blot analysis and corresponding quantifications of WT and PINK1 KO iNeurons treated with 100 µM IU1 for 24Hand 48H. Treated samples display a significant increase of LC3II:LC3I ratio compared to control. Graph bars represent mean±SEM. N=4 independent experiments. **(B)** (up) Representative EM images of WT and PINK1 KO iNeurons treated with 100 µM IU1 for 48H. Scale bar are represented in each image. (down) Corresponding quantification of # of autophagosome (down) counted in each cell of WT and PINK1 KO iNeurons treated with 100 µM IU1 for 24H and 48H. Box plot represent mean±SEM. N=3 independent experiments. **(C)** (up) Representative EM images of USP14 KO iNeurons treated with 100 µM IU1 for 24H and 48H. Scale bar are represented in each image. (down) Corresponding quantification of # of autophagosome (down) counted in each cell of USP14 KOiNeurons treated with 100 µM IU1 for 24H and 48H. Box plot represent mean±SEM. N=1 independent experiments. **(D)** Western Blot analysis of USP14 KO iNeurons treated with 100 µM IU1 for 24Hand 48H. Treated samples display a significant increase of LC3II:LC3I ratio compared to control.

Supplementary Figure S4. Relevant to Figure 4

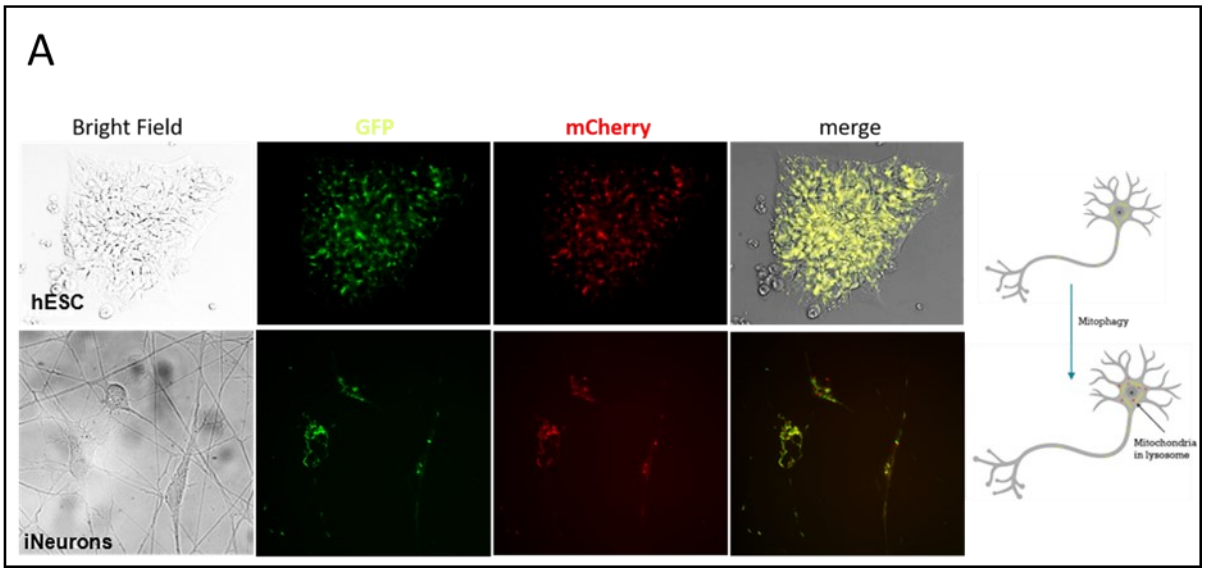

Figure S4. (A) Representative images of stable H9-hESCs expressing mtx-QCXL. Expression is maintained after differentiation. GFP(green), mCherry (red), Brightfield (grey).

Supplementary Figure S5. Relevant to Figure 6

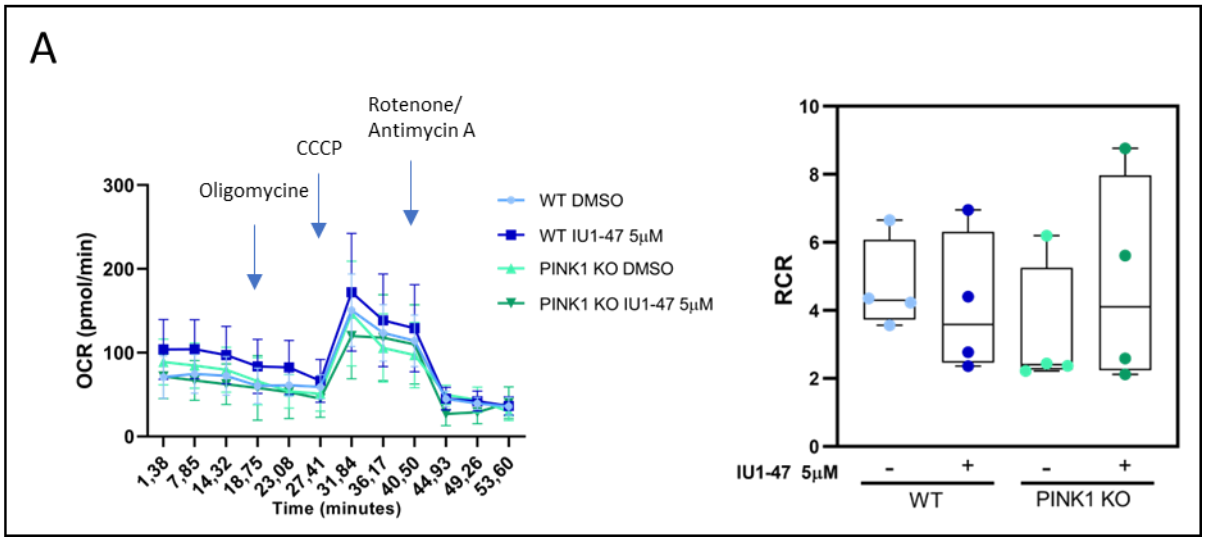

Figure S5. (A) (Left) Plot showing mitochondrial oxygen consumption rate measurements (OCR) of WT and PINK1 KO iNeurons treated with 5µM IU1-47 for 24H. OCR measurements were performed using the Seahorse XFe24 using the indicated treatments. (Right) Corresponding quantification of respiratory control ratio (RCR) calculated as State 3/ State 4. N=4 independent experiments represented by dots. Box plot represents Mean±SEM.

Materials and methods

All details and catalogue numbers can be found in the Materials Table.

Cell culture and iNeurons differentiation

H9 hESCs (WiCell Institute) were cultured in TeSR™-E8™ medium (StemCell Technologies) on Matrigel (Corning) -coated tissue culture plates with daily medium change. Cells were passaged every 4-5 days with 0.5 mM EDTA in DMEM/F12 (Sigma). Introduction of the TRE3G-NGN2 insert into the AAVS1 site, necessary for iNeurons differentiation, and gene editing to obtain the desired mutants (PINK1 KO, Parkin KO, USP14 KO, MUL1 KO, MARCH5 KO, and BNIP3L KO) was performed by the gene editing core facility in the Dept of Cell Biology at HMS. The cells were kindly provided by our collaborators Prof. Dan Finley (Harvard Medical School, Department of Cell Biology) and Prof. Wade Harper (Harvard Medical School, Department of Cell Biology). Details on the gene editing methods can be found in previously published studies by Harper's lab [20,21,113]. For H9 hESCs conversion to iNeurons, cells were treated with Accutase (Thermo Fisher Scientific) and plated on Matrigel-coated tissue plates in DMEM/F12 supplemented with 1x N2, 1x NEAA (Thermo Fisher Scientific), human brain-derived neurotrophic factor (BDNF, 10 ng/ml, PeproTech), human Neurotrophin-3 (NT-3, 10 ng/l, PeproTech), human recombinant laminin (0.2 mg/ml, Life Technologies), Y-27632 (10 mM, PeproTech) and Doxycycline (2 mg/ml,Sigma-Aldrich) on Day 0. On Day 1, Y-27632 was withdrawn. On Day 2, medium was replaced with Neurobasal medium supplemented with 1x B27 and 1x Glutamax (Thermo Fisher Scientific) containing BDNF, NT-3 and 2 mg/ml Doxycycline. Starting on Day 4, half of the medium was replaced every other day thereafter. On Day 7, the cells were treated with Accutase (Thermo Fisher Scientific) and plated on Matrigel-coated tissue plates. Doxycycline was

withdrawn on Day 10. Treatments and experiments were performed between day 11 and 13.

Generation of stable mitophagic flux reporters hESC lines

H9 hESC harbouring the mitochondrial matrix mCherry-GFP flux reporter were generated by transfection of $1x10^5$ cells with 1µg pAC150-PiggyBac-matrix-mCherry-eGFPXL (Harper's lab) and 1µg pCMV- HypBAC-PiggyBac-Helper (Sanger Institute) in conjunction with the transfection reagent FuGENE HD (Promega). The cells were selected and maintained in TeSR™-E8™ medium supplemented with 200 mg/ml Hygromycin (Thermo Fisher Scientific). Hygromycin was kept in the medium during differentiation to iNeurons.

Compounds and treatments

Cells were treated in the corresponding cell culture medium. USP14 inhibition was performed using IU1-47 inhibitor (Sigma Aldrich) for 24 hours at different final concentrations depending on the experiment. Antimycin 0,5 µM/Oligomycin 0,5 µM (Sigma Aldrich) were used in combination as a positive control to induce stress mediated. The late-stage autophagy inhibitor Bafilomycin A (Sigma Aldrich) was used at a final concentration of 10nM as a control for the blockage of the autophagic flux. DMSO was used for control condition.

Immunoblotting

At the indicated times, hES cells or iNeurons were washed on ice with 1xPBS, harvested and pellet was resuspended in RIPA buffer (140mM NaCl; 65mM Tris-HCl pH 7,4; 1% NP-40; 0,25% NaDeoxycholate, 1mM EDTA, 1x protease Inhibitor Cocktail, 1xPhosSTOP phosphatase inhibitor cocktail). Resuspended cell lysates

were incubated on ice for 30 min, vortexed every 10 min and debris pelleted at 20.000 rcf for 15 min. Protein concentration was determined by BCA assay according to manufacturer's instructions (Thermo Fisher Scientific). 30 µg of proteins were resuspended in 1xLDS with 100mM DTT and boiled for 10 min at 95°C. Equal amount of protein and volume were loaded and run on homemade 15% Tris-glycine SDS-Polyacrylamide gels (for LC3I and II detection) or on 4%-20% Bis-Tris ExpressPlus™ PAGE Gels (GenScript). Gels were run respectively in 1x Tris-Glycine Running Buffer (25mM Tris; 192 mM Glycine; 0,1% SDS; pH 8,3) or 1xTris-MOPS-SDS Running buffer (GenScript) for 5 minutes at 70 V, and then run at 130 V for the required time. Gels were transferred via semi-dry Trans Blot Turbo transfer system (BioRad) for 30 min at 25V onto PVDF membrane for immunoblotting. PVDF membrane were blocked for 1 hour at RT in 5% BSA in TTBS (0.5 M Tris-HCl pH 7,4; 1,5 M NaCl; Tween 20 0,05%(v/v)) and subsequently incubated with the desired primary antibody diluted in 1% BSA in TTBS overnight at 4°C. For detection, membranes were washed 3-4 times for 10' with TTBS and then incubated 1h at room temperature with polyclonal horseradish-peroxidase (HRP)-conjugated secondary antibodies followed by 3 TTBS washes. Immunoreactivity was detected with Luminata Forte Western HRP substrate (Sigma Aldrich) and images were acquired using the ImageQuant LAS 4000 instrument (GE Healthcare). Images from Western Blots were exported and analysed using ImageJ/FiJi[199].

MTT cell viability assay

To assess cytotoxicity and cell tolerance upon treatment with the IU1-47 inhibitor, we used the 3-(4,5-dimethylthiazol-2yl)-2,5-diphenyltetrazolium bromide (MTT) tetrazolium assay (Thermos Fisher Scientific). This is a colorimetric assay that measures cellular metabolic activity as an indicator of

cell viability, proliferation and cytotoxicity. To perform this assay, 3000 cells were seeded on 96-well plates and then treated with different concentration (5, 10, 20, 50, 75, 100, 200 µM) of IU1-47 for 24 hours. After 24 hours, 10 µL of MTT solution (12 mM, Thermo Fisher Scientific) was added to each well and the plate was incubated at 37º C for 4 hours. The formazan crystal formed were subsequently dissolved with 50 µL DMSO per well and the absorbance at 560 nm was acquired after an incubation of 10 min at 37°C using a multi-well spectrophotometer.

RealTime qPCR

Total RNA was extracted from the cells using ReliaPrep RNA Cell Miniprep isolation kit (Promega). RNA was quantified using Nanodrop spectrophotometer, 500 ng of total RNA was used to synthesize cDNA in 20 µl reaction mix using SensiFast cDNA synthesis kit (Meridian Life Science) according to the manufacturer's protocol. HOT FIREPol SolisGreen qPCR mix (Solis BioDyne) was used for real-time PCR with the following conditions: 95°C 10 min/40 cycles (95°C 15 sec, 60°C 1 min). Dissociation curve was generated for checking the amplification specificity. All the samples were run in triplicate and negative controls without cDNA were run each time together with the samples for both internal control and gene of interest. The data were analyzed by comparative CT method[200] to determine fold differences in expression of target genes with respect to the internal control.

Measurement of Oxygen Consumption Rate (Sea Horse assay)

OCR was measured using a Seahorse XFe24 (Agilent Technologies) running Wave Controller Software 2.6 according to manufacturer's manual. 3,5 x 10^4 iNeurons were plated in Matrigel-coated Seahorse XF24 V7 PS cell culture microplates

(Agilent) in appropriate growth or differentiation medium at day 7 of differentiation. The day before the assay cells were treated with 5µM IU1-47 for 24 hours. On day of assay, cell culture medium was removed stepwise with DMEM Base (Sigma Aldrich) supplemented with 31,8 mM NaCl, 1mM sodium pyruvate, 10 mM Glucose, 2mM L-glutamine, 5mM HEPES and equilibrated for 30 min-1hour at 37°C. All assays and drug dilutions were performed in this media. Measurements were taken for a total for 50 minutes, in 3 min periods with mixing and incubation intervals between treatments. After measurement of baseline respiration, 1,5µM oligomycin was added in a single injection, mixed, and followed by 3 measurements. This step was repeated after the injection of 1,5µM CCCP and 1µM Antimycin A + 1µM Rotenone. Protein concentration per well was determined using a BCA kit after lysis in RIPA buffer and used as normalization for OCR measurements.

PROTEOMICS

Proteomics – general sample preparation

Sample preparation of proteomic analysis of whole-cell extract from iNeurons was performed according to previously published studies [113,201,202]. Flash frozen cell pellets were lysed in 8M urea buffer (8M urea, 150 mM NaCl, 50 mM HEPES pH 7.5, 1x protease Inhibitor Cocktail, 1xPhosSTOP phosphatase inhibitor cocktail). Lysates were clarified by centrifugation at 17,000 x g for 15 min at 4°C. Protein concentration of the supernatant was quantified by BCA assay according to manufacturer's instructions. To reduce and alkylate cysteines, 150 µg of protein was sequentially incubated with 5mM TCEP for 30 mins, 14 mM iodoacetamide for 30 mins, and 10 mM DTT for 15 mins. All reactions were performed at RT. Next, proteins were chloroform-methanol precipitated and the pellet resuspended in 200 mM EPPS pH 8.5. Then, the protease LysC (Wako) was

added at 1:100 (LysC:protein) ratio and incubated overnight at RT. The day after, samples were further digested for 5 hours at 37ºC with trypsin at 1:75 (trypsin:protein) ratio. Both digestions were performed in an orbital shaker at 1,500 rpm. After digestion, samples were clarified by centrifugation at 17,000 x g for 10 min. Peptide concentration of the supernatant was quantified using a quantitative colorimetric peptide assay (Thermo Fisher Scientific).

Proteomics – quantitative proteomics using TMT

Tandem mass tag labeling of each sample was performed using the TMT-11plex kit (Thermo Fisher Scientific)[20,21,113,201]. Briefly, 25 µg of peptides was brought to 1 µg/µl with 200 mM EPPS (pH 8.5), acetonitrile (ACN) was added to a final concentration of 30% followed by the addition of 50µg of each TMT reagents. After 1 h of incubation at RT, the reaction was stopped by the addition of 0.3% hydroxylamine (Sigma) for 15 min at RT. After labelling, samples were combined, desalted with tC18 SepPak solid-phase extraction cartridges (Waters), and dried in the SpeedVac. Next, desalted peptides were resuspended in 5% ACN, 10 mM NH 4 HCO 3 pH 8 and fractionated in a basic pH reversed phase chromatography using a HPLC equipped with a 3.5 µm Zorbax 300 Extended-C18 column (Agilent). Fractions were collected in a 96-well plate, then combined into 24 samples. Twelve of them were desalted following the C18 Stop and Go Extraction Tip (STAGE-Tip) and dried down in a SpeedVac. Finally, peptides were resuspended in 1% formic acid, 3% ACN, and analyzed by LC-MS3 in an Orbitrap Fusion Lumos (Thermo Fisher Scientific) mounted with FAIMS and running in HR-MS^2 mode[203].

Proteomics – data analysis

A suite of in-house pipeline (GFY-Core Version 3.8, Harvard University) was used to obtain final protein quantifications from all RAW files collected. RAW data were converted to mzXML format using a modified version of RawFileReader

(5.0.7) and searched using the search engine Comet[204] against a human target-decoy protein database (downloaded from UniProt in June 2019) that included the most common contaminants. Precursor ion tolerance was set at 20 ppm and product ion tolerance at 0.02 Da. Cysteine carbamidomethylation (+57.0215 Da) and TMT tag (+229.1629 Da) on lysine residues and peptide N-termini were set as static modifications. Up to 2 variable methionine oxidations (+15.9949 Da) and 2 miss cleavages were allowed in the searches. Peptide-spectrum matches (PSMs) were adjusted to a 1% FDR with a linear discriminant analysis[205] and proteins were further collapsed to a final protein-level FDR of 1%. TMT quantitative values we obtained from MS2 scans. Only those with a signal-to-noise ratio >100 and an isolation specificity > 0.7 were used for quantification. Each TMT was normalized to the total signal in each column. Quantifications are represented as relative abundances. RAW files will be made available upon request. Enrichment of GO-terms (CC, Cellular Component and KEGG pathways) was performed using DAVID Functional Annotation Tool[206]. For these analyses, all proteins significantly (p-value>0,05) up-or downregulated between WT and treated cells. The annotation list for the subcellular localization of organellar protein markers was derived from previously published high confidence HeLa dataset[207]; “high” and “very high” confidence. MitoCarta 3.0[208] was used for mitochondrial annotation. Figures were generated using a combination of Excel, Perseus (v1.6.5)[209], GraphPad Prism (v8.0), and SRplot (https://www.bioinformatics.com.cn/en).

MICROSCOPY

Live-cell confocal microscopy for mitophagic flux analysis

For quantitative mtx-QC(mCherry-GFP)^{XL} flux analysis iNeurons were plated onto µ-Slide 8 well ibiTreat (Ibidi) on day 7 of the differentiation. On day 11-12,

the cells were treated with IU1-47 (5-10μM) or Antimycin A (0,5 μM) and Oligomycin (0,5 μM) for 24H. Cell were imaged using the laser spinning disk confocal iMIC-Andromeda imaging workstation (TILL Photonics, Graefelfing, Germany) equipped with UPlanSApo 60X/1.35 objective lens. Images for mCherry and eGFP were collected sequentially using 561 nm and 488 nm solid state lasers and emission collected with 615/20 and 525/39 filters, respectively. Consistent laser intensity and exposure time were applied to all the samples, and brightness and contrast were adjusted equally by applying the same minimum and maximum display values in FiJi software[199].

Image Quantitation: For each condition, 5 Z-stacks (0,2 μm increments) were acquired for each channel and a minimum of 10 image sections were taken with a 60x objective lens and analyzed using Fiji software[199]. All the sections were included for the analysis except the cells that showed lower GFP-mCherry expression levels compared to the average fluorescent intensity. Step 1) Following z-projection stack and background subtraction, a threshold (Otsu) was applied for each channel to create two binary images (green mask and red mask). Step 2) Binary images were subtracted (red mask – green mask) resulting in a binary image of “red only puncta” representing the mitolysosomes. The "Analyze Particles..." command (pixel size exclusion: 0.2-exclude edge objects) was used to measure the total puncta number puncta and mean area for each image. The number of cells present in each image was counted manually. Step 3) Mitophagy index was calculated for each image applying the following equation: [(n° of mitolysosome/n° of cells) x mean area of mitolysosomes]. The average value for each replicate in each condition was normalized by the average value obtained from replicates of the untreated condition.

Immunocytochemical analysis

hESCs or iNeurons were plated on 13 mm round glass coverslips. For membrane potential assessment the cells were treated with IU1-47 (5-10µM) or Antimycin A (0,5 µM) and Oligomycin (0,5 µM) for 24H on day 11 and stained with 50 nM MitoTracker RED CMX Ros (Thermo Fisher Scientific) for 30 minutes before fixation. The iNeurons were fixed in 4% PFA in PBS for 15 min at room temperature, permeabilized with 0.1% Triton X-100 in 1xPBS/0,05% Tween20 for 15 min at RT and blocked for 1 hour at RT in 4% BSA in 1xPBS/0,05% Tween20. Anti-MAP2 antibody (Cell Signaling), anti-β3 tubulin antibody (Cell Signaling), anti-OCT3/4 antibody (SIGMA), anti-SOX2 antibody (Santa Cruz) and anti-TOM20 antibody (Santa Cruz) were diluted at 1:200 in 1xPBS/0,05% Tween20 and 1% BSA and applied overnight at 4°C. Secondary antibodies (Thermo Fisher Scientific) were diluted at 1:400 in 1xPBS/0,05% Tween20 and 1% BSA and applied for 1h at room temperature. Coverslip were mounted on cover slides using Moviol mounting medium.

Cells were imaged using the laser spinning disk confocal iMIC-Andromeda imaging workstation (TILL Photonics, Graefelfing, Germany) equipped with UPlanSApo 60X/1.35 objective lens. Images were collected using 561 nm and 488 nm solid state lasers and emission collected with 615/20 and 525/39 filters,respectively according to the secondary antibody used in the experiment. Consistent laser intensity and exposure time were applied to all the samples, and brightness and contrast were adjusted equally by applying the same minimum and maximum display values in FiJi software[199].

Transmission electron microscopy

Samples were fixed with 2.5% glutaraldehyde in 0.1M sodium cacodylate buffer pH 7.4 ON at 4°C. The samples were postfixed with 1% osmium tetroxide plus potassium ferrocyanide 1% in 0.1M sodium cacodylate buffer for 1 hour at 4°.

After three water washes, samples were dehydrated in a graded ethanol series and embedded in an epoxy resin (Sigma- Aldrich). Ultrathin sections (60-70nm) were obtained with an Ultrotome V (LKB) ultramicrotome, counterstained with uranyl acetate and lead citrate and viewed with a Tecnai G2 (FEI) transmission electron microscope operating at 100 kV. Images were captured with a Veleta (Olympus Soft Imaging System) digital camera.

Statistical analysis

Data are presented as mean ± SEM from at least three independent experiments. Exact number of replicates (N) is indicated for each experiment in the figure legend. Statistical significance was determined using unpaired t-test, or multiple comparison test (One-way or Two-way ANOVA), and p-values are indicated (GraphPad Prism 8 software).

Materials Table

REAGENTS	SOURCE	IDENTIFIER
Antibodies		
anti-LC3A	Novus Biologicals	Cat#NB100-2331
anti-GAPDH	Sigma Aldrich	Cat#G9545-100ul
anti-Vinculin	Sigma Aldrich	Cat#V9264-25ul
anti-SOX2	Sigma Aldrich	Cat#AB5603-25ug
anti-OCT3/4	Santa Cruz Biotechnology	Cat#sc-5279
anti-β3 Tubulin	Thermo Fisher Scientific	Cat#MA1-118
anti-MAP2	Cell Signaling Technology	Cat#4542S
anti-Parkin	ABclonal	Cat#A0968
anti-PINK1	Novus Biologicals	Cat#BC100-494
anti-BNIP3L	Sigma-Aldrich	Cat#HPA015652
anti-USP14	Cell Signaling Technology	Cat#11931
anti-TOM20	Santa Cruz Biotechnology	Cat#sc-11415
Anti-Rabbit IgG (H+L), HRP Conjugate	Fisher Scientific	Cat#NA934V
Anti-Mouse IgG (H+L), HRP Conjugate	Fisher Scientific	Cat#NXA931V
Alexa Fluor 488 Goat anti-mouse	Thermo Fisher Scientific	Cat#A10667
Alexa Fluor 488 Goat anti-rabbit	Thermo Fisher Scientific	Cat#A11034
Alexa Fluor 555 Goat anti-mouse	Thermo Fisher Scientific	Cat#A21147
Alexa Fluor 555 Goat anti-rabbit	Thermo Fisher Scientific	Cat#A21430
Chemicals		
Oligomycin A	Sigma Aldrich	Cat#O4876
Antimycin A	Sigma Aldrich	Cat#A8674
CCCP	Sigma Aldrich	Cat#C2759
Rotenone	Sigma Aldrich	Cat#R8875
Bafilomycin A	Sigma Aldrich	Cat#B1793
Doxycycline	Sigma Aldrich	Cat#D9891
Y-27632 Dihydrochloride (ROCK inhibitor)	PeproTech	Cat#1293823
Hygromycin B	Thermo Fisher Scientific	Cat#10687-010
Corning Matrigel Matrix, Growth Factor Reduced	Corning	Cat#354230
MitoTracker RED CMX Ros	Thermo Fisher Scientific	Cat#M7512
IU1	Sigma Aldrich	Cat#I1911
IU1-47	Sigma Aldrich	Cat#SML2240
DMEM/F12	Thermo Fisher Scientific	Cat#31331028
Neurobasal	Thermo Fisher Scientific	Cat#21103049
NEAA	Thermo Fisher Scientific	Cat#11140-035
GlutaMax	Thermo Fisher Scientific	Cat#35050038
N-2 Supplement (100X)	Thermo Fisher Scientific	Cat#17502-048
Neurotrophin-3(NT3) Recombinant human	PeproTech	Cat#450-03
Brain-derived neurotrophic factor (BDNF)	PeproTech	Cat#450-02
B27 Supplement	Thermo Fisher Scientific	Cat#17504044
Accutase	Thermo Fisher Scientific	Cat#A1110501
TeSR™-E8™	StemCell Technologies	Cat#5990
EDTA	Thermo Fisher Scientific	Cat#AM9260G
DMEM Base	Sigma Aldrich	Cat#D5030
HOT FIREPol SolisGreen qPCR mix	Solis BioDyne	Cat#08-46-00001

FuGene HD	Promega	Cat#E2311
MTT	Thermo Fisher Scientific	Cat#M6494
1x Protease Inhibitor Cocktail	Thermo Fisher Scientific	Cat#78442
1xPhosSTOP Phosphatase Inhibitor Cocktail	Thermo Fisher Scientific	Cat#78428
Luminata Forte Western HRP substrate	Thermo Fisher Scientific	Cat#WBLUF0500
Commercial assays and kits		Cat#
SensiFast cDNA synthesis kit	Meridian Life Science	Cat#BIO-65054
Pierce BCA Protein assay kits and reagents	Thermo Fisher Scientific	Cat#23227
ReliaPrep RNA Cell Miniprep System	Promega	Cat#Z6011
Seahorse XFe24 FluxPak mini	Agilent Technologies	Cat#102342-100
TMT10plex Isobaric Label Reagent Set plus TMT11-131C Label Reagent	Thermo Fisher Scientific	Cat#A34808
Oligonucleotides and Recombinant DNA		
pCMV-hyPBase – hyperactive piggyBac transposase	Sanger Institute	
pAC150-PBLHL-4xHS-EF1a – mtx-QC(mCherry-GFP)XL	Ordureau et al. 2020	
Primers for OCT3/4	5'-AGAACATGTGTAAGCTGCGG and 5'-GTTGCCTCTCACTCGGTTC	
Primers for Ngn2	5'-TACCTCCTCTTCCTCCTTCA and 5'-GACATTCCCGGACACACAC	
Primers for NeuN	5'-GTAGAGGGACGGAAAATTGAGG and 5'-CATAGAATTCAGGCCCGTAGAC	
Primers for MAP2	5'-CAGGAGACAGAGATGAGAATTCC and 5'-CAGGAGTGATGGCAGTAGAC	
Primers for β3-Tubulin	5'-TTTGGACATCTCTTCAGGCC and 5'-TTTCACACTCCTTCCGCAC	
Primers for GAPDH	5'-GGCCATCCACAGTCTTCTG and 5'-TCATCAGCAATGCCTCCTG	
Primers for Actin	5'-GATCATTGCTCCTCCTGAGC and 5'-ACATCTGCTGGAAGGTGGAC	

REFERENCES

1. WHO. Dementia. (2019). Available at: https://www.who.int/news-room/fact-sheets/detail/dementia.
2. Dhapola, R., Sarma, P., Medhi, B., Prakash, A. & Reddy, D. H. Recent Advances in Molecular Pathways and Therapeutic Implications Targeting Mitochondrial Dysfunction for Alzheimer's Disease. *Mol. Neurobiol.* **59**, 535–555 (2022).
3. Helley, M. P., Pinnell, J., Sportelli, C. & Tieu, K. Mitochondria: A Common Target for Genetic Mutations and Environmental Toxicants in Parkinson's Disease. *Front. Genet.* **8**, 177 (2017).
4. Doxaki, C. & Palikaras, K. Neuronal Mitophagy: Friend or Foe? *Front. Cell Dev. Biol.* **8**, (2021).
5. Lou, G. *et al.* Mitophagy and Neuroprotection. *Trends in Molecular Medicine* **26**, 8–20 (2020).
6. Pohl, C. & Dikic, I. Cellular quality control by the ubiquitin-proteasome system and autophagy. *Science (80-.).* **366**, 818–822 (2019).
7. Dikic, I. Proteasomal and Autophagic Degradation Systems. *Annu. Rev. Biochem.* **86**, 193–224 (2017).
8. Gatica, D., Lahiri, V. & Klionsky, D. J. Cargo recognition and degradation by selective autophagy. *Nat. Cell Biol.* **20**, 233–242 (2018).
9. McWilliams, T. G. & Muqit, M. M. PINK1 and Parkin: emerging themes in mitochondrial homeostasis. *Curr. Opin. Cell Biol.* **45**, 83–91 (2017).
10. Yamano, K., Matsuda, N. & Tanaka, K. The ubiquitin signal and autophagy: an orchestrated dance leading to mitochondrial degradation. *EMBO Rep.* **17**, 300–316 (2016).
11. Nijman, S. M. B. *et al.* A Genomic and Functional Inventory of Deubiquitinating Enzymes. *Cell* **123**, 773–786 (2005).
12. Ristic, G., Tsou, W. L. & Todi, S. V. An optimal ubiquitin-proteasome pathway in the nervous system: The role of deubiquitinating enzymes. *Frontiers in Molecular Neuroscience* **7**, 72 (2014).
13. Kim, H. T. & Goldberg, A. L. The deubiquitinating enzyme Usp14 allosterically inhibits multiple proteasomal activities and ubiquitin-independent proteolysis. *J. Biol. Chem.* **292**, 9830–9839 (2017).

14. Lee, B.-H. *et al.* Enhancement of proteasome activity by a small-molecule inhibitor of USP14. *Nature* **467**, 179–84 (2010).

15. Xu, D. *et al.* USP14 regulates autophagy by suppressing K63 ubiquitination of Beclin. *Genes Dev.* **30**, 1718–1730 (2016).

16. Xu, F. *et al.* Typically inhibiting USP14 promotes autophagy in M1-like macrophages and alleviates CLP-induced sepsis. *Cell Death Dis.* **11**, 666 (2020).

17. Han, K. H. *et al.* USP14 Inhibition Regulates Tumorigenesis by Inducing Autophagy in Lung Cancer In Vitro. *Int. J. Mol. Sci.* **20**, 5300 (2019).

18. Boselli, M. *et al.* An inhibitor of the proteasomal deubiquitinating enzyme USP14 induces tau elimination in cultured neurons. *J. Biol. Chem.* **292**, 19209–19225 (2017).

19. Chakraborty, J. *et al.* USP 14 inhibition corrects an in vivo model of impaired mitophagy. *EMBO Mol. Med.* **10**, 1–17 (2018).

20. Ordureau, A. *et al.* Dynamics of PARKIN-Dependent Mitochondrial Ubiquitylation in Induced Neurons and Model Systems Revealed by Digital Snapshot Proteomics. *Mol. Cell* **70**, 211-227.e8 (2018).

21. Ordureau, A. *et al.* Global Landscape and Dynamics of Parkin and USP30-Dependent Ubiquitylomes in iNeurons during Mitophagic Signaling. *Mol. Cell* **77**, 1124-1142.e10 (2020).

22. Ferraiuolo, L., Kirby, J., Grierson, A. J., Sendtner, M. & Shaw, P. J. Molecular pathways of motor neuron injury in amyotrophic lateral sclerosis. *Nat. Rev. Neurol.* **7**, 616–630 (2011).

23. Wu, Y., Chen, M. & Jiang, J. Mitochondrial dysfunction in neurodegenerative diseases and drug targets via apoptotic signaling. *Mitochondrion* **49**, 35–45 (2019).

24. Wallace, D. C. Mitochondrial diseases in man and mouse. *Science* **283**, 1482–1488 (1999).

25. Palikaras, K., Lionaki, E. & Tavernarakis, N. Coordination of mitophagy and mitochondrial biogenesis during ageing in C. elegans. *Nature* **521**, 525–528 (2015).

26. Aman, Y. *et al.* Enhancing mitophagy as a therapeutic approach for neurodegenerative diseases. *Int. Rev. Neurobiol.* **155**, 169–202 (2020).

27. Zimorski, V., Ku, C., Martin, W. F. & Gould, S. B. Endosymbiotic theory for

organelle origins. *Curr. Opin. Microbiol.* **22**, 38–48 (2014).

28. Giacomello, M., Pyakurel, A., Glytsou, C. & Scorrano, L. The cell biology of mitochondrial membrane dynamics. *Nat. Rev. Mol. Cell Biol.* **21**, 204–224 (2020).

29. Frank, S. *et al.* The Role of Dynamin-Related Protein 1, a Mediator of Mitochondrial Fission, in Apoptosis. *Dev. Cell* **1**, 515–525 (2001).

30. Scorrano, L. *et al.* A distinct pathway remodels mitochondrial cristae and mobilizes cytochrome c during apoptosis. *Dev. Cell* **2**, 55–67 (2002).

31. Gomes, L. C., Di Benedetto, G., Scorrano, L., Benedetto, G. Di & Scorrano, L. During autophagy mitochondria elongate, are spared from degradation and sustain cell viability. *Nat. Cell Biol.* **13**, 589–98 (2011).

32. Wade, S. & Khacho, M. MITOCHONDRIA: Mitochondrial dynamics in the regulation of stem cells. *Int. J. Biochem. Cell Biol.* **144**, 106158 (2022).

33. Vringer, E. & Tait, S. W. G. Mitochondria and cell death-associated inflammation. *Cell Death Differ.* (2022). doi:10.1038/s41418-022-01094-w

34. Bader, V. & Winklhofer, K. F. Mitochondria at the interface between neurodegeneration and neuroinflammation. *Semin. Cell Dev. Biol.* **99**, 163–171 (2020).

35. Lackner, L. L. Determining the shape and cellular distribution of mitochondria: the integration of multiple activities. *Curr. Opin. Cell Biol.* **25**, 471–476 (2013).

36. Kühlbrandt, W. Structure and function of mitochondrial membrane protein complexes. *BMC Biol.* **13**, 89 (2015).

37. Giacomello, M. & Pellegrini, L. The coming of age of the mitochondria–ER contact: a matter of thickness. *Cell Death Differ.* **23**, 1417–1427 (2016).

38. Basso, V. *et al.* Regulation of ER-mitochondria contacts by Parkin via Mfn2. *Pharmacol. Res.* **138**, 43–56 (2018).

39. Cisneros, J., Belton, T. B., Shum, G. C., Molakal, C. G. & Wong, Y. C. Mitochondria-lysosome contact site dynamics and misregulation in neurodegenerative diseases. *Trends Neurosci.* **45**, 312–322 (2022).

40. Shai, N. *et al.* Systematic mapping of contact sites reveals tethers and a function for the peroxisome-mitochondria contact. *Nat. Commun.* **9**, 1761 (2018).

41. Montes de Oca Balderas, P. Mitochondria–plasma membrane interactions and communication. *J. Biol. Chem.* **297**, 101164 (2021).

42. Desai, R. *et al.* Mitochondria form contact sites with the nucleus to couple prosurvival retrograde response. *Sci. Adv.* **6**, (2020).

43. Moore, A. S. & Holzbaur, E. L. Mitochondrial-cytoskeletal interactions: dynamic associations that facilitate network function and remodeling. *Curr. Opin. Physiol.* **3**, 94–100 (2018).

44. Glancy, B., Kim, Y., Katti, P. & Willingham, T. B. The Functional Impact of Mitochondrial Structure Across Subcellular Scales. *Front. Physiol.* **11**, (2020).

45. Kondadi, A. K. *et al.* Cristae undergo continuous cycles of membrane remodelling in a MICOS-dependent manner. *EMBO Rep.* **21**, (2020).

46. Cogliati, S. *et al.* Mitochondrial cristae shape determines respiratory chain supercomplexes assembly and respiratory efficiency. *Cell* **155**, 160–71 (2013).

47. Frezza, C., Cipolat, S. & Scorrano, L. Measuring mitochondrial shape changes and their consequences on mitochondrial involvement during apoptosis. *Methods Mol. Biol.* **372**, 405–20 (2007).

48. Cogliati, S., Enriquez, J. A. & Scorrano, L. Mitochondrial Cristae: Where Beauty Meets Functionality. *Trends Biochem. Sci.* **41**, 261–273 (2016).

49. Judge, A. & Dodd, M. S. Metabolism. *Essays Biochem.* **64**, 607–647 (2020).

50. D. L. Nelson, M. M. C. *Lehninger principles of biochemistry*. (W.H. Freeman, 2017).

51. Chaudhry, R. & Varacallo, M. *Biochemistry, Glycolysis*. *StatPearls* (2022).

52. Melkonian, E. A. & Schury, M. P. *Biochemistry, Anaerobic Glycolysis*. *StatPearls* (2022).

53. Naifeh, J., Dimri, M. & Varacallo, M. *Biochemistry, Aerobic Glycolysis*. *StatPearls* (2022).

54. Wanders, R. J. A., Ruiter, J. P. N., IJlst, L., Waterham, H. R. & Houten, S. M. The enzymology of mitochondrial fatty acid beta-oxidation and its application to follow-up analysis of positive neonatal screening results. *J. Inherit. Metab. Dis.* **33**, 479–494 (2010).

55. Van Der Bliek, A. M., Sedensky, M. M. & Morgan, P. G. Cell biology of the

mitochondrion. *Genetics* **207**, 843–871 (2017).

56. Papa, S. *et al. The oxidative phosphorylation system in mammalian mitochondria*. *Advances in Experimental Medicine and Biology* **942**, (2012).

57. Chan, D. C. Mitochondria: Dynamic Organelles in Disease, Aging, and Development. *Cell* **125**, 1241–1252 (2006).

58. Legros, F., Lombès, A., Frachon, P. & Rojo, M. Mitochondrial fusion in human cells is efficient, requires the inner membrane potential, and is mediated by mitofusins. *Mol. Biol. Cell* **13**, 4343–54 (2002).

59. Smirnova, E., Griparic, L., Shurland, D. L. & Van der Bliek, A. M. Dynamin-related protein Drp1 is required for mitochondrial division in mammalian cells. *Mol. Biol. Cell* **12**, 2245–56 (2001).

60. Palmer, C. S. *et al.* MiD49 and MiD51, new components of the mitochondrial fission machinery. *EMBO Rep.* **12**, 565–73 (2011).

61. James, D. I., Parone, P. A., Mattenberger, Y. & Martinou, J.-C. hFis1, a novel component of the mammalian mitochondrial fission machinery. *J. Biol. Chem.* **278**, 36373–9 (2003).

62. Kasahara, A. & Scorrano, L. Mitochondria: From cell death executioners to regulators of cell differentiation. *Trends in Cell Biology* **24**, 761–770 (2014).

63. Benard, G. & Rossignol, R. Ultrastructure of the mitochondrion and its bearing on function and bioenergetics. *Antioxidants and Redox Signaling* **10**, 1313–1342 (2008).

64. Liu, W. *et al.* Pink1 regulates the oxidative phosphorylation machinery via mitochondrial fission. *Proc. Natl. Acad. Sci. U. S. A.* **108**, 12920–12924 (2011).

65. Kann, O. & Kovács, R. Mitochondria and neuronal activity. *American Journal of Physiology - Cell Physiology* **292**, (2007).

66. Bertholet, A. M. *et al.* Mitochondrial fusion/fission dynamics in neurodegeneration and neuronal plasticity. *Neurobiology of Disease* **90**, 3–19 (2016).

67. Gao, J. *et al.* Abnormalities of mitochondrial dynamics in neurodegenerative diseases. *Antioxidants* **6**, 25 (2017).

68. Misrani, A., Tabassum, S. & Yang, L. Mitochondrial Dysfunction and

Oxidative Stress in Alzheimer's Disease. *Frontiers in Aging Neuroscience* **13**, (2021).

69. Tran, M. & Reddy, P. H. Defective Autophagy and Mitophagy in Aging and Alzheimer's Disease. *Front. Neurosci.* **14**, 1297 (2021).

70. Santos, D. & Cardoso, S. M. Mitochondrial dynamics and neuronal fate in Parkinson's disease. *Mitochondrion* **12**, 428–437 (2012).

71. Delettre, C. *et al.* Nuclear gene OPA1, encoding a mitochondrial dynamin-related protein, is mutated in dominant optic atrophy. *Nat. Genet.* **26**, 207–210 (2000).

72. Züchner, S. *et al.* Mutations in the mitochondrial GTPase mitofusin 2 cause Charcot-Marie-Tooth neuropathy type 2A. *Nat. Genet.* **36**, 449–451 (2004).

73. Ishihara, N. *et al.* Mitochondrial fission factor Drp1 is essential for embryonic development and synapse formation in mice. *Nat. Cell Biol.* **11**, 958–966 (2009).

74. Waterham, H. R. *et al.* A Lethal Defect of Mitochondrial and Peroxisomal Fission. *N. Engl. J. Med.* **356**, 1736–1741 (2007).

75. Course, M. M. & Wang, X. Transporting mitochondria in neurons. *F1000Research* **5**, (2016).

76. Devine, M. J. & Kittler, J. T. Mitochondria at the neuronal presynapse in health and disease. *Nature Reviews Neuroscience* **19**, 63–80 (2018).

77. El Fissi, N. *et al.* Mitofusin gain and loss of function drive pathogenesis in Drosophila models of CMT 2A neuropathy . *EMBO Rep.* **19**, (2018).

78. Baloh, R. H., Schmidt, R. E., Pestronk, A. & Milbrandt, J. Altered axonal mitochondrial transport in the pathogenesis of Charcot-Marie-Tooth disease from mitofusin 2 mutations. *J. Neurosci.* **27**, 422–430 (2007).

79. Wang, X. *et al.* Impaired balance of mitochondrial fission and fusion in Alzheimer's disease. *J. Neurosci.* **29**, 9090–9103 (2009).

80. Wang, X. *et al.* Amyloid-β overproduction causes abnormal mitochondrial dynamics via differential modulation of mitochondrial fission/fusion proteins. *Proc. Natl. Acad. Sci. U. S. A.* **105**, 19318–19323 (2008).

81. Pilling, A. D., Horiuchi, D., Lively, C. M. & Saxton, W. M. Kinesin-1 and dynein are the primary motors for fast transport of mitochondria in Drosophila motor axons. *Mol. Biol. Cell* **17**, 2057–2068 (2006).

82. Schwarz, T. L. Mitochondrial trafficking in neurons. *Cold Spring Harb. Perspect. Biol.* **5**, (2013).

83. Saxton, W. M. & Hollenbeck, P. J. The axonal transport of mitochondria. *J. Cell Sci.* **125**, 2095–104 (2012).

84. López-Doménech, G. *et al.* Loss of Dendritic Complexity Precedes Neurodegeneration in a Mouse Model with Disrupted Mitochondrial Distribution in Mature Dendrites. *Cell Rep.* **17**, 317–327 (2016).

85. Kay, L., Pienaar, I. S., Cooray, R., Black, G. & Soundararajan, M. Understanding Miro GTPases: Implications in the Treatment of Neurodegenerative Disorders. *Molecular Neurobiology* **55**, 7352–7365 (2018).

86. Hsieh, C. H. *et al.* Functional Impairment in Miro Degradation and Mitophagy Is a Shared Feature in Familial and Sporadic Parkinson's Disease. *Cell Stem Cell* **19**, 709–724 (2016).

87. Wang, X. *et al.* PINK1 and Parkin target miro for phosphorylation and degradation to arrest mitochondrial motility. *Cell* **147**, 893–906 (2011).

88. Hernandez, D. G., Reed, X. & Singleton, A. B. Genetics in Parkinson disease: Mendelian versus non-Mendelian inheritance. *Journal of Neurochemistry* **139 Suppl 1**, 59–74 (2016).

89. Shaltouki, A., Hsieh, C. H., Kim, M. J. & Wang, X. Alpha-synuclein delays mitophagy and targeting Miro rescues neuron loss in Parkinson's models. *Acta Neuropathol.* **136**, 607–620 (2018).

90. Lee, S. & Min, K. T. The interface between ER and mitochondria: Molecular compositions and functions. *Mol. Cells* **41**, 1000–1007 (2018).

91. Iijima-Ando, K. *et al.* Loss of Axonal Mitochondria Promotes Tau-Mediated Neurodegeneration and Alzheimer's Disease–Related Tau Phosphorylation Via PAR-1. *PLoS Genet.* **8**, e1002918 (2012).

92. Martinez-Vicente, M. Neuronal mitophagy in neurodegenerative diseases. *Frontiers in Molecular Neuroscience* **10**, (2017).

93. Zhang, Q. *et al.* Role of PGC-1α in Mitochondrial Quality Control in Neurodegenerative Diseases. *Neurochemical Research* **44**, 2031–2043 (2019).

94. Sheng, B. *et al.* Impaired mitochondrial biogenesis contributes to mitochondrial dysfunction in Alzheimer's disease. *J. Neurochem.* **120**, 419–429 (2012).

95. Lee, Y. *et al.* PINK1 Primes Parkin-Mediated Ubiquitination of PARIS in Dopaminergic Neuronal Survival. *Cell Rep.* **18**, 918–932 (2017).

96. Shirendeb, U. P. *et al.* Mutant Huntingtin's interaction with mitochondrial protein Drp1 impairs mitochondrial biogenesis and causes defective axonal transport and synaptic degeneration in Huntington's disease. *Hum. Mol. Genet.* **21**, 406–420 (2012).

97. Dominy, J. E. & Puigserver, P. Mitochondrial biogenesis through activation of nuclear signaling proteins. *Cold Spring Harb. Perspect. Biol.* **5**, (2013).

98. Popov, L. D. Mitochondrial biogenesis: An update. *Journal of Cellular and Molecular Medicine* **24**, 4892–4899 (2020).

99. Uittenbogaard, M. & Chiaramello, A. Mitochondrial Biogenesis: A Therapeutic Target for Neurodevelopmental Disorders and Neurodegenerative Diseases. *Curr. Pharm. Des.* **20**, 5574–5593 (2014).

100. Burtscher, J. *et al.* Boosting mitochondrial health to counteract neurodegeneration. *Prog. Neurobiol.* **215**, 102289 (2022).

101. Rappe, A. & McWilliams, T. G. Mitophagy in the aging nervous system. *Front. Cell Dev. Biol.* **10**, 1–14 (2022).

102. McWilliams, T. G. *et al.* mito-QC illuminates mitophagy and mitochondrial architecture in vivo. *J. Cell Biol.* **214**, 333–345 (2016).

103. Sun, N. *et al.* Measuring In Vivo Mitophagy. *Mol. Cell* **60**, 685–96 (2015).

104. McWilliams, T. G. *et al.* Basal Mitophagy Occurs Independently of PINK1 in Mouse Tissues of High Metabolic Demand. *Cell Metab.* **27**, 439-449.e5 (2018).

105. Lee, J. J. *et al.* Basal mitophagy is widespread in Drosophila but minimally affected by loss of Pink1 or parkin. *J. Cell Biol.* **217**, 1613–1622 (2018).

106. Youle, R. J. & Narendra, D. P. Mechanisms of mitophagy. *Nat. Rev. Mol. Cell Biol.* **12**, 9–14 (2011).

107. Frank, M. *et al.* Mitophagy is triggered by mild oxidative stress in a mitochondrial fission dependent manner. *Biochim. Biophys. Acta* **1823**, 2297–310 (2012).

108. Eiyama, A., Kondo-Okamoto, N. & Okamoto, K. Mitochondrial degradation during starvation is selective and temporally distinct from bulk autophagy in yeast. *FEBS Lett.* **587**, 1787–92 (2013).

109. Wu, H. & Chen, Q. Hypoxia activation of mitophagy and its role in disease pathogenesis. *Antioxid. Redox Signal.* **22**, 1032–46 (2015).

110. Rojansky, R., Cha, M.-Y. & Chan, D. C. Elimination of paternal mitochondria in mouse embryos occurs through autophagic degradation dependent on PARKIN and MUL1. *Elife* **5**, (2016).

111. Al Rawi, S. *et al.* Postfertilization autophagy of sperm organelles prevents paternal mitochondrial DNA transmission. *Science* **334**, 1144–7 (2011).

112. Cairns, G., Thumiah-Mootoo, M., Burelle, Y. & Khacho, M. Mitophagy: A New Player in Stem Cell Biology. *Biology (Basel).* **9**, 1–24 (2020).

113. Ordureau, A. *et al.* Temporal proteomics during neurogenesis reveals large-scale proteome and organelle remodeling via selective autophagy. *Mol. Cell* **81**, 5082-5098.e11 (2021).

114. Esteban-Martínez, L. *et al.* Programmed mitophagy is essential for the glycolytic switch during cell differentiation. *EMBO J.* **36**, 1688 (2017).

115. Sin, J. *et al.* Mitophagy is required for mitochondrial biogenesis and myogenic differentiation of C2C12 myoblasts. *Autophagy* **12**, 369–380 (2016).

116. Lampert, M. A. *et al.* BNIP3L/NIX and FUNDC1-mediated mitophagy is required for mitochondrial network remodeling during cardiac progenitor cell differentiation. *Autophagy* **15**, 1182 (2019).

117. Onishi, M., Yamano, K., Sato, M., Matsuda, N. & Okamoto, K. Molecular mechanisms and physiological functions of mitophagy. *EMBO J.* **40**, (2021).

118. Narendra, D., Tanaka, A., Suen, D.-F. & Youle, R. J. Parkin is recruited selectively to impaired mitochondria and promotes their autophagy. *J. Cell Biol.* **183**, 795–803 (2008).

119. Matsuda, N. *et al.* PINK1 stabilized by mitochondrial depolarization recruits Parkin to damaged mitochondria and activates latent Parkin for mitophagy. *J. Cell Biol.* **189**, 211–21 (2010).

120. Narendra, D. P. *et al.* PINK1 is selectively stabilized on impaired mitochondria to activate Parkin. *PLoS Biol.* **8**, e1000298 (2010).

121. Wauer, T., Simicek, M., Schubert, A. & Komander, D. Mechanism of phospho-ubiquitin-induced PARKIN activation. *Nature* **524**, 370–374 (2015).

122. Tanaka, A. *et al.* Proteasome and p97 mediate mitophagy and degradation of mitofusins induced by Parkin. *J. Cell Biol.* **191**, 1367–80 (2010).

123. Sarraf, S. A. *et al.* Landscape of the PARKIN-dependent ubiquitylome in response to mitochondrial depolarization. *Nature* **496**, 372–6 (2013).

124. Palikaras, K., Lionaki, E. & Tavernarakis, N. Mechanisms of mitophagy in cellular homeostasis, physiology and pathology. *Nat. Cell Biol.* **20**, 1013–1022 (2018).

125. Li, W. *et al.* Genome-Wide and Functional Annotation of Human E3 Ubiquitin Ligases Identifies MULAN, a Mitochondrial E3 that Regulates the Organelle's Dynamics and Signaling. *PLoS One* **3**, e1487 (2008).

126. Cilenti, L. *et al.* Inactivation of Omi/HtrA2 protease leads to the deregulation of mitochondrial Mulan E3 ubiquitin ligase and increased mitophagy. *Biochim. Biophys. Acta - Mol. Cell Res.* **1843**, 1295–1307 (2014).

127. Choubey, V., Zeb, A. & Kaasik, A. Molecular Mechanisms and Regulation of Mammalian Mitophagy. *Cells* **11**, 38 (2021).

128. Murakawa, T. *et al.* Bcl-2-like protein 13 is a mammalian Atg32 homologue that mediates mitophagy and mitochondrial fragmentation. *Nat. Commun.* **6**, 7527 (2015).

129. Sowter, H. M., Ratcliffe, P. J., Watson, P., Greenberg, A. H. & Harris, A. L. HIF-1-dependent regulation of hypoxic induction of the cell death factors BNIP3 and NIX in human tumors. *Cancer Res.* **61**, 6669–73 (2001).

130. Zhu, Y. *et al.* Modulation of Serines 17 and 24 in the LC3-interacting Region of Bnip3 Determines Pro-survival Mitophagy versus Apoptosis. *J. Biol. Chem.* **288**, 1099–1113 (2013).

131. Rogov, V. V. *et al.* Phosphorylation of the mitochondrial autophagy receptor Nix enhances its interaction with LC3 proteins. *Sci. Rep.* **7**, 1131 (2017).

132. Zhang, T. *et al.* BNIP3 Protein Suppresses PINK1 Kinase Proteolytic Cleavage to Promote Mitophagy. *J. Biol. Chem.* **291**, 21616–21629 (2016).

133. Gao, F. *et al.* The mitochondrial protein BNIP3L is the substrate of PARK2 and mediates mitophagy in PINK1/PARK2 pathway. *Hum. Mol. Genet.* **24**, 2528–2538 (2015).

134. Chen, G. *et al.* A Regulatory Signaling Loop Comprising the PGAM5

Phosphatase and CK2 Controls Receptor-Mediated Mitophagy. *Mol. Cell* **54**, 362–377 (2014).

135. Liu, L. *et al.* Mitochondrial outer-membrane protein FUNDC1 mediates hypoxia-induced mitophagy in mammalian cells. *Nat. Cell Biol.* **14**, 177–185 (2012).

136. Chen, Z. *et al.* Mitochondrial E3 ligase MARCH 5 regulates FUNDC 1 to fine-tune hypoxic mitophagy . *EMBO Rep.* **18**, 495–509 (2017).

137. Koyano, F., Yamano, K., Kosako, H., Tanaka, K. & Matsuda, N. Parkin recruitment to impaired mitochondria for nonselective ubiquitylation is facilitated by MITOL. *J. Biol. Chem.* **294**, 10300–10314 (2019).

138. Shiiba, I., Takeda, K., Nagashima, S. & Yanagi, S. Overview of Mitochondrial E3 Ubiquitin Ligase MITOL/MARCH5 from Molecular Mechanisms to Diseases. *Int. J. Mol. Sci.* **21**, (2020).

139. Berndsen, C. E. & Wolberger, C. New insights into ubiquitin E3 ligase mechanism. *Nat. Struct. Mol. Biol.* **21**, 301–307 (2014).

140. Yau, R. & Rape, M. The increasing complexity of the ubiquitin code. *Nat. Cell Biol.* **18**, 579–86 (2016).

141. Rousseau, A. & Bertolotti, A. Regulation of proteasome assembly and activity in health and disease. *Nat. Rev. Mol. Cell Biol.* **19**, 697–712 (2018).

142. Kerr, J. S. *et al.* Mitophagy and Alzheimer's Disease: Cellular and Molecular Mechanisms. *Trends in Neurosciences* **40**, 151–166 (2017).

143. Fang, E. F. *et al.* Mitophagy inhibits amyloid-β and tau pathology and reverses cognitive deficits in models of Alzheimer's disease. *Nat. Neurosci.* **22**, 401–412 (2019).

144. Nixon, R. A. *et al.* Extensive involvement of autophagy in Alzheimer disease: an immuno-electron microscopy study. *J. Neuropathol. Exp. Neurol.* **64**, 113–22 (2005).

145. Grubman, A. *et al.* A single-cell atlas of entorhinal cortex from individuals with Alzheimer's disease reveals cell-type-specific gene expression regulation. *Nat. Neurosci.* **22**, 2087–2097 (2019).

146. Hu, Y. *et al.* Tau accumulation impairs mitophagy via increasing mitochondrial membrane potential and reducing mitochondrial Parkin. *Oncotarget* **7**, 17356–68 (2016).

147. Pérez, M. J., Jara, C. & Quintanilla, R. A. Contribution of Tau Pathology to Mitochondrial Impairment in Neurodegeneration. *Front. Neurosci.* **12**, (2018).

148. Hardiman, O. *et al.* Amyotrophic lateral sclerosis. *Nat. Rev. Dis. Prim.* **3**, 17071 (2017).

149. Wong, Y. C. & Holzbaur, E. L. F. Optineurin is an autophagy receptor for damaged mitochondria in parkin-mediated mitophagy that is disrupted by an ALS-linked mutation. *Proc. Natl. Acad. Sci. U. S. A.* **111**, E4439-48 (2014).

150. Jankovic, J. Parkinson ' s disease : clinical features and diagnosis. *J. Neurol. Neurosurg. Psychiatry* 368–376 (2008).

151. Mantri, B. S. & Morley, J. F. Prodromal and Early Parkinson ' s Disease Diagnosis. **2**, 28–32 (2018).

152. Goldman, S. M. Environmental toxins and Parkinson's disease. *Annu. Rev. Pharmacol. Toxicol.* **54**, 141–64 (2014).

153. Kitada, T. *et al.* Mutations in the parkin gene cause autosomal recessive juvenile parkinsonism. *Nature* **392**, 605–8 (1998).

154. Sliter, D. A. *et al.* Parkin and PINK1 mitigate STING-induced inflammation. *Nature* **561**, 258–262 (2018).

155. Ge, P., Dawson, V. L. & Dawson, T. M. PINK1 and Parkin mitochondrial quality control: a source of regional vulnerability in Parkinson's disease. *Mol. Neurodegener.* **15**, 20 (2020).

156. Kumar, M. *et al.* Defects in Mitochondrial Biogenesis Drive Mitochondrial Alterations in PARKIN-Deficient Human Dopamine Neurons. *Stem Cell Reports* **15**, 629–645 (2020).

157. Rey, F., Ottolenghi, S., Zuccotti, G., Samaja, M. & Carelli, S. Mitochondrial dysfunctions in neurodegenerative diseases: role in disease pathogenesis, strategies for analysis and therapeutic prospects. *Neural Regen. Res.* **17**, 754–758 (2022).

158. Schöndorf, D. C. *et al.* The NAD+ Precursor Nicotinamide Riboside Rescues Mitochondrial Defects and Neuronal Loss in iPSC and Fly Models of Parkinson's Disease. *Cell Rep.* **23**, 2976–2988 (2018).

159. Trammell, S. A. J. *et al.* Nicotinamide riboside is uniquely and orally bioavailable in mice and humans. *Nat. Commun.* **7**, (2016).

160. Gilmour, B. C. *et al.* Targeting NAD+ in translational research to relieve diseases and conditions of metabolic stress and ageing. *Mechanisms of Ageing and Development* **186**, 111208 (2020).

161. Song, Y. M. *et al.* Metformin restores parkin-mediated mitophagy, suppressed by cytosolic p53. *Int. J. Mol. Sci.* **17**, (2016).

162. Li, Q. *et al.* Rapamycin Enhances Mitophagy and Attenuates Apoptosis After Spinal Ischemia-Reperfusion Injury. *Front. Neurosci.* **12**, 865 (2018).

163. Bartolomé, A. *et al.* MTORC1 Regulates both General Autophagy and Mitophagy Induction after Oxidative Phosphorylation Uncoupling. *Mol. Cell. Biol.* **37**, (2017).

164. Nardin, A., Schrepfer, E. & Ziviani, E. Counteracting PINK/Parkin Deficiency in the Activation of Mitophagy: A Potential Therapeutic Intervention for Parkinson's Disease. *Curr. Neuropharmacol.* **14**, 250–259 (2016).

165. Wang, Y. *et al.* Deubiquitinating enzymes regulate PARK2-mediated mitophagy. *Autophagy* **11**, 595–606 (2015).

166. Cornelissen, T. *et al.* The deubiquitinase USP15 antagonizes Parkin-mediated mitochondrial ubiquitination and mitophagy. *Hum. Mol. Genet.* **23**, 5227–5242 (2014).

167. Bingol, B. *et al.* The mitochondrial deubiquitinase USP30 opposes parkin-mediated mitophagy. *Nature* **510**, 370–5 (2014).

168. Cunningham, C. N. *et al.* USP30 and parkin homeostatically regulate atypical ubiquitin chains on mitochondria. *Nat. Cell Biol.* **17**, 160–9 (2015).

169. Kluge, A. F. *et al.* Novel highly selective inhibitors of ubiquitin specific protease 30 (USP30) accelerate mitophagy. *Bioorganic Med. Chem. Lett.* **28**, 2655–2659 (2018).

170. Rusilowicz-Jones, E. V *et al.* Benchmarking a highly selective USP30 inhibitor for enhancement of mitophagy and pexophagy. *Life Sci. Alliance* **5**, e202101287 (2022).

171. Wang, Y. *et al.* Small molecule inhibitors reveal allosteric regulation of USP14 via steric blockade. *Cell Res.* **28**, 1186–1194 (2018).

172. Wang, F., Ning, S., Yu, B. & Wang, Y. USP14: Structure, Function, and Target Inhibition. *Front. Pharmacol.* **12**, (2022).

173. Kim, E. *et al.* Dual Function of USP14 Deubiquitinase in Cellular Proteasomal Activity and Autophagic Flux. *Cell Rep.* **24**, 732–743 (2018).

174. Zhu, Y., Zhang, C., Gu, C., Li, Q. & Wu, N. Function of Deubiquitinating Enzyme USP14 as Oncogene in Different Types of Cancer. *Cell. Physiol. Biochem.* **38**, 993–1002 (2016).

175. Wang, D., Ma, H., Zhao, Y. & Zhao, J. Ubiquitin-specific protease 14 is a new therapeutic target for the treatment of diseases. *J. Cell. Physiol.* **236**, 3396–3405 (2021).

176. Rowinsky, E. K. *et al.* Phase 1 study of the protein deubiquitinase inhibitor VLX1570 in patients with relapsed and/or refractory multiple myeloma. *Invest. New Drugs* **38**, 1448–1453 (2020).

177. Palikaras, K., Lionaki, E. & Tavernarakis, N. Balancing mitochondrial biogenesis and mitophagy to maintain energy metabolism homeostasis. *Cell Death Differ.* **22**, 1399–1401 (2015).

178. Harper, J. W., Ordureau, A. & Heo, J.-M. Building and decoding ubiquitin chains for mitophagy. *Nat. Rev. Mol. Cell Biol.* **19**, 93–108 (2018).

179. Whitworth, A. J. *et al.* Increased glutathione S-transferase activity rescues dopaminergic neuron loss in a Drosophila model of Parkinson's disease. *Proc. Natl. Acad. Sci. U. S. A.* **102**, 8024–9 (2005).

180. Park, J. *et al.* Mitochondrial dysfunction in Drosophila PINK1 mutants is complemented by parkin. *Nature* **441**, 1157–61 (2006).

181. Blesa, J. & Przedborski, S. Parkinson's disease: animal models and dopaminergic cell vulnerability. *Front. Neuroanat.* **8**, 155 (2014).

182. Chen, C., Turnbull, D. M. & Reeve, A. K. Mitochondrial dysfunction in Parkinson's disease—cause or consequence? *Biology (Basel).* **8**, 1–26 (2019).

183. Chakraborty, J. & Ziviani, E. Deubiquitinating Enzymes in Parkinson's Disease. *Front. Physiol.* **11**, 1–6 (2020).

184. Nehme, R. *et al.* Combining NGN2 Programming with Developmental Patterning Generates Human Excitatory Neurons with NMDAR-Mediated Synaptic Transmission. *Cell Rep.* **23**, 2509–2523 (2018).

185. Ho, S. M. *et al.* Rapid Ngn2-induction of excitatory neurons from hiPSC-derived neural progenitor cells. *Methods* **101**, 113–124 (2016).

186. Zhang, Y. *et al.* Rapid single-step induction of functional neurons from

human pluripotent stem cells. *Neuron* **78**, 785–798 (2013).

187. Ortuno, D., Carlisle, H. J. & Miller, S. Does inactivation of USP14 enhance degradation of proteasomal substrates that are associated with neurodegenerative diseases? *F1000Research* **5**, 137 (2016).

188. Rodger, C. E., McWilliams, T. G. & Ganley, I. G. Mammalian mitophagy – from in vitro molecules to in vivo models. *FEBS J.* **285**, 1185–1202 (2018).

189. Wilhelm, L. P. *et al.* BNIP3L/NIX regulates both mitophagy and pexophagy. *EMBO J.* e111115 (2022). doi:10.15252/EMBJ.2022111115

190. Yun, J. *et al.* MUL1 acts in parallel to the PINK1/parkin pathway in regulating mitofusin and compensates for loss of PINK1/parkin. *Elife* **3**, (2014).

191. Prudent, J. *et al.* MAPL SUMOylation of Drp1 Stabilizes an ER/Mitochondrial Platform Required for Cell Death. *Mol. Cell* **59**, 941–955 (2015).

192. Ambivero, C. T., Cilenti, L., Main, S. & Zervos, A. S. Mulan E3 ubiquitin ligase interacts with multiple E2 conjugating enzymes and participates in mitophagy by recruiting GABARAP. *Cell. Signal.* **26**, 2921–2929 (2014).

193. Li, J. *et al.* Mitochondrial outer-membrane E3 ligase MUL1 ubiquitinates ULK1 and regulates selenite-induced mitophagy. *Autophagy* **11**, 1216–1229 (2015).

194. Puri, R., Cheng, X. T., Lin, M. Y., Huang, N. & Sheng, Z. H. Mul1 restrains Parkin-mediated mitophagy in mature neurons by maintaining ER-mitochondrial contacts. *Nat. Commun. 2019 101* **10**, 1–19 (2019).

195. Pickrell, A. M. *et al.* Endogenous Parkin Preserves Dopaminergic Substantia Nigral Neurons following Mitochondrial DNA Mutagenic Stress. *Neuron* **87**, 371–81 (2015).

196. Tian, T., McLean, J. W., Wilson, J. A. & Wilson, S. M. Examination of genetic and pharmacological tools to study the proteasomal deubiquitinating enzyme ubiquitin-specific protease 14 in the nervous system. *J. Neurochem.* **156**, 309–323 (2021).

197. Valente, E. M. *et al.* Hereditary early-onset Parkinson's disease caused by mutations in PINK1. *Science (80-.).* **304**, 1158–1160 (2004).

198. Ryan, B. J., Hoek, S., Fon, E. A. & Wade-Martins, R. Mitochondrial dysfunction and mitophagy in Parkinson's: From familial to sporadic disease. *Trends in Biochemical Sciences* **40**, 200–210 (2015).

199. Schindelin, J. *et al.* Fiji: an open-source platform for biological-image analysis. *Nat. Methods* **9**, 676–682 (2012).

200. Schmittgen, T. D. & Livak, K. J. Analyzing real-time PCR data by the comparative CT method. *Nat. Protoc.* **3**, 1101–1108 (2008).

201. Rose, C. M. *et al.* Highly Multiplexed Quantitative Mass Spectrometry Analysis of Ubiquitylomes. *Cell Syst.* **3**, 395-403.e4 (2016).

202. Whiteley, A. M. *et al.* Global proteomics of Ubqln2-based murine models of ALS. *J. Biol. Chem.* **296**, 100153 (2021).

203. Paulo, J. A., O'Connell, J. D. & Gygi, S. P. A Triple Knockout (TKO) Proteomics Standard for Diagnosing Ion Interference in Isobaric Labeling Experiments. *J. Am. Soc. Mass Spectrom.* **27**, 1620–1625 (2016).

204. Eng, J. K., Jahan, T. A. & Hoopmann, M. R. Comet: An open-source MS/MS sequence database search tool. *Proteomics* **13**, 22–24 (2013).

205. Huttlin, E. L. *et al.* A Tissue-Specific Atlas of Mouse Protein Phosphorylation and Expression. *Cell* **143**, 1174–1189 (2010).

206. Sherman, B. T. *et al.* DAVID: a web server for functional enrichment analysis and functional annotation of gene lists (2021 update). *Nucleic Acids Res.* **50**, W216–W221 (2022).

207. Itzhak, D. N., Tyanova, S., Cox, J. & Borner, G. H. Global, quantitative and dynamic mapping of protein subcellular localization. *Elife* **5**, (2016).

208. Rath, S. *et al.* MitoCarta3.0: an updated mitochondrial proteome now with sub-organelle localization and pathway annotations. *Nucleic Acids Res.* **49**, D1541–D1547 (2021).

209. Tyanova, S. *et al.* The Perseus computational platform for comprehensive analysis of (prote)omics data. *Nat. Methods* **13**, 731–740 (2016).

210. Ni, Y.-Q., Xu, H. & Liu, Y.-S. Roles of Long Non-coding RNAs in the Development of Aging-Related Neurodegenerative Diseases. *Front. Mol. Neurosci.* **15**, (2022).

211. Zuo, Z. *et al.* Mechanisms and Functions of Mitophagy and Potential Roles in Renal Disease. *Front. Physiol.* **11**, (2020).